The Catalytic Dehydrocoupling of Amine–Boranes and Phosphine–Boranes

Heather C. Johnson, Thomas N. Hooper, and Andrew S. Weller

Contents

H.C. Johnson • T.N. Hooper • A.S. Weller (✉)
Department of Chemistry, University of Oxford, Oxford OX1 3TA, UK
e-mail: andrew.weller@chem.ox.ac.uk

E. Fernández, A. Whiting (eds.), *Synthesis and Application of Organoboron Compounds*, Topics in Organometallic Chemistry 49,
DOI 10.1007/978-3-319-13054-5_6

Abstract Mechanistic studies into the catalysed dehydrocoupling of amine–boranes and phosphine–boranes have seen a rapid development over the last 5 years. The primary driver for this intense research effort has been the development of catalysts that might offer significant benefits with regard to the kinetics of hydrogen release, for potential use when linked with a fuel cell. Secondary to this, although becoming increasingly important, is the use of dehydrocoupling approaches to afford well-defined polymeric materials with B–N or B–P backbones that offer potential as high-performance polymers, as pre-ceramic materials and as precursors to white graphene. There have been many systems studied using catalysts incorporating metals from across the periodic table. This review attempts to bring together the insight revealed from these studies, which shows a rich and complex mechanistic landscape for the dehydrocoupling of phosphine–boranes and amine–boranes.

Keywords Amine–Borane • Catalysis • Dehydrocoupling • Mechanism • Phosphine–Borane

1 Introduction

The transition-metal-catalysed dehydrocoupling of amine–boranes and, to a lesser extent, phosphine–boranes has received much attention in recent years [1, 2]. For amine–boranes, the parent compound, $H_3B \cdot NH_3$, is an air-stable solid containing a high weight percentage of hydrogen (19.6%) and thus has been explored extensively as a potential candidate for chemical hydrogen storage vectors [3]. Although $H_3B \cdot NH_3$ can release dihydrogen on heating to temperatures above 120°C, leading to mixtures of products including polyborazylene and polyaminoboranes, metal catalysts have led to more efficient and controlled dehydrogenation [4]. Amine–boranes have also been studied with respect to the formation of BN-based materials. In particular polyaminoboranes, which are isoelectronic with societally and technologically ubiquitous polyolefins, have potential applications as piezoelectric materials or as precursors to BN-based ceramics [5] or white graphene [6]. Likewise, the analogous dehydrocoupling of phosphine–boranes produces oligomeric and polymeric materials that show promise as electron beam resists and precursors to semiconducting boron phosphide [7].

In this review we outline recent developments to elucidate, and thus harness, the mechanism of catalytic dehydrocoupling of amine–boranes and phosphine–boranes. Although there is yet to be developed a common, detailed, overarching mechanism that encompasses all catalysed systems, we hope that this contribution serves to mark the current state of the art in the field and provide a background to aid future developments in the area. It is the control of these processes, to either afford well-defined final products or the maximum rate and yield of hydrogen evolution, that makes catalytic routes attractive for dehydrocoupling. This is not

the first time that dehydrocoupling of amine–boranes and phosphine–boranes has been reviewed, and there have been recent overviews dealing with their general chemistry and properties [1, 2], role in hydrogen storage applications [4, 8, 9], as well as dehydrocoupling processes [5, 7, 10, 11]. We do not attempt to review the extensive literature on the catalysed hydrolysis of amine–boranes to produce H_2 as the principal product of interest [3].

2 Transition-Metal-Catalysed Dehydrocoupling of Amine–Boranes

2.1 General Considerations

A generalised scheme for the products observed from amine–borane dehydrocoupling is shown in Scheme 1. The parent $H_3B \cdot NH_3$ can also lose over 2 equiv. of hydrogen to form polyborazylene, as well as often insoluble oligomeric and polymeric materials that arise from loss of less than 2 equiv. of H_2 [8]. Primary amine–boranes, $H_3B \cdot NRH_2$, can undergo loss of 1 equiv. of hydrogen during dehydrocoupling to afford polyaminoboranes $[H_2BNRH]_n$ (R=H, Me, ^{n}Bu), while borazines, $[HBNR]_3$ (R=H, Me, ^{n}Bu), can result from the loss of 2 equiv. of dihydrogen and should be considered to be the thermodynamic product of the dehydrocoupling of primary amine–boranes. Secondary amine–boranes $H_3B \cdot NR_2H$ can lose 1 equiv. of dihydrogen and dehydrocouple through soluble and well-defined intermediates; for $H_3B \cdot NMe_2H$, the most commonly observed are the aminoborane $H_2B{=}NMe_2$ and the linear diborazane $H_3B \cdot NMe_2BH_2 \cdot NMe_2H$ (see Sect. 2.2 and 2.3). Consequently, $H_3B \cdot NMe_2H$ is often used as a model for the dehydrocoupling of $H_3B \cdot NH_3$ and $H_3B \cdot NMeH_2$ [12, 13], the products of which are often insoluble or poorly defined polymeric or oligomeric materials [14]. The cyclic dimer $[H_2BNR_2]_2$ (R=e.g. Me, Et) is generally formed as the major dehydrocoupling product of $H_3B \cdot NR_2H$. With bulky *N*-substituents, e.g. ^{i}Pr or Cy, dimerisation is prevented and instead the aminoborane $H_2B{=}NR_2$ results [15, 16].

2.2 Aminoboranes: Observation and Trapping

The dehydrocoupling of amine–boranes is often proposed to proceed via formation of aminoboranes $H_2B{=}NRR'$ that arise from initial dehydrogenation, and aminoboranes such as $H_2B{=}N^tBuH$ and $H_2B{=}NMe_2$ have been directly observed as intermediates in catalytic dehydrocoupling of their respective amine–boranes [17, 18]. The kinetics for the "off-metal" dimerisation of $H_2B{=}NMe_2$ to form $[H_2BNMe_2]_2$ have been explored and found to be a second-order process with a large negative entropy of activation [19]. Interestingly, a significant solvent effect on the relative rate of dimerisation has also been noted, with acetonitrile

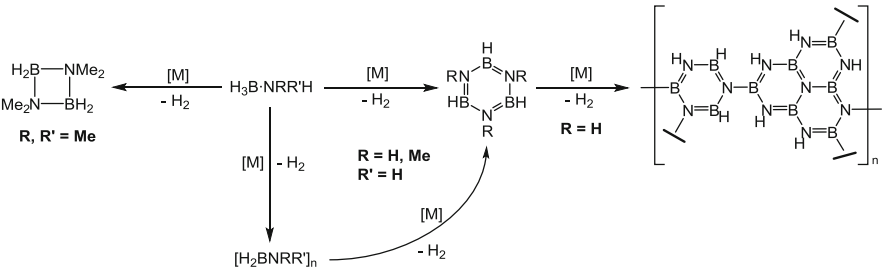

Scheme 1 Simplified dehydrocoupling pathway for $H_3B \cdot NMe_2H$, $H_3B \cdot NMeH_2$ and $H_3B \cdot NH_3$. The generation of intermediate aminoboranes is not shown but is implicit for many processes

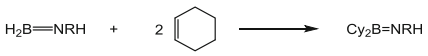

Scheme 2 Trapping of aminoboranes by cyclohexene. R=Me, H

accelerating the process [13, 20]. The less bulky congeners $H_2B{=}NH_2$ [21] and $H_2B{=}NMeH$ [22, 23], however, have not been directly observed as intermediates in dehydrocoupling, although they have been isolated coordinated to a transition metal fragment, being formed from dehydrogenation of the corresponding amine–borane [24]. In 2008, Baker, Dixon and co-workers proposed that $H_2B{=}NH_2$ liberated from the metal results in the eventual production of borazine, whereas $H_2B{=}NH_2$ (or derivatives thereof) remaining bound to the metal results in oligomeric or polymeric products [25]. To detect free aminoborane, cyclohexene was added to reaction mixtures, as cyclohexene can be hydroborated by $H_2B{=}NRH$ (R=H, Me), forming $Cy_2B{=}NRH$ (Scheme 2) thereby acting as a useful marker for free aminoboranes.

Accordingly, when cyclohexene was added to a reaction mixture of $H_3B \cdot NH_3$ and $[Rh(1,5\text{-cod})(\mu\text{-Cl})]_2$, $Cy_2B{=}NH_2$ was the major product observed, instead of the expected borazine (see Sect. 2.4 [26]). However, upon addition of cyclohexene to a solution of $H_3B \cdot NH_3$ and catalyst $Ir(^t\text{BuPOCOP}^t\text{Bu})(H)_2$ [27], the same oligomeric products were observed as in the absence of cyclohexene, i.e. no hydroboration product was observed (Sect. 2.8.3). Although cyclohexene trapping is still regarded as a useful method for detecting free aminoboranes, more recent studies have suggested that the absence of hydroboration does not necessarily reflect an absence of free aminoborane. It has been suggested that, if borazine formation (from aminoborane trimerisation/dehydrogenation) or hydroboration of cyclohexene are not kinetically competitive with metal-based BN oligomerisation/polymerisation processes, $Cy_2B{=}NH_2$ will not be observed even if $H_2B{=}NH_2$ is present [21, 28, 29].

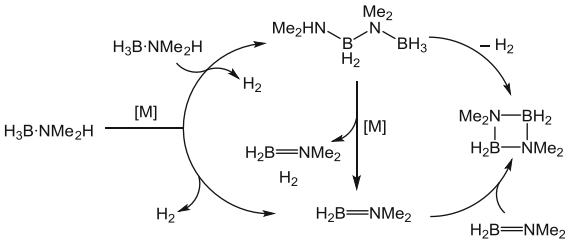

Scheme 3 Schneider's early model for dehydrocoupling $H_3B \cdot NMe_2H$ to form $[H_2BNMe_2]_2$

2.3 *Linear Diborazanes*

Another intermediate often observed in the dehydrocoupling of $H_3B \cdot NMe_2H$ is the linear diborazane $H_3B \cdot NMe_2BH_2 \cdot NMe_2H$ [15]. Schneider has calculated that the pathway for B–N bond cleavage of $H_3B \cdot NMe_2BH_2 \cdot NMe_2H$ to generate $H_3B \cdot NMe_2H$ and $H_2B{=}NMe_2$ is close to thermoneutral ($\Delta G = -2.3$ kcal mol^{-1}) [30]. Therefore, if this process is reversible, the position of the equilibrium (and hence whether $H_3B \cdot NMe_2BH_2 \cdot NMe_2H$ is observed in catalysis) is likely to be dependent upon these species relative concentrations and rates of formation with a particular catalyst. A general pathway for the dehydrocoupling of $H_3B \cdot NMe_2H$ with Schneider's ruthenium catalysts (see Sect. 2.8.4) was developed (Scheme 3), suggesting that the formation of $H_3B \cdot NMe_2BH_2 \cdot NMe_2H$ is a metal-based process. The role of this diborazane in the dehydrocoupling of $H_3B \cdot NMe_2H$ has been further discussed by others [15, 19, 28, 31, 32].

Weller and Manners have since reported that the diborazane $H_3B \cdot NMeHBH_2 \cdot NMeH_2$, the product of one dehydrooligomerisation of $H_3B \cdot NMeH_2$, can be formed by catalytic methods [33], and its role as a possible intermediate in dehydropolymerisation has been further explored (see Sect. 2.8.3) [28]. Shore and co-workers have also reported the synthesis by stoichiometric methods of the $H_3B \cdot NH_3$ analogue, $H_3B \cdot NH_2BH_2 \cdot NH_3$ [34], while Sneddon and co-workers have reported the synthesis of triborazanes, such as $H_3B \cdot (NH_2BH_2)_2 \cdot NH_3$ [35], which are implicated in dehydropolymerisation processes [36].

2.4 *Early Examples of Metal-Catalysed Dehydrocoupling*

The first example of transition-metal-catalysed dehydrocoupling was reported in 1989 by Roberts and co-workers. The amine–borane $H_3B \cdot N^tBuMeH$ was dehydrogenated at 120°C by 10% Pd on charcoal to form the aminoborane $H_2B{=}N^tBuMe$, which dimerised to form $[H_2BN^tBuMe]_2$ [37]. In 2001, Manners and co-workers reported that Rh^I or Rh^{III} precursors catalytically dehydrocoupled secondary amine–boranes $H_3B \cdot NR_2H$ ($R_2{=}Me_2$, *cyclo*-C_4H_8) to yield the corresponding cyclic dimer $[H_2BNR_2]_2$ (Scheme 4). The Rh^I precursor was also

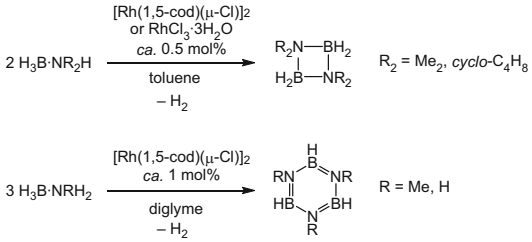

Scheme 4 Dehydrocoupling of amine–boranes by $[Rh(1,5\text{-cod})(\mu\text{-Cl})]_2$ and $RhCl_3 \cdot 3H_2O$

an effective catalyst for the dehydrocoupling of $H_3B \cdot NH_3$ and $H_3B \cdot NMeH_2$ to form their respective borazines, although in both cases insoluble material, indicative of oligomeric chains, was also observed in the reaction mixtures [26].

2.5 *Heterogeneous Catalysts for the Dehydrocoupling of Amine–Boranes*

Various systems act as heterogeneous catalysts for amine–borane dehydrocoupling by the formation in situ of catalytically active nanoparticles, although the nature of the actual catalytic component has been the subject of debate. Nonetheless, heterogeneous catalysis is attractive due to the facile separation of the products and catalyst. The dehydrocoupling of $H_3B \cdot NMe_2H$ by $[Rh(1,5\text{-cod})(\mu\text{-Cl})]_2$ showed a reaction profile with an induction period, during which a black precipitate was observed to form. Tests, originally developed by Finke [38], were performed to probe for heterogeneous catalysis. For example, both filtration and catalyst poisoning with mercury halted catalysis (Fig. 1), suggesting a heterogeneous system in which the dehydrocoupling is catalysed by rhodium nanoparticles [39].

Later EXAFS studies by Autrey and co-workers suggested that, instead, soluble Rh_6 clusters are responsible for the dehydrocoupling activity in this system [40]. Interestingly, the catalytic dehydrocoupling of $H_3B \cdot PPh_2H$ with $[Rh(1,5\text{-cod})(\mu\text{-Cl})]_2$ to form $H_3B \cdot PPh_2BH_2 \cdot PPh_2H$ was reported by Manners as homogeneous (see Sect. 3.2) [39].

Some heterogeneous systems are among the fastest reported dehydrocoupling catalysts. A system using $[Fe(NCMe)_2(PNNP)][BF_4]_2/KO^tBu$ [PNNP= $(Ph_2PC_6H_4CH{=}NCH_2)_2$], reported by Morris and co-workers, was highly active in the dehydrogenation of $H_3B \cdot NH_3$. At 2.5 mol% catalyst loading, an equivalent of H_2 is released within a minute, representing a turnover frequency (TOF) of approximately 2,400 h^{-1}, to yield a mixture of products: borazine, polyborazylene and B–N oligomers or partially cross-linked polyborazylene, as well as unreacted $H_3B \cdot NH_3$ [41]. The active species are proposed to be iron(0) nanoparticles stabilised by PNNP ligands. Catalysis slowed after the initial fast dehydrogenation, and free PNNP ligand was observed by $^{31}P\{^1H\}$ NMR spectroscopy, implying that

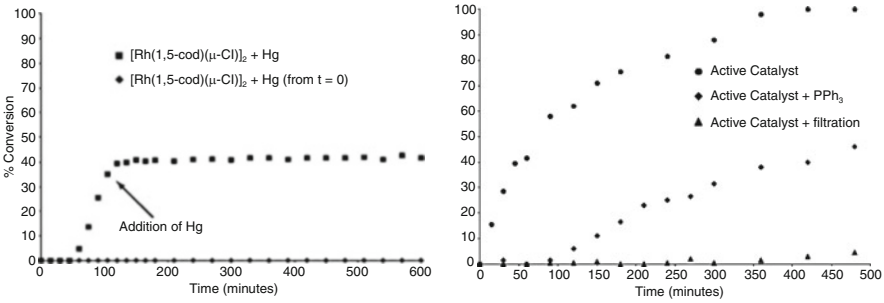

Fig. 1 *Left*: addition of mercury to the reaction mixture. *Right*: the effect of filtration and poisoning with PPh_3. Both figures reprinted (adapted) with permission from Jaska and Manners [39]. Copyright 2004 American Chemical Society

catalyst deactivation was occurring and active sites on the iron nanoparticle were being blocked. Consistent with this, attempts to recycle the catalyst resulted in slower dehydrocoupling.

Systems based upon ruthenium nanoparticles have been explored by Ozkar et al. for the dehydrocoupling of $H_3B \cdot NMe_2H$ to yield $[H_2BNMe_2]_2$ and show good activities. Oleylamine-stabilised ruthenium(0) nanoparticles (generated in situ from $RuCl_3$) effect dehydrocoupling of this amine–borane with a TOF of 137 h^{-1} [42], while ruthenium(0) nanoparticles stabilised by 3–aminopropyltriethoxysilane gave a TOF of 55 h^{-1} [43]. Ozkar also obtained turnover frequencies of ~60 h^{-1} for the dehydrocoupling of $H_3B \cdot NMe_2H$ when using rhodium(0) nanoclusters (~Rh_{190}–Rh_{460}), produced from $[(C_5H_{11}CO_2)_2Rh]_2$ [44]. Zahmakiran and co-workers dehydrogenated $H_3B \cdot NH_3$ to form $[H_2BNH_2]_n$ and polyborazylene (average TOF ~24 h^{-1}) with a ruthenium nanocatalyst that is formed from the in situ hydrogenation of [Ru(cod)(cot)]. Poisoning experiments suggested sub-nanometer Ru_n clusters as the dominant catalytically active species rather than Ru(0) nanoparticles [45]. Iron-doped $H_3B \cdot NH_3$ (5 mol% Fe) has been shown to produce crystalline $[H_2BNH_2]_n$ on heating the solid to 60°C, the mechanism being proposed to operate via an FeB alloy [46].

A skeletal nickel catalyst, produced from base-leaching a Ni/Al alloy, for the heterogeneous dehydrocoupling of amine–boranes was reported by Manners and co-workers [22]. Although the dehydrocoupling is relatively slow (TOF ~3 h^{-1} for $H_3B \cdot NMe_2H$, 5 mol% Ni), mechanistic insight into heterogeneous dehydrocoupling was obtained. The major route for dehydrocoupling $H_3B \cdot NMe_2H$ was proposed to be dehydrogenation to afford the aminoborane $H_2B{=}NMe_2$, which dimerises off-metal to form the final product $[H_2BNMe_2]_2$. A minor pathway was also suggested, involving the on-metal formation of the linear dimer $H_3B \cdot NMe_2BH_2 \cdot NMe_2H$, followed by on-metal dehydrocyclisation to form $[H_2BNMe_2]_2$ (Scheme 5).

Dehydrocoupling of the primary amine–borane $H_3B \cdot NMeH_2$ was also investigated with this system. At a catalyst loading of 5 mol%, slow conversion (TOF ~0.2 h^{-1}) to form the cyclic triborazane $[H_2BNMeH]_3$ resulted. Interestingly at

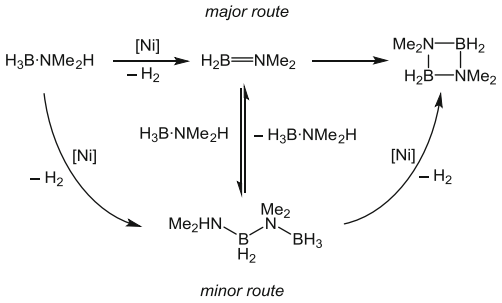

Scheme 5 Suggested dehydrocoupling pathway for the dehydrocoupling of $H_3B \cdot NMe_2H$ by skeletal Ni (5 mol%, toluene)

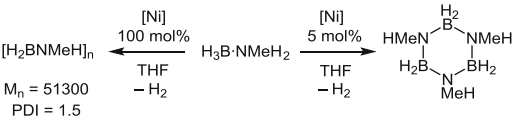

Scheme 6 Dehydrocoupling of $H_3B \cdot NMeH_2$ with skeletal Ni

100 mol% Ni, polyaminoborane $[H_2BNMeH]_n$ was formed ($M_n = 51{,}300$ g mol^{-1}, PDI = 1.5), Scheme 6. This effect of catalyst loading on the identity of the final product was attributed to initial dehydrogenation of $H_3B \cdot NMeH_2$ to form the monomer $H_2B{=}NMeH$, which is formed in higher concentrations with higher catalyst loadings and, under such a kinetic regime, polymerisation is favoured over cyclisation. Similarly, in the dehydrocoupling of $H_3B \cdot NH_3$, 5 mol% of Ni produced *B*-(cyclodiborazanyl)-aminoborohydride, whereas stoichiometric quantities of Ni formed polyaminoborane $[H_2BNH_2]_n$.

An important result for the potential development of amine–boranes as hydrogen storage materials originated from Liu and co-workers using a heterogeneous system. The cyclic amine–borane BN-methylcyclopentane (**1**, Scheme 7), an air- and moisture-stable liquid at room temperature, was shown to release 2 equiv. of H_2 (4.7 wt%) at 80°C to cleanly generate the trimer **2**, also a liquid, using 5 mol% $FeCl_2$ (TOF 120 h^{-1}) in a neat solution of **1** [47]. The reaction profile showed an induction period, and a black powder was produced during the reaction, with mercury experiments suggesting a heterogeneous catalyst as the active species. The catalyst was recyclable, with three successive experiments all showing similar activities. Significantly **2** could be treated with MeOH (to form **3**), followed by $LiAlH_4$ to regenerate **1** (Scheme 7) in 92% yield. Although a more efficient regeneration method is desirable, these results illustrate the potential of this system as a hydrogen storage candidate, with the additional benefit of using cheap and abundant iron as the catalyst. The properties of the materials produced by this process have been described (e.g. viscosity, thermal stability, purity) [48]. A related system was recently reported in which $MeH_2B \cdot NMeH_2$ is dehydrogenated by $CoCl_2$ (5 mol%, 80°C, diglyme) to form the borazine product $[MeBNMe]_3$ in

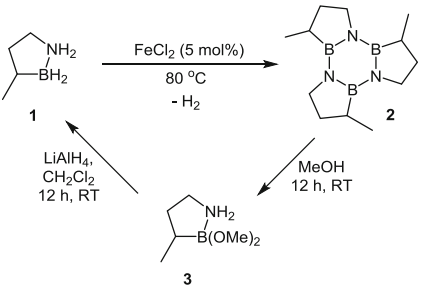

Scheme 7 Dehydrogenation of **1** to yield **2** and regeneration of **1** from **2**

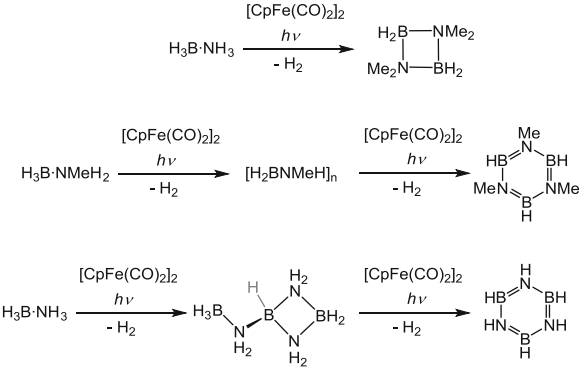

Scheme 8 Catalytic dehydrocoupling of $H_3B \cdot NMe_2H$, $H_3B \cdot NMeH_2$ and $H_3B \cdot NH_3$ with 5 mol % $[FeCp(CO)_2]_2$

71% yield. Subsequent treatment of $[MeBNMe]_3$ with HCOOH and then $LiAlH_4$ regenerated $MeH_2B \cdot NMeH_2$ in a 46% yield [49].

Manners and co-workers recently illustrated that subtle changes in the ligand set can have significant effects on whether the catalysis is homogeneous or heterogeneous. $[CpFe(CO)_2]_2$ (5 mol%) dehydrocouples the amine–boranes $H_3B \cdot NMe_2H$, $H_3B \cdot NMeH_2$ and $H_3B \cdot NH_3$ under photoirradiation (Scheme 8). With $H_3B \cdot NMeH_2$, high molecular weight $[H_2BNMeH]_n$ was produced ($M_n = 64{,}300$ g mol^{-1}, PDI = 1.8) after 3 h (90% conversion), although after 16 h of irradiation, the borazine $[HBNMe]_3$ was the major product [50].

Further mechanistic investigations were undertaken with a range of iron carbonyl cyclopentadienyl complexes and $H_3B \cdot NMe_2H$ [51]. When using $[CpFe(CO)_2]_2$ under photoirradiation and $Cp_2Fe_2(CO)_3(NCMe)$ (no photoirradiation), $H_2B{=}NMe_2$ was observed as the sole intermediate during the dehydrocoupling. With $CpFe(CO)_2I$, however, under photoirradiation, the linear diborazane $H_3B \cdot NMe_2BH_2 \cdot NMe_2H$ was observed as an intermediate, with $H_2B{=}NMe_2$ observed in no significant quantities. Investigations into the nature of the reaction mixtures showed that $[CpFe(CO)_2]_2$ and $Cp_2Fe_2(CO)_3(NCMe)$ were producing iron nanoparticles as the active catalyst, thought to form via the loss of CO and NCMe,

respectively. The heterogeneous mechanism is thought to involve initial dehydrogenation of $H_3B \cdot NMe_2H$ on the nanoparticle surface to form $H_2B{=}NMe_2$, which then dimerises off-metal. By contrast, $CpFe(CO)_2I$ appeared to be acting as a homogeneous catalyst, and this mechanism is discussed in more detail in Sect. 2.8.3.

2.6 *Transition-Metal-Catalysed Dehydrocoupling of $H_3B \cdot NH_3$ Promoted by Ionic Liquids*

In 2006 Sneddon and co-workers noted that dissolving $H_3B \cdot NH_3$ in ionic liquids increased the rate and extent of *thermal* dehydrocoupling relative to that of solid $H_3B \cdot NH_3$ [52, 53]. In 2011, Baker and Sneddon sought to utilise this enhancement by combining transition metal catalysts with ionic liquid solvents. A range of transition metal catalysts were screened for the dehydrocoupling of $H_3B \cdot NH_3$ in the ionic liquid [bmim][Cl] (bmim=1-butyl-3-methylimidazole) [54], all at 5 mol% loading, including $[Rh(1,5\text{-cod})(\mu\text{-Cl})]_2$, $Ru(1,5\text{-cod})Cl_2$, $RhCl_3$, $Ni(1,5\text{-cod})_2$ and $NiCl_2$. All showed enhanced dehydrocoupling activity at 65°C compared with the analogous reaction in [bmim][Cl] in the absence of catalyst. However, increasing the temperature to 85°C with the catalyst $[Rh(1,5\text{-cod})(\mu\text{-Cl})]_2$ led to lower total H_2 release than that in the absence of catalyst. Similar effects were observed with $[RuCl_2(PMe_3)_4]$ (0.78 mol%) in [emim][O_3SOEt] (emim = 1-ethyl-3-methylimidazole), implying that transition metal catalysts can enhance the rate of H_2 release in ionic liquids, but the advantage is most apparent below 85°C. Moreover, different products were observed with changing the ionic liquid: catalysis with $[RuCl_2(PMe_3)_4]$ in [emim][O_3SOEt] resulted in borazine and polyborazylene, whereas the same reaction in [bmim][NTf_2] resulted in $[H_2BNH_2]_n$ (Scheme 9).

This selectivity could have useful implications in the future design of chemical hydrogen storage systems, which was exploited by Baker in the dehydrocoupling of mixtures of $H_3B \cdot NH_3$ and *sec*-butylamine-borane, $H_3B \cdot N^sBuH_2$ [55]. $H_3B \cdot N^sBuH_2$ can solubilise $H_3B \cdot NH_3$, resulting in liquid fuel mixtures that have an upper limit for H_2 release of 12.8 wt%. With the $[RuCl_2(PMe_3)_4]$ catalyst (~1 mol%), the system released over 5.0 wt% of hydrogen in 1 h at 80°C, affording $[HBN^sBu]_3$, $[HBNH]_3$ and polyborazylene. However, insoluble $[H_2BNH_2]_n$ was also observed in the reaction mixture, which is undesirable for a liquid fuel cell, and prevailed on testing diglyme and sulfolane as co-solvents (Scheme 10). The addition of [emim][O_3SOEt] as the co-solvent, however, released 3.6 wt% H_2 at 80°C over 18 h (a lower overall storage capacity due to the ionic liquid) with no insoluble $[H_2BNH_2]_n$ observed, making $H_3B \cdot N^sBuH_2/H_3B \cdot NH_3$ mixtures more appealing as potential liquid fuel cells.

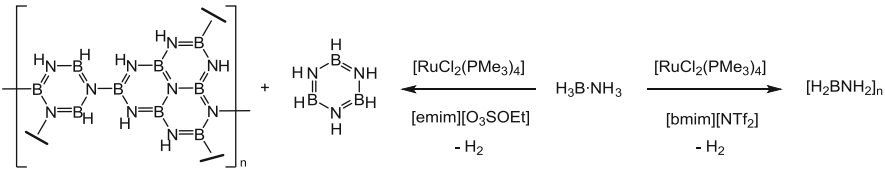

Scheme 9 Different product distributions for the Ru-catalysed dehydrocoupling of $H_3B \cdot NH_3$ with different ionic liquids

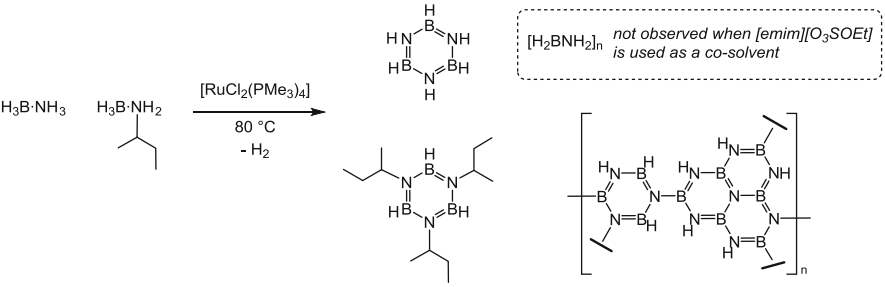

Scheme 10 Products resulting from the dehydrogenation of $H_3B \cdot N^sBuH_2/H_3B \cdot NH_3$ with $[RuCl_2(PMe_3)_4]$ (~1 mol%) with and without [emim][O_3SOEt] as co-solvent

2.7 *Homogeneous Dehydrocoupling of Amine–Boranes*

Although heterogeneous catalysts can produce high turnover numbers, homogeneous catalysts are more readily studied due to the well-defined coordination sites that can allow for control of catalytic processes by modification of the metal and ligand environment. Homogeneous catalysts can operate via inner-sphere or outer-sphere mechanisms. Outer-sphere mechanisms allow dehydrogenation of amine–boranes without the direct coordination to the metal centre by using metal–ligand cooperativity [21, 30, 56–59]. By contrast, inner-sphere mechanisms involve initial coordination of the amine–borane to the metal forming a sigma complex, followed by dehydrogenation of the amine–borane (Scheme 11). Various mechanistic scenarios have been implicated for the mechanism of dehydrogenation and will be discussed in detail in Sect. 2.8.

2.7.1 Sigma Complexes of Amine–Boranes

Inner-sphere mechanisms for the dehydrocoupling of amine–boranes often invoke coordination of an amine–borane to the metal via 3-centre, 2-electron M–H–B interactions [60], forming a sigma complex, $[L_nM\text{-}H_3B \cdot NR_3]$. These weak interactions arise primarily from donation from the σ B–H orbital to the metal; the B–H σ* orbital is high in energy, meaning that back-donation from the metal is negligible [11, 61]. Often, sigma complexes are isolated using tertiary amine–boranes,

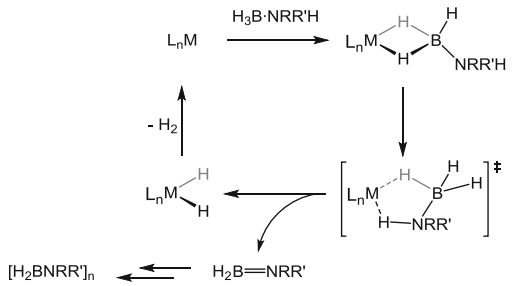

Scheme 11 Simplified pathway for inner-sphere dehydrogenation

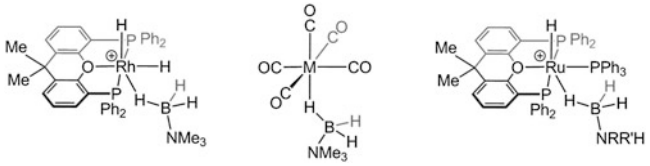

Fig. 2 Examples of η^1-sigma amine–borane complexes. M=Cr, Mo or W. NRR′H=N^{t}BuH$_2$, NMe$_2$H or NH$_3$. [BAr$^F{}_4$]$^-$ anions not shown

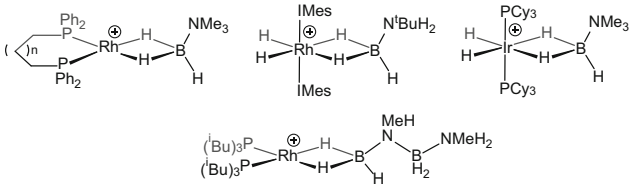

Fig. 3 Examples of η^2-sigma amine–borane complexes. [BAr$^F{}_4$]$^-$ anions not shown. IMes=*N*,*N*′-bis(2,4,6-trimethylphenyl)imidazol-2-ylidene, $n = 1$–3

e.g. $H_3B \cdot NMe_3$, as the lack of N–H bonds generally prevents further reactivity. The first example of a simple amine–borane coordinated to a metal was reported by Shimoi and co-workers in 1999, in which [M(CO)$_5$(η^1-$H_3B \cdot NMe_3$)] (M=Cr, Mo, W) is formed through photolysis of [M(CO)$_6$] in the presence of $H_3B \cdot NMe_3$ [61]. This "end-on" η^1 binding of the amine–borane occurs through one B–H bond, and various other η^1 sigma complexes of amine–boranes have since been reported (a selection shown in Fig. 2) [61–63].

Amine–boranes can also bind to the metal centre through two B–H sigma bonds, resulting in η^2 complexes [19, 64, 65]. Oligomeric species such as $H_3B \cdot NMe_2BH_2 \cdot NMe_2H$ have also been observed to bind in this manner (Fig. 3) [31, 66, 67].

Examples have also been isolated in which multiple amine–borane moieties are bound to a metal centre, similar to intermediates often invoked for dimerisation and polymerisation mechanisms (vide infra) [12, 62, 68–70]. In

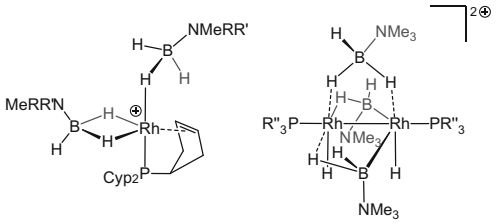

Fig. 4 Examples of multiple amine–borane bonding to transition metal fragments. R″=^{i}Pr, Cy. Cyp=cyclopentyl. R=Me, H. R′=Me, H. $[BAr^{F}_{4}]^{-}$ not shown

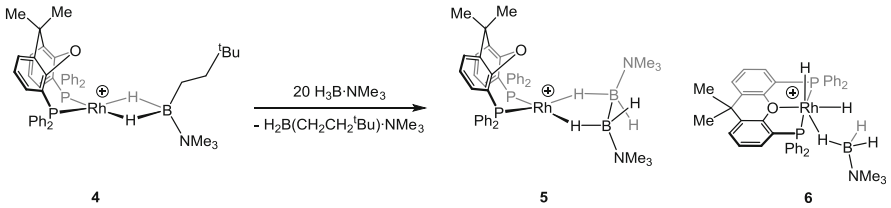

Scheme 12 B–B homocoupling using the $[Rh(Xantphos)]^{+}$ fragment. $[BAr^{F}_{4}]^{-}$ not shown

2010, Weller and co-workers reported a bimetallic hydridoboryl species formed from two $\{Rh(PR_3)\}^{+}$ (R=^{i}Pr, Cy) fragments bridged by three $H_3B \cdot NMe_3$ ligands, two of which have undergone B–H activation (Fig. 4) [71]. The same group also reported cationic rhodium species with two amine–boranes bound to one rhodium centre, $[Rh\{P(C_5H_9)_2(\eta^2\text{-}C_5H_7)\}(\eta^2\text{-}H_3B \cdot NMeRR')(\eta^1\text{-}H_3B \cdot NMeRR')][BAr^{F}_{4}]$ (R, R′=Me, H) [72].

In 2013, Weller and MacGregor reported the first well-characterised example of the B–B homocoupling of an amine–borane to yield the diborane (4) $Me_3N \cdot BH_2BH_2 \cdot NMe_3$ ligand sigma bound to rhodium [62]. B–B homocoupling of boranes has been otherwise limited to B–B bond formation in polyhedral boranes [73, 74], guanidine bases [75] and catechol- and pinacolboranes [76–78]. Pd^{II} catalysts have been demonstrated to rapidly (TOF ~2,000 h^{-1}) dehydrocouple $H_3B \cdot NH_3$ to yield poorly defined materials proposed to contain B–B bonds [79]. Addition of excess $H_3B \cdot NMe_3$ to the sigma complex $[Rh(\kappa^2\text{-}_{P,P}\text{-Xantphos})(\eta^2\text{-}H_2B(CH_2CH_2{}^{t}Bu) \cdot NMe_3)][BAr^{F}_{4}]$ (**4**) yielded $[Rh(\kappa^2\text{-}_{P,P}\text{-Xantphos})(\eta^2\text{-}H_4B_2 \cdot 2NMe_3)][BAr^{F}_{4}]$ (**5**) alongside the Rh^{III} complex $[Rh(\kappa^3\text{-}_{P,O,P}\text{-Xantphos})(H)_2(\eta^1\text{-}H_3B \cdot NMe_3)][BAr^{F}_{4}]$ (**6**) in an approximate 50:50 ratio (Scheme 12).

The homocoupling mechanism was probed by DFT calculations. Starting from the putative complex $[Rh(\kappa^2\text{-}_{P,P}\text{-Xantphos})(\eta^2\text{-}H_3B \cdot NMe_3)][BAr^{F}_{4}]$, a low-energy initial B–H activation of the coordinated $H_3B \cdot NMe_3$ is followed by the coordination of a second $H_3B \cdot NMe_3$ molecule, with a higher-energy combined second B–H activation/B–B coupling step. Addition of excess cyclohexene to the reaction mixture resulted in nearly quantitative yields of **5** by reducing **6** to $[Rh(\kappa^2\text{-}_{P,P}\text{-Xantphos})(\eta^2\text{-}H_3B \cdot NMe_3)][BAr^{F}_{4}]$, enabling further homocoupling at a Rh^{I} centre.

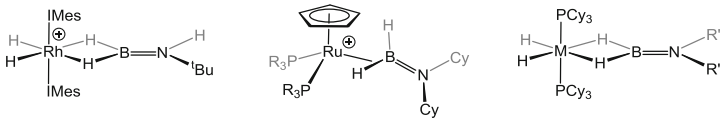

Fig. 5 Aminoborane complexes. $(PR_3)_2$=$(Ph_3P)_2$ or $(Cy_2PCH_2CH_2PCy_2)$. M=Ru, R′=^{i}Pr, Me, H; M=Rh^+ or Ir^+, R′=^{i}Pr, Me. $[BAr^F{}_4]^-$ not shown

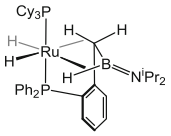

Fig. 6 Sabo-Etienne and Alcaraz's bis(agostic) phosphinobenzyl-(amino)borane ruthenium complex

Sigma complexes of aminoboranes have also been isolated, where donation from the B–H bonds into a vacant metal orbital is reinforced by π back-donation from the metal into the π* B–N orbital of the aminoborane [80]. Various examples have been characterised with rhodium [13, 66, 80, 81], iridium [17, 19, 80, 82] and ruthenium [24, 80, 83, 84], and a selection is presented in Fig. 5. Sabo-Etienne and Alcaraz have recently reported an unusual aminoborane complex exhibiting adjacent agostic B–H and C–H interactions (Fig. 6) [85]. The isolation of aminoborane complexes is of interest mechanistically, as aminoboranes bound to the metal centre have been implicated in dehydrocoupling mechanisms, although often not observed directly (vide infra) [12, 70, 86]. These aminoborane complexes are also closely related to transition metal complexes of three-coordinate boranes, e.g. H_2BR or HBR_2 [87].

2.8 *Mechanistic Studies on Homogeneous Dehydrocoupling Systems*

2.8.1 Early Transition Metals

In 2006, Manners demonstrated the first well-defined homogeneous catalytic dehydrocoupling of $H_3B \cdot NMe_2H$ to form $[H_2BNMe_2]_2$ by using the $[Cp_2Ti]$ fragment, generated in situ from Cp_2TiCl_2/^{n}BuLi [88]. After this initial report, calculations by Ohno and Luo suggested a stepwise mechanism for dehydrocoupling in which N–H bond activation is followed by B–H activation to form $H_2B{=}NMe_2$, which dimerises off-metal [89]. A more detailed kinetic–mechanistic study by Manners, Lloyd-Jones and co-workers on the $[Cp_2Ti]$ system contradicted this mechanism; significantly, the linear diborazane $H_3B \cdot NMe_2BH_2 \cdot NMe_2H$ was identified as an intermediate in the dehydrocoupling reaction (2 mol% $[Cp_2Ti]$, TOF = 12.5 h^{-1}) [69]. The proposed mechanism

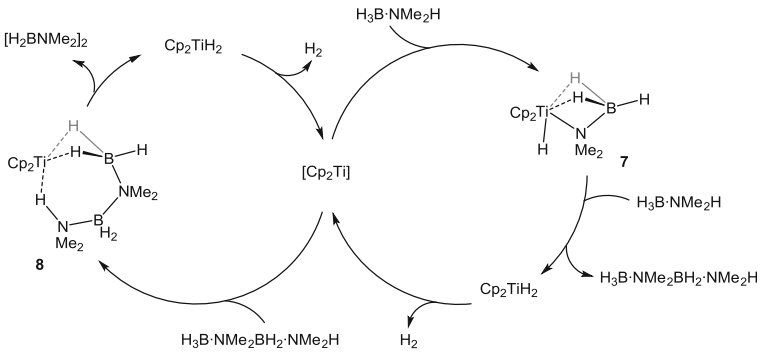

Scheme 13 Mechanism proposed by Manners and Lloyd-Jones for the dehydrocoupling of $H_3B \cdot NMe_2H$

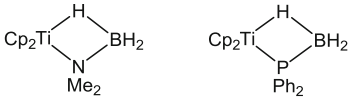

Fig. 7 Ti^{III} complexes **9** and **10**

(Scheme 13) involves two cycles. Initial coordination of $H_3B \cdot NMe_2H$ to $[Cp_2Ti]$ to form $[Cp_2Ti(\eta^2\text{-}H_3B \cdot NMe_2H)]$ is suggested to be followed by N–H activation of the protic hydrogen with the Ti^{II} centre to yield the amidoborane $[Cp_2Ti(H)(NMe_2 \cdot BH_3)]$, **7**. A second equivalent of $H_3B \cdot NMe_2H$ reacts with **7**, resulting in B–N bond formation to give Cp_2TiH_2 with loss of $H_3B \cdot NMe_2BH_2 \cdot NMe_2H$. The second cycle invokes reaction of $H_3B \cdot NMe_2BH_2 \cdot NMe_2H$ with $[Cp_2Ti]$ to form **8**, which undergoes on-metal dehydrocyclisation to form $[H_2BNMe_2]_2$ and Cp_2TiH_2. The proposed scheme is consistent with experimental and kinetic observations, in particular that reaction of independently prepared $H_3B \cdot NMe_2BH_2 \cdot NMe_2H$ with $[Cp_2Ti]$ resulted in the complete consumption of $H_3B \cdot NMe_2BH_2 \cdot NMe_2H$ to form $[H_2BNMe_2]_2$, with only negligible amounts of $H_2B{=}NMe_2$ observed. This implies that $H_3B \cdot NMe_2BH_2 \cdot NMe_2H$ is the sole intermediate in the formation of $[H_2BNMe_2]_2$ in this case, contrary to Luo and Ohno's mechanism. Interestingly, the same system was unreactive towards $H_3B \cdot NMeH_2$ (20°C) and $H_3B \cdot PPh_2H$ (up to 40°C). Zirconium analogues of amidoboranes such as **7** have been synthesised and structurally characterised by Roesler and co-workers [90].

More recent work has found that paramagnetic Ti^{III} species may play a significant role in the $[Cp_2Ti]$ system. Following the report of the isolation of the Ti^{III} complex $[Cp_2Ti(NH_2 \cdot BH_3)]$ by McGrady [91], the analogous complexes $[Cp_2Ti(NMe_2 \cdot BH_3)]$ (**9**) and $[Cp_2Ti(PPh_2 \cdot BH_3)]$ (**10**) (Fig. 7) were synthesised and employed as catalysts under the same conditions as with the titanocene fragment (2 mol%, toluene) [92]. **9** and **10** were shown to be effective catalysts, promoting 83 and 97% consumption of $H_3B \cdot NMe_2H$ after 2 h, respectively. Similar to $[Cp_2Ti]$, both reaction profiles showed $H_3B \cdot NMe_2BH_2 \cdot NMe_2H$ as an

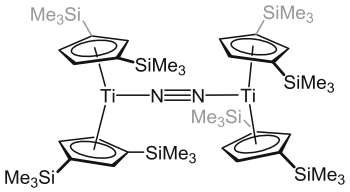

11

Fig. 8 Chirik's dehydrocoupling catalyst **11**

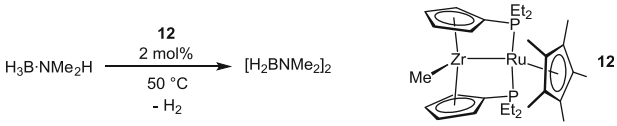

Scheme 14 Dehydrocoupling of $H_3B \cdot NMe_2H$ using **12**

intermediate, followed by the formation of $[H_2BNMe_2]_2$, with **9** showing comparable activity to $[Cp_2Ti]$ (TOF of 10.7 h^{-1} for **9**, cf. 12.5 h^{-1} for $[Cp_2Ti]$). Analysis by UV/Vis and EPR spectroscopies of reaction solutions using $[Cp_2Ti]$ and **9** as precatalysts resulted in spectra comparable with those of isolated **9**. These results imply that the Ti^{III} complex **9** may be of importance in the catalytic dehydrocoupling by titanocene, in contrast to the Ti^{II} and Ti^{IV} cycle depicted in Scheme 13. The zirconocene analogue of **10**, $[Cp_2Zr(PPh_2 \cdot BH_3)]$, was a far less active catalyst, achieving negligible consumption of $H_3B \cdot NMe_2H$ after 2 h. Related work on metallocene complexes by Rosenthal and co-workers using the alkyne complex $[Cp_2M(\eta^2\text{-}Me_3SiCCSiMe_3)(L)]$ (M=Ti, Zr; L=pyridine for Zr, no L for Ti) as a source of $[Cp_2M]$ showed turnover frequencies of 3 h^{-1} and 1 h^{-1} for M=Ti and M=Zr, respectively, for the dehydrocoupling of $H_3B \cdot NMe_2H$ [93]. The closely related precatalyst $[(\eta^5\text{-}C_5H_4{}^iPr)_2Ti(\eta^2\text{-}Me_3SiCCSiMe_3)]$ was explored shortly afterwards and showed improved dehydrocoupling activity (TOF = 32 h^{-1} at 40°C, 6 h^{-1} at 24°C) [94]. The Cp* analogue, however, showed no dehydrocoupling activity, highlighting the importance of sterics in designing systems for dehydrocoupling with early transition metal systems [93].

The fastest group IV systems reported include Chirik's Ti^{II} complex **11** (Fig. 8), which dehydrocoupled $H_3B \cdot NMe_2H$ with a TOF of 420 h^{-1} [95]. Based on kinetic and isotopic labelling experiments, a mechanism was proposed that involved reversible B–H oxidative addition followed by β-H elimination. A rapid Zr^{IV} catalyst based on a frustrated Lewis pair (TOF ~600 h^{-1}) published by Wass is discussed further in Sect. 2.8.4.

Nishibayashi and co-workers reported the heterobimetallic group IV/VIII complex $[ZrMe(\mu\text{-}\eta^5\text{:}\eta^1\text{-}C_5H_4PEt_2)_2RuCp^*]$, **12**, and showed that it was a slow catalyst for the dehydrocoupling of $H_3B \cdot NMe_2H$ to form $[H_2BNMe_2]_2$ (2 mol% **12**, TOF ~8 h^{-1}, 50°C) (Scheme 14) [96]. The system was less active for the dehydrocoupling of $H_3B \cdot NMeH_2$ and $H_3B \cdot NH_3$, reaching 92 and 56% completion, respectively, after 24 h (10 mol% **12** at 50°C) to form B–N oligomeric

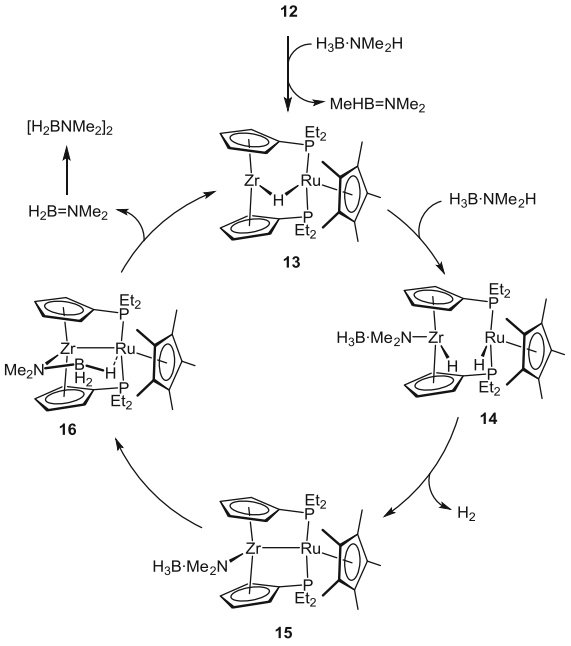

Scheme 15 Proposed mechanism for the dehydrocoupling of $H_3B \cdot NMe_2H$ with **12**

materials. Accordingly, mechanistic studies were conducted with $H_3B \cdot NMe_2H$, and the proposed catalytic cycle is presented in Scheme 15.

The initial conversion of **12** to **13** is proposed to occur via ligand exchange of the hydride on $H_3B \cdot NMe_2H$ with the methyl group at Zr, forming $MeH_2B \cdot NMe_2H$ and **13**, which is suggested to be the true catalyst. The thus formed $MeH_2B \cdot NMe_2H$ undergoes dehydrogenation to afford $MeHB{=}NMe_2$ (observed) in an analogous manner to the subsequent catalytic dehydrogenation of $H_3B \cdot NMe_2H$. From **13**, the dehydrogenation of $H_3B \cdot NMe_2H$ proceeds via initial N–H activation of $H_3B \cdot NMe_2H$ on the Zr centre, forming the amidoborane dihydride **14**. Bimetallic reductive elimination of H_2 forms **15**, and B–H activation by the Ru centre can then occur (**16**), releasing $H_2B{=}NMe_2$, which yields $[H_2BNMe_2]_2$ upon dimerisation, and reforming **13**. This cycle highlights that the cooperative effect of two metals in close proximity could be of potential use in designing future catalysts, although the activity of **12** is only moderate compared with some other homogeneous systems [12, 21, 59, 65]. Rousseau has also explored multimetallic dehydrocoupling of $H_3B \cdot NMe_2H$ with Rh_4 clusters [97].

2.8.2 Mid-Transition Metals

Shimoi and co-workers have shown that photoactivated $[M(CO)_6]$ (M=Cr, Mo, W) act as dehydrocoupling catalysts yielding $[H_2BNMe_2]_2$ from $H_3B \cdot NMe_2H$ (TOF 19 h^{-1} when M=Cr) and a mixture of $[HBNMe]_3$ and $[H_2BNMeH]_n$ from

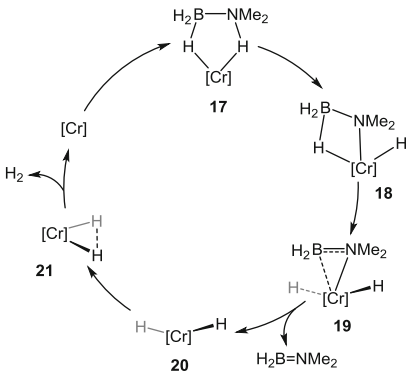

Scheme 16 Shimoi's proposed mechanism for the dehydrocoupling of $H_3B \cdot NMe_2H$. [Cr]=[Cr $(CO)_4$]

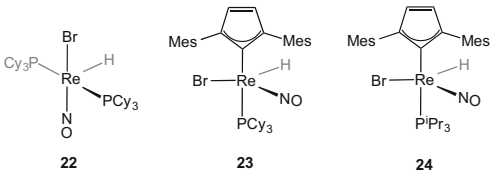

Fig. 9 Rhenium catalysts for the dehydrocoupling of $H_3B \cdot NMe_2H$

$H_3B \cdot NMeH_2$ [98]. The mechanism of dehydrocoupling $H_3B \cdot NMe_2H$ with [Cr $(CO)_6$] was investigated by DFT calculations and suggested that the active species is the 14-electron [$Cr(CO)_4$] fragment, which can coordinate $H_3B \cdot NMe_2H$ to form the sigma complex **17** (Scheme 16). From this, N–H activation to form an amidoborane (**18**) precedes B–H activation to release $H_2B{=}NMe_2$ from **19**. [Cr $(CO)_4$] is regenerated from [$Cr(CO)_4(H)_2$] (**20**) (Scheme 16). Interestingly, although the sigma complex [$Cr(CO)_5(\eta^1$-$H_3B \cdot NMe_2H)$] was observed in the reaction mixture, it was calculated to sit outside the cycle, acting simply as a source of [$Cr(CO)_4$].

In 2009, Berke and co-workers explored a range of nitrosyl rhenium catalysts for the dehydrocoupling of $H_3B \cdot NMe_2H$ to form $[H_2BNMe_2]_2$ [86]. The most active catalysts were **22**, **23** and **24** (Fig. 9), showing turnover frequencies of 77, 100 and 92 h^{-1}, respectively. All three catalysts were also active for the transfer hydrogenation of *n*-octene using $H_3B \cdot NMe_2H$ as the hydrogen source. Two possible mechanisms for the dehydrocoupling reaction using **22** were suggested (Scheme 17). Cycle A involves coordination of $H_3B \cdot NMe_2H$ to **22**, forming the sigma complex **25**. Loss of a PCy_3 ligand reveals a vacant coordination site, allowing B–H activation to form the base-stabilised boryl species **26**. Reductive elimination of H_2 forms **27**, from which a β-H elimination yields free $H_2B{=}NMe_2$ and reforms **22**. An alternative pathway (B) involves the formation of the sigma compound **28**, followed by N–H protonation of Re–H to form **29**. B–H cleavage

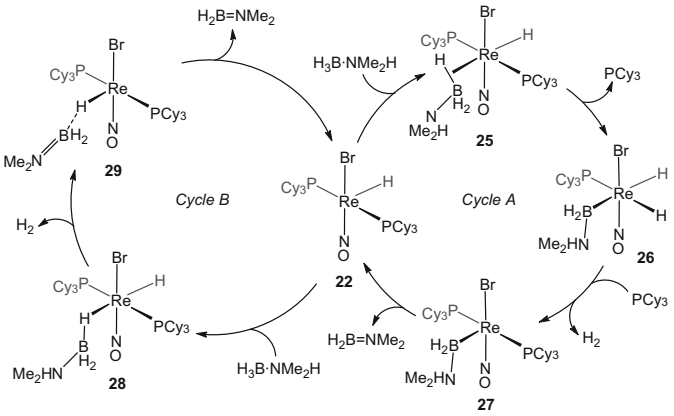

Scheme 17 Suggested mechanisms for the dehydrocoupling of $H_3B \cdot NMe_2H$ using **22**

then forms $H_2B{=}NMe_2$ and **22**. During catalysis, a dihydrogen complex [ReBr $(PCy_3)_2(H)(H_2)(NO)$] was the observed resting state in the presence of hydrogen, being in equilibrium with the active species **22**.

2.8.3 Late Transition Metals

Many studies regarding the mechanisms of catalytic dehydrocoupling have used late transition metal systems. Early reports by Manners on Rh systems indicated that these were operating as heterogeneous catalysts (see Sect. 2.5) [15, 26]. In 2006 Heinekey and Goldberg used Brookhart's Ir(^{t}BuPOCOP^{t}Bu)H_2 (^{t}BuPOCOP^{t}Bu = κ^3-$_{P,C,P}$-1,3-$(OP^tBu_2)_2C_6H_3$) catalyst (**30**) to efficiently dehydrocouple $H_3B \cdot NH_3$ to form the purported cyclic pentamer $[H_2BNH_2]_5$ [27], although this product was later reassigned by Manners and co-workers as $[H_2BNH_2]_n$ ($n \sim 20$) [23]. At 1 mol% an impressive ToF of 1,500 h^{-1} was recorded. At long reaction times, a dormant new species is formed, assigned as the sigma-borane complex Ir(^{t}BuPOCOP^{t}Bu)$H_2(BH_3)$ **31** (Fig. 10) [99], which can be regenerated to form a catalytically active species on addition of H_2. Related sigma complexes of **30** bound to pinacolborane and 9-BBN have also been reported. Various kinetic data of the hydrogen release using catalyst **30** have been determined, and follow a first-order dependence on amine–borane, for both $H_3B \cdot NH_3$ and $H_3B \cdot NMeH_2$ [100]. Interestingly, for this system, dehydrocoupling of $H_3B \cdot NMe_2H$ is sluggish at best. Calculations suggest a concerted process for B–H/N–H activation at the Ir centre [101].

In 2007 Baker reported that $Ni(NHC)_2$ systems were active catalysts for the dehydrogenation of ammonia–borane [102]. A variety of NHC ligands were used, with Enders' carbene (1,3,4-triphenyl-4,5-dihydro-1H-1,2,4-triazol-5-ylidene) affording the most active catalyst (Scheme 18). First-order rate constants were determined, and KIE experiments indicated that both B–H and N–H bonds were being broken in the rate-determining step(s). This report generated considerable

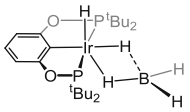

Fig. 10 The structure of Ir(^{t}BuPOCOP^{t}Bu)(H)$_2$(BH$_3$) (**31**)

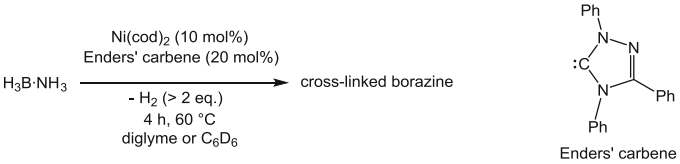

Scheme 18 Dehydrocoupling of $H_3B \cdot NH_3$ with Ni(cod)$_2$ and Enders' carbene

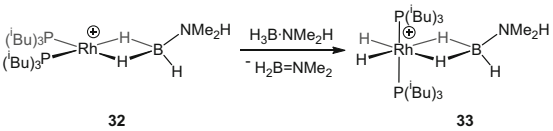

Scheme 19 Initial dehydrogenation of **32**. [BAr$^F{}_4$]$^-$ anions not shown

interest with regard to mapping the processes occurring using computational methods [103–107]. In particular the non-innocent role of the NHC ligands, by mediating hydrogen transfer from the amine–borane to the Ni centre, and the role of free carbene in dehydrogenation were revealed.

In 2009, Weller and Hall conducted a detailed experimental and computational study [66] on the dehydrocoupling of $H_3B \cdot NMe_2H$ by the latent low-coordinate complex [Rh(P^{i}Bu$_3$)$_2$][BAr$^F{}_4$] [108] (5 mol%, TOF = 34 h^{-1}) to afford [H$_2$BNMe$_2$]$_2$. Coordination of $H_3B \cdot NMe_2H$ to [Rh(P^{i}Bu$_3$)$_2$][BAr$^F{}_4$] forms the sigma complex [Rh(P^{i}Bu$_3$)$_2$(η^2-H$_3$B · NMe$_2$H)][BAr$^F{}_4$] (**32**, Scheme 19). This is short–lived in the presence of excess $H_3B{\cdot}NMe_2H$, rapidly forming [Rh(^{i}Bu$_3$)$_2$(H)$_2$(η^2–H$_3$B·NMe$_2$H)][BAr$^F{}_4$] (**33**). A complex pathway was calculated for the lowest energy dehydrogenation of **32**. Either initial B–H activation and N–H transfer or initial N–H activation and B–H transfer occurs to yield the aminoborane complex [Rh(P^{i}Bu$_3$)$_2$(H$_2$)(η^2-H$_2$B=NMe$_2$)][BAr$^F{}_4$], which is observed at the end of catalysis. N–H activation was calculated to be rate limiting in either pathway. Then, H$_2$ loss followed by dissociation of H$_2$B=NMe$_2$, or vice versa, forms [H$_2$BNMe$_2$]$_2$ and regenerates the Rh^I fragment. A constant oxidation state Rh^{III} cycle was also proposed. Experimentally $H_3B \cdot NMe_2BH_2 \cdot NMe_2H$ was observed as an intermediate during catalytic dehydrocoupling and its role probed further. The linear diborazane complex [Rh(P^{i}Bu$_3$)$_2$(η^2-$H_3B \cdot NMe_2BH_2 \cdot NMe_2H$)][BAr$^F{}_4$] was stable in 1,2-C$_6H_4F_2$ solution but, upon addition of excess $H_3B \cdot NMe_2BH_2 \cdot NMe_2H$, formed [H$_2$BNMe$_2$]$_2$ with H$_2$B=NMe$_2$ also observed, suggesting that B–N cleavage is occurring rather than a simple intramolecular dehydrocyclisation.

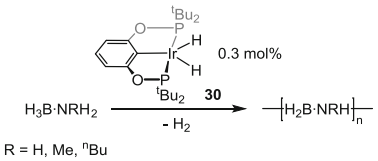

Scheme 20 Catalytic dehydropolymerisation of amine–boranes using **30**

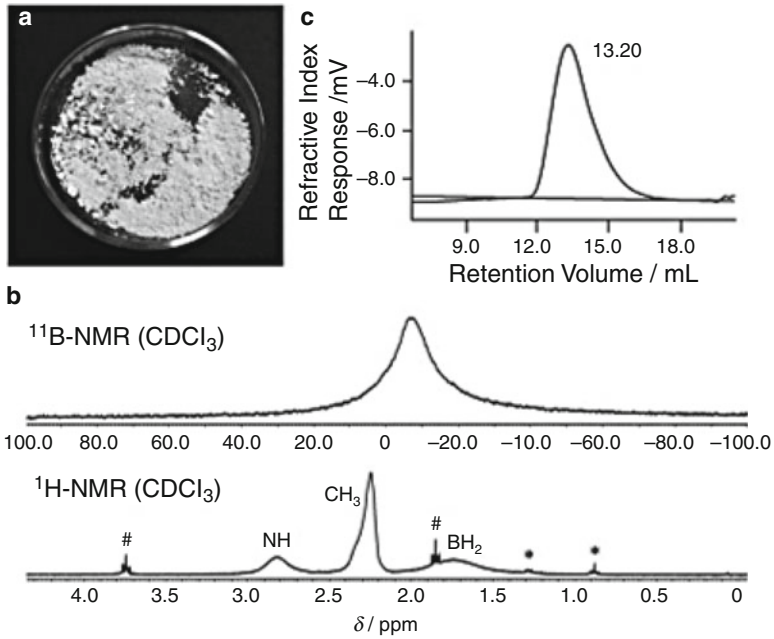

Fig. 11 (**a**) $[H_2BNMeH]_n$. (**b**) ^{11}B and ^{1}H NMR spectra. # = THF, * = butane. (**c**) GPC trace (THF with 0.1% w/w $^{n}Bu_4NBr$). Staubitz et al. [14]. Copyright 2008 Wiley-VCH

The first example of well-defined homogeneous catalytic dehydropolymerisation of amine–boranes was reported by Manners and co-workers in 2008 [14]. The dehydropolymerisation of $H_3B \cdot NRH_2$ (R=H, Me, ^{n}Bu) mediated by **30** formed $[H_2BNRH]_n$ (Scheme 20). With R=Me, high molecular weight $[H_2BNMeH]_n$ was isolated ($M_n = 55{,}200$ g mol^{-1}, PDI = 2.9, Fig. 11c). The ^{11}B NMR spectrum of the polymer shows a broad resonance consistent with multiple ^{11}B environments within the polymer chain (Fig. 11b).

In a detailed follow-up paper, on the basis of molecular weight versus conversion experiments alongside other markers, a modified chain growth mechanism was proposed for this system, in which a slow initial dehydrogenation of $H_3B \cdot NMeH_2$ is followed by fast insertion of the resulting $H_2B{=}NMeH$ [23]. A variety of other catalysts based on rhodium and ruthenium were also active in dehydropolymerisation. A recent computational study explored the mechanism of

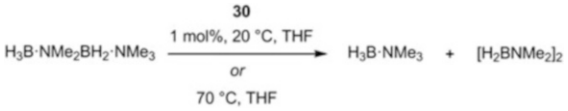

Scheme 21 Hydrogen redistribution reaction of $H_3B \cdot NMe_2BH_2 \cdot NMe_3$

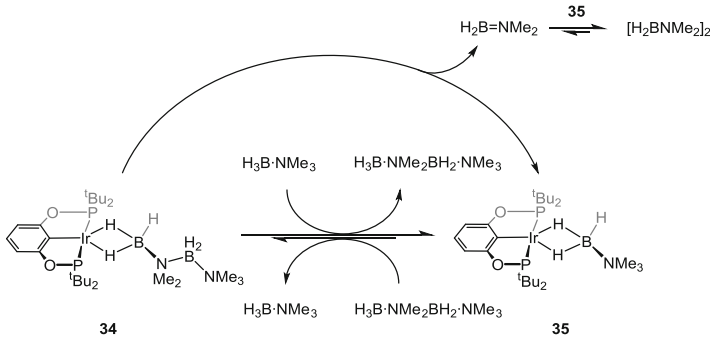

Scheme 22 Model suggested for the metal-catalysed hydrogen redistribution reaction

the polymerisation of $H_2B{=}NH_2$ by **30** (although concomitant dehydrogenation of the amine–borane was not probed) and also implicated a chain growth mechanism, as suggested experimentally by Manners. The proposed mechanism for propagation involves end chain growth; the lone pair on the NH_2 end of the chain interacts with the Lewis acidic BH_2 group of the entering $H_2B{=}NH_2$ molecule [29]. This suggested mechanism contrasts with a coordination insertion mechanism, in which a transient aminoborane inserts into a growing polymer chain at the metal centre, similar to Ziegler–Natta olefin polymerisation.

The role of **30** in the redistribution of linear diborazanes has also been probed [28]. The diborazane $H_3B \cdot NMe_2BH_2 \cdot NMe_3$ was prepared as a "model" diborazane as it does not have a functional N–H group. This can undergo both thermal (70°C, THF) and metal-catalysed (20°C, 1 mol% [Ir], THF) redistribution reactions to form $H_3B \cdot NMe_3$ and $[H_2BNMe_2]_2$ (Scheme 21). Kinetic analyses and simulations were used to probe the metal-catalysed pathway. The model suggested that **30** reacts with $H_3B \cdot NMe_2BH_2 \cdot NMe_3$ to form a proposed sigma complex **34**, from which a direct redistribution reaction gives $H_2B{=}NMe_2$ and a sigma complex **35** (Scheme 22). Dimerisation of $H_2B{=}NMe_2$ affords $[H_2BNMe_2]_2$, and the kinetic simulations showed that, as well as the expected off-metal dimerisation, the dimerisation was also being catalysed by **35**, or a closely related fragment. Related to this, the pincer complex $[Pd(^tBuPCP^tBu)(OH_2)][PF_6]$ ($^tBuPCP^tBu = 2,6\text{-}C_6H_3(CH_2P^tBu_2)_2$) has been shown to release 1 equiv. of H_2 upon reaction with $H_3B \cdot NH_3$, and DFT modelling also suggested an on-metal cyclodimerisation to form $[H_2BNH_2]_2$ [109].

The redistribution chemistry of the more complex (i.e. containing N–H groups) linear diborazane $H_3B \cdot NMeHBH_2 \cdot NMeH_2$, first noted by Weller and Manners as the product of a single oligomerisation of $H_3B \cdot NMeH_2$ [33], was also explored by

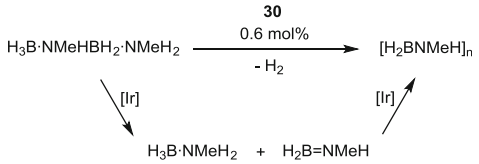

Scheme 23 Proposed mechanism for the metal-catalysed redistribution of $H_3B \cdot NMeHBH_2 \cdot NMeH_2$

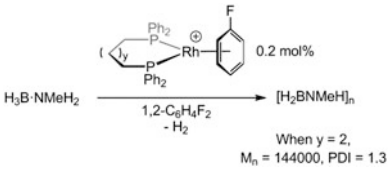

Scheme 24 Dehydropolymerisation by $[Rh(Ph_2P(CH_2)_xPPh_2)(\eta^6\text{-}C_6H_5F)][BAr^F{}_4]$ ($x = 3$–5). $[BAr^F{}_4]^-$ not shown

Manners and co-workers [110]. Treatment of $H_3B \cdot NMeHBH_2 \cdot NMeH_2$ with 0.6 mol% **30** yielded high molecular weight $[H_2BNMeH]_n$ ($M_n = 67{,}400$, PDI = 1.4), with the parent amine–borane $H_3B \cdot NMeH_2$ observed as an intermediate (Scheme 23). Hydroboration trapping experiments with cyclohexene (Sect. 2.2) did not lead to $Cy_2B{=}NMeH$. Nonetheless, the observation of $H_3B \cdot NMeH_2$ suggests that $H_2B{=}NMeH$ is formed, either remaining on-metal or polymerising rapidly relative to the rate of hydroboration. By contrast, metal-free thermolysis of $H_3B \cdot NMeHBH_2 \cdot NMeH_2$ at 70°C in THF led to the formation of $H_3B \cdot NMeH_2$ and the cyclic trimer $[H_2BNMeH]_3$, presumed to arise from trimerisation of $H_2B{=}NMeH$. Addition of cyclohexene resulted in the formation of the trapping product $Cy_2B{=}NMeH$, implying free $H_2B{=}NMeH$ is present in the solution and that hydroboration is kinetically competitive with trimerisation.

In 2011, Weller and Manners reported that the dehydrocoupling of $H_3B \cdot NMeH_2$ with the cationic rhodium chelating phosphine system $[Rh(Ph_2P(CH_2)_xPPh_2)(\eta^6\text{-}C_6H_5F)][BAr^F{}_4]$ ($x = 3$–5) produced high molecular weight and narrow polydispersity polyaminoborane $[H_2BNMeH]_n$ (when $x = 4$, $M_n = 144{,}000$ g mol^{-1}, PDI = 1.3) (Scheme 24) [65].

These catalysts were also efficient in dehydrocoupling $H_3B \cdot NMe_2H$ to form $[H_2BNMe_2]_2$ (fastest TOF ~1,250 h^{-1} when $x = 3$) following an induction period of approximately 5 min. The bite angle correlated with binding strength in the related sigma complexes $[Rh(Ph_2P(CH_2)_xPPh_2)(\eta^2\text{-}H_3B \cdot NMe_3)][BAr^F{}_4]$ ($x = 3$–5); the smallest bite angle ($x = 3$) has the weakest sigma binding of $H_3B \cdot NMe_3$ and the fastest dehydrocoupling activity of $H_3B \cdot NMe_2H$. Tests indicated a homogeneous catalyst, and, although the reason for the induction period is yet to be deduced, it was speculated on the basis of ESI–MS experiments that this temporal profile was due to the formation of an initial inactive dimeric species, possibly in a slow equilibrium with an active monomeric species. Independent computational work

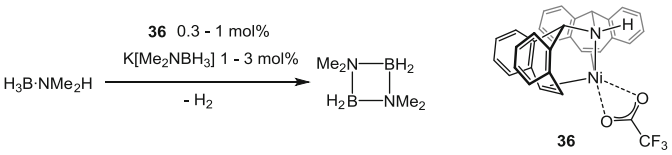

Scheme 25 Dehydrocoupling of $H_3B \cdot NMe_2H$ with **36**

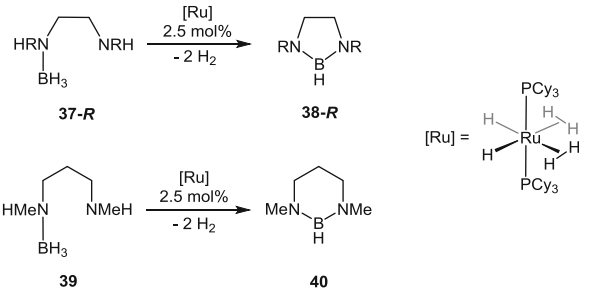

Scheme 26 Dehydrocyclisation of amine–boranes using $[Ru(PCy_3)_2(H)_2(H_2)_2]$. R=Me, ^{i}Pr

on this system has suggested that dimerisation forms an inactive hydridoboryl species, and the active catalyst is monomeric [111].

One of the fastest dehydrocoupling catalysts that has been reported is the Ni^I species $[Ni(trop_2NH)(OOCCF_3)]$ ($trop_2NH$=bistropylidenylamine) (**36**, Scheme 25) [112]. At 0.3 mol% of **36**, one molar equivalent of hydrogen is released from a solution of $H_3B \cdot NMe_2H$ in less than 1 min (TOF ~20,000 h^{-1}) to form $[H_2BNMe_2]_2$. Interestingly the amidoborane $K[NMe_2BH_3]$ is used as cocatalyst (1–3 mol%), and, although its role was not commented upon, it is tempting to speculate that the active species is a Ni-amidoborane. During dehydrocoupling, the aminoborane $H_2B{=}NMe_2$ is observed as an intermediate, although further mechanistic details were not reported.

Alcaraz and Sabo-Etienne reported the novel dehydrogenative cyclisation of the diamine–monoboranes **37-*Me***, **37-*^{i}Pr*** and **39** leading to cyclic diaminoboranes **38-*Me***, **38-*^{i}Pr*** and **40**, respectively, using the $[Ru(PCy_3)_2(H)_2(H_2)_2]$ catalyst at 2.5 mol% loading (Scheme 26) [113]. The reaction was slower in the presence of bulkier *N*-substituents (3 h for complete formation of **38-*Me*** versus 8 h for complete formation of **38-*^{i}Pr***), but lengthening the alkyl chain length of the starting amine–borane (**37-*Me*** versus **39**) did not significantly affect the rate. $[Ru(PCy_3)_2(H)_2(H_2)_2]$ remained the resting state throughout catalysis and could be reused twice.

In 2013, Weller explored the mechanism of the dehydrocoupling of $H_3B \cdot NMe_2H$ with the neutral rhodium catalyst $Rh(PCy_3)_2(H)_2Cl$ after its catalytic activity had been implicated in an earlier study with $[Rh(PCy_3)_2][BAr^F{}_4]$ (vide infra) [13, 32]. Investigations showed that $Rh(PCy_3)_2(H)_2Cl$ is a moderate catalyst for dehydrogenation of $H_3B \cdot NMe_2H$ (2 mol% [Rh], TOF = 28 h^{-1}) to form $H_2B{=}NMe_2$, which dimerises to form $[H_2BNMe_2]_2$ (Scheme 27) [32].

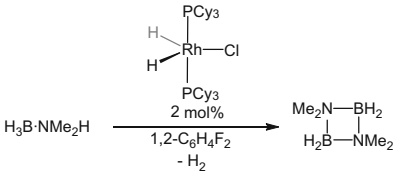

Scheme 27 Dehydrocoupling of $H_3B \cdot NMe_2H$ with $Rh(PCy_3)_2(H)_2Cl$

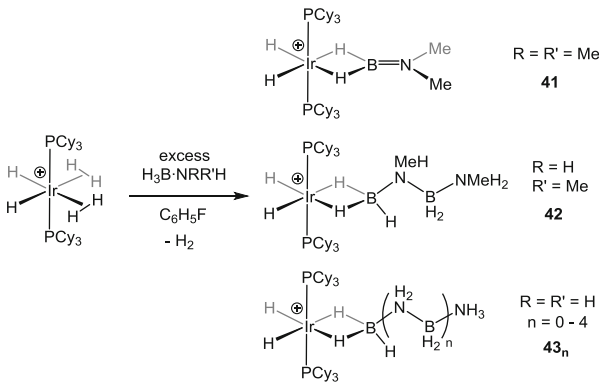

Scheme 28 Metal-bound products in the reaction of excess amine–borane with $\{Ir(PCy_3)_2(H)_2\}^+$. $[BAr^F{}_4]^-$ not shown

Mechanistic investigations indicated that N–H activation (either preceding or following B–H activation) is turnover-limiting in this system, indicated by a large primary kinetic isotope effect observed using $H_3B \cdot NMe_2D$.

The $\{Ir(PCy_3)_2(H)_2\}^+$ fragment has proved a useful, albeit slow (10–20 mol%, TOF ~0.1 h^{-1}), catalyst for the dehydrogenation and dehydrocoupling of $H_3B \cdot NMe_2H$ [19], $H_3B \cdot NMeH_2$ [33] and $H_3B \cdot NH_3$ [70], in which metal-bound products and intermediates can be observed, allowing direct comparisons between the different amine–boranes. Reaction of the bis-dihydrogen complex $[Ir(PCy_3)(H)_2(H_2)_2][BAr^F{}_4]$, a source of $\{Ir(PCy_3)_2(H)_2\}^+$, with $H_3B \cdot NMe_2H$ forms ultimately $[H_2BNMe_2]_2$, and the major metal-containing product is the bound aminoborane complex $[Ir(PCy_3)_2(H)_2(\eta^2\text{-}H_2B{=}NMe_2)][BAr^F{}_4]$ (**41**). The mechanism of dehydrogenation of $[Ir(PCy_3)_2(H)_2(\eta^2\text{-}H_3B \cdot NMe_2H)][BAr^F{}_4]$ to form **41** has been suggested by calculation to be sequential B–H activation, H_2 loss from the metal and rate-limiting N–H activation [19]. By contrast, $H_3B \cdot NMeH_2$ catalytically undergoes an on-metal oligomerisation event to yield the diborazane $H_3B \cdot NMeHBH_2 \cdot NMeH_2$, with the sigma complex $[Ir(PCy_3)_2(H)_2(\eta^2\text{-}H_3B \cdot NMeHBH_2 \cdot NMeH_2)][BAr^F{}_4]$ (**42**) observed during the dehydrocoupling. Furthermore, $H_3B \cdot NH_3$ undergoes additional oligomerisation events, yielding insoluble $[H_2BNH_2]_n$. During the dehydrocoupling, various species with bound oligomeric units, $[Ir(PCy_3)_2(H)_2(\eta^2\text{-}H_3B \cdot (NH_2BH_2)_n \cdot NH_3)][BAr^F{}_4]$ (**43**$_n$) ($n = 0$–4), were observed using ESI–MS techniques (Scheme 28).

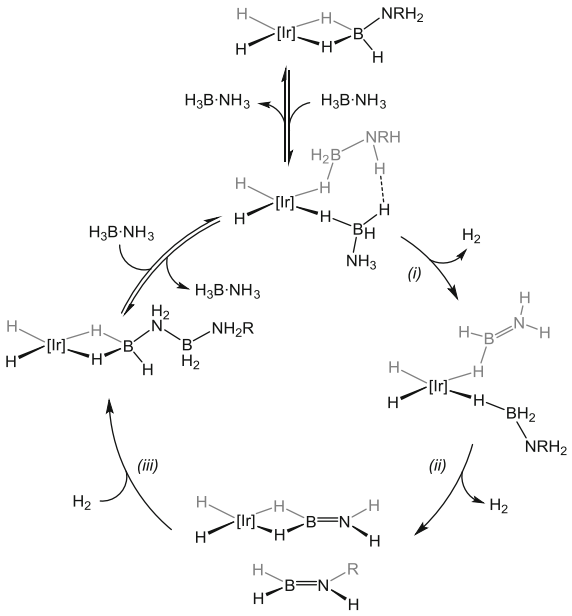

Scheme 29 Calculated pathway by MacGregor and Weller for the dehydrogenation and coupling of $H_3B \cdot NH_3$. R=H (first oligomerisation), R=BH_2NH_2 (second oligomerisation). [Ir]={Ir$(PR'_3)_2$}$^+$ (R′=Cy, experiment; Me, computation)

Calculations conducted on the model system $\{Ir(PMe_3)_2(H)_2\}^+$ for the dehydrogenation and oligomerisation of $H_3B \cdot NH_3$ propose a pathway (Scheme 29) involving (*i*) initial dehydrogenation of the amine–borane, (*ii*) dehydrogenation of a second amine–borane and (*iii*) B–N coupling. Step (*i*) was calculated to have the highest barrier, and the B–N coupling step (*iii*) had the lowest barrier. Calculations showed that subsequent oligomerisations were also viable for this system, as observed experimentally. With $H_3B \cdot NMeH_2$, the B–N coupling barrier for subsequent oligomerisations was significantly raised, consistent with the experimental observations of a single oligomerisation event. With the more sterically encumbered $H_3B \cdot NMe_2H$, the calculated B–N coupling barrier was prohibitively high, consistent with no experimental observation of linear diborazane. Although likely to be system specific, this selectivity illustrates the potential importance of sterics in the dehydrocoupling of amine–boranes. Moreover, the calculations point to outer-sphere N–H$\cdots$H–B interactions as being important to lowering barriers to dehydrogenation processes, as has been reviewed by others more generally for amine–boranes [114].

As introduced in Sect. 2.5, Manners and co-workers recently found that [CpFe$(CO)_2$I], under conditions of photoirradiation, acts as a homogeneous catalyst in the dehydrocoupling of $H_3B \cdot NMe_2H$ to form $[H_2BNMe_2]_2$ [51]. A two-stage mechanism was proposed for this system to account for the formation of $H_3B \cdot NMe_2BH_2 \cdot NMe_2H$ and the on-metal dehydrocyclisation to yield $[H_2BNMe_2]_2$ (Scheme 30), similar to that invoked for Cp_2Ti systems [69].

Experimental evidence and DFT calculations support initial coordination of $H_3B \cdot NMe_2H$ to the photogenerated $[FeCp(CO)]^+$ fragment, forming the sigma

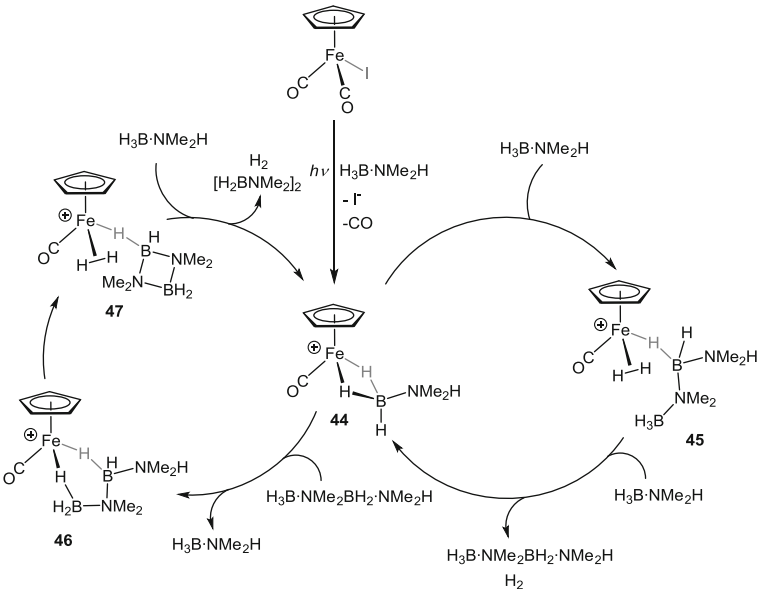

Scheme 30 Proposed two-stage mechanism for the homogeneous dehydrocoupling of $H_3B \cdot NMe_2H$ using $CpFe(CO)_2I$

complex **44**. Addition of a second equivalent of $H_3B \cdot NMe_2H$ results in a B–N bond formation process to yield the bound $H_3B \cdot NMe_2BH_2 \cdot NMe_2H$ complex **45**. Complex $H_3B \cdot NMe_2BH_2 \cdot NMe_2H$ and dihydrogen are displaced by $H_3B \cdot NMe_2H$ to reform **44**. The second cycle proposes that the just formed $H_3B \cdot NMe_2BH_2 \cdot NMe_2H$ displaces $H_3B \cdot NMe_2H$ in **44** to form the chelate sigma complex **46**, not unrelated to Rh complexes crystallographically characterised with this motif [31]. Subsequent on-metal dehydrocyclisation occurs to form $[H_2BNMe_2]_2$ sigma bound to the metal (**47**). $[H_2BNMe_2]_2$ and dihydrogen are displaced by $H_3B \cdot NMe_2H$, reforming **44**. It was speculated that the electronegative iodide ligand enables heterolytic Fe–I cleavage under photoirradiation, maintaining an Fe^{II} species. However, the dimeric complexes $[CpFe(CO)_2]_2$ and $Cp_2Fe_2(CO)_3(NCMe)$ formally are in the lower Fe^{I} oxidation state and already have Fe–Fe interactions; these factors aid nanoparticle formation and hence heterogeneous catalysis is observed (Sect. 2.5).

A recent report by Weller, Manners and Lloyd-Jones has explored in detail the catalytic dehydrocoupling of $H_3B \cdot NMe_2H$ and $H_3B \cdot NMeH_2$ with **4** (Scheme 31) [12]. Open to argon, thus allowing for release of H_2, complex **4** (0.2 mol%) dehydrocouples $H_3B \cdot NMe_2H$ rapidly, forming $[H_2BNMe_2]_2$ (TOF ~1,000 h^{-1}), following an induction period of approximately 5 min. $H_2B{=}NMe_2$ was observed as an intermediate with only negligible amounts of $H_3B \cdot NMe_2BH_2 \cdot NMe_2H$ detected, a similar reaction profile to the closely related $[Rh(Ph_2P(CH_2)_xPPh_2)(\eta^6\text{-}C_6H_5F)][BAr^F{}_4]$ system (TOF ~1,250 h^{-1} for $x = 3$). Under these conditions, the decay of $[H_3B \cdot NMe_2H]$ appeared *pseudo*-zero order at high $[H_3B \cdot NMe_2H]$

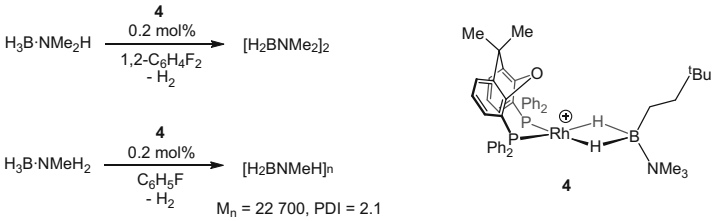

Scheme 31 Dehydrocoupling of $H_3B \cdot NMe_2H$ and $H_3B \cdot NMeH_2$ using **4**. $[BAr^F{}_4]^-$ not shown

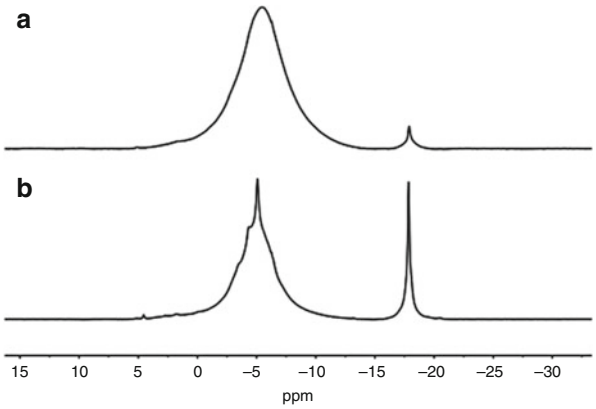

Fig. 12 (**a**) $^{11}B\{^1H\}$ NMR spectrum of $[H_2BNMeH]_n$ ($\delta \sim -5$) isolated after dehydropolymerisation of $H_3B \cdot NMeH_2$ (**4**, 0.2 mol%) under open conditions (signal at δ-17 is unreacted $H_3B \cdot NMeH_2$). (**b**) $^{11}B\{^1H\}$ NMR spectrum of material isolated after reaction under sealed conditions (**4**, 0.2 mol%). Johnson et al. [115]. Copyright 2014 American Chemical Society

(approximately 0.1 M), becoming *pseudo*-first order at lower $[H_3B \cdot NMe_2H]$. This suggested that saturation kinetics were operating, corroborated by kinetic modelling. By contrast, under closed conditions, in which a pressure of H_2 can build, the reaction profile appeared *pseudo*-first order over the entire concentration range (post induction period). With $H_3B \cdot NMeH_2$, in an open system, 0.2 mol% **4** catalysed the formation of $[H_2BNMeH]_n$ ($M_n = 22{,}700$ g mol^{-1}, PDI = 2.1) in C_6H_5F solution within 2 h, also with an induction period observed. Similar to $H_3B \cdot NMe_2H$, saturation kinetics were apparent. Molecular weight versus conversion experiments indicated a chain growth mechanism; in particular, high molecular weights were achieved at less than 20% conversion. In THF solvent, the catalysis was slower (85% completion, 19 h) but produced higher molecular weight $[H_2BNMeH]_n$ ($M_n = 52{,}200$ g mol^{-1}, PDI = 1.4). Conversely, in a sealed system, the molecular weight was significantly lower ($M_n = 2{,}800$ g mol^{-1}, PDI = 1.8) and took approximately 24 h to reach ~95% completion. $^{11}B\{^1H\}$ NMR spectroscopy of the product isolated from the closed system provided evidence for the presence of shorter-chain oligomers (Fig. 12).

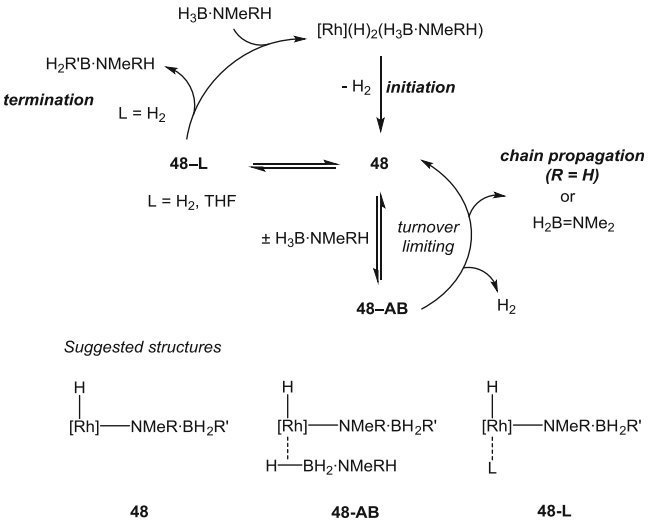

Scheme 32 Suggested cycle for the dehydropolymerisation of $H_3B \cdot NMeH_2$ (R′=H or growing polymer chain; R=H) and dehydrogenation of $H_3B \cdot NMe_2H$ (R′=H, R=Me). [Rh]={Rh(Xantphos)}$^+$

Exploring the rationale behind the induction period, heterogeneous catalysis was ruled out. Additionally, the authors noted that the induction period was approximately twice as long using $H_3B \cdot NMe_2D$ compared with $H_3B \cdot NMe_2H$, whereas no change was observed using $D_3B \cdot NMe_2H$. This implied that N–H activation was rate limiting in the formation of the active species, which is proposed to be an amido-boryl complex **48**. These, and other observations, led to a proposed catalytic cycle applicable for both the dehydropolymerisation of $H_3B \cdot NMeH_2$ and dehydrogenation of $H_3B \cdot NMe_2H$ (Scheme 32).

Stoichiometric reactions of **4** with 2 equiv. of $H_3B \cdot NMe_2H$ or $H_3B \cdot NMeH_2$ led to the immediate formation of the Rh^{III} dihydride [Rh(κ^3-$_{P,O,P}$-Xantphos)(H)$_2$(η^1-$H_3B \cdot NMeRH$)][$BAr^F{}_4$] (R=Me, H), and it was speculated that these species were the starting points in the catalytic cycle. The induction period (i.e. initiation) occurs, involving N–H activation, to yield **48**. Complex **48**, as written, would have a vacant site, allowing the reversible binding of another equivalent of amine–borane, forming **48**-**AB**, as implicated by saturation kinetics. From **48**-**AB**, dehydrogenation (with $H_3B \cdot NMe_2H$) or chain propagation (with $H_3B \cdot NMeH_2$) occurs, for the latter leading to a growing polymer from the metal centre. At high [amine–borane], the turnover-limiting step occurs after the formation of **48**-**AB**, resulting in a *pseudo*-zero-order decay of [amine–borane], but at lower [amine–borane], the formation of **48**-**AB** is dependent upon [amine–borane], giving *pseudo*-first-order kinetics. Chain termination can arise from H_2 binding to **48** and undergoing heterolytic H_2 cleavage [116], consistent with the observations of shorter polymer chains, and first-order decay of [$H_3B \cdot NMe_2H$], under an atmosphere of H_2. THF can also bind competitively with H_2 and $H_3B \cdot NMeH_2$, slowing catalysis but

attenuating chain termination, resulting in higher molecular weight $[H_2BNMeH]_n$. This tuning of molecular weight has provided valuable insight into methods of controlling polyaminoborane formation.

2.8.4 Dehydrocoupling of Amine–Boranes Involving Ligand Cooperativity

In 2008, Fagnou and co-workers reported the rapid dehydrogenation of $H_3B \cdot NH_3$ to form $[H_2BNH_2]_n$ with 0.03 mol% loadings of the catalyst [Ru($P^iPr_2CH_2CH_2NH_2)_2Cl_2$] (**49**), activated by 0.9 mol% KO^{t}Bu (TOF ~20,000 h^{-1}) [59]. Furthermore, 0.5 mol% of **49** could promote the release of 2 equiv. of H_2 from $H_3B \cdot NMeH_2$ within 10 min. An outer-sphere mechanism was proposed using DFT calculations on the model complex [Ru($PMe_2CH_2CH_2NH_2$)($PMe_2CH_2CH_2NH$)H] (**50-*Me***), the product of the activation of [Ru($PMe_2CH_2CH_2NH_2)_2Cl_2$] (**49-*Me***) with KO^{t}Bu (Scheme 33). The mechanism proposed invokes protonation of the ligand by the amine (**51-*Me***), loss of $H_2B{=}NH_2$ to form **52-*Me*** and rate-limiting formation of the dihydrogen complex **53-*Me***.

In 2009, Schneider and co-workers reported that the related bifunctional catalyst [Ru(PNP)(H)(PMe_3)] {Fig. 13, PNP=N($CH_2CH_2P^iPr_2)_2$} (**54**) was extremely active in the dehydrocoupling of $H_3B \cdot NH_3$ to release approximately 1 equiv. of dihydrogen (TOF ~12,000 h^{-1} at 0.1 mol% **54**) to form $[H_2BNH_2]_n$, with small amounts of borazine also observed [57]. $H_3B \cdot NMe_2H$ was also rapidly dehydrocoupled by **54** (2 mol%), forming $[H_2BNMe_2]_2$, until approximately 70% conversion (initial TOF ~3,600 h^{-1}); after this point, a much slower regime operates (TOF ~1.5 h^{-1}), suggesting a change in mechanism [30]. During the fast regime, the species *trans*-[Ru(PNP^H)$(H)_2$(PMe_3)] {PNP^H=HN($CH_2CH_2P^iPr_2)_2$} (**55**) was observed as the resting state and, indeed, starting catalysis with **55** showed very similar kinetics as with **54**. However, a new species evolved throughout the dehydrocoupling, [Ru(PNP^B)$(H)_2$(PMe_3)] {PNP^B=$NMe_2BH_2N(CH_2CH_2P^iPr_2)_2$}

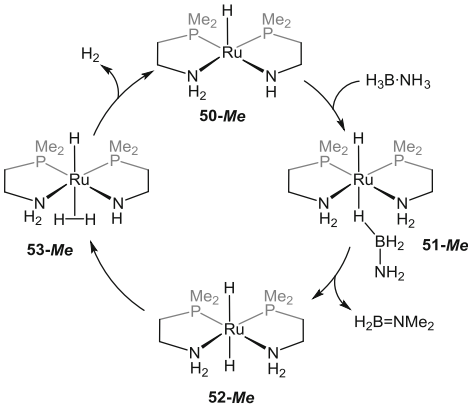

Scheme 33 Proposed mechanism for the dehydrogenation of $H_3B \cdot NH_3$ by **50-*Me***

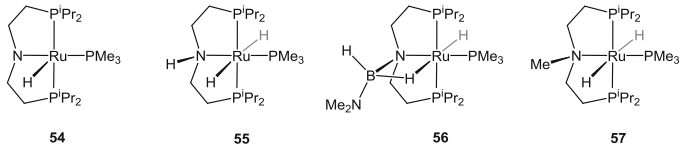

Fig. 13 Schneider's bifunctional ruthenium complexes

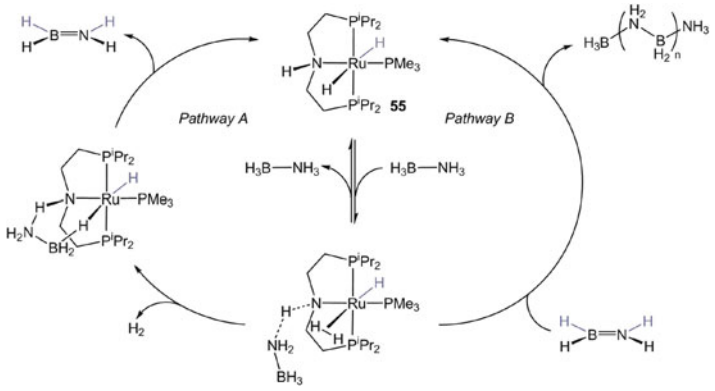

Scheme 34 Dehydrogenation and dehydrocoupling pathways proposed by Schneider and co-workers

(**56**), containing a four-membered bora-metallacycle. The use of isolated **56** as the dehydrocoupling catalyst gave essentially the same catalytic activity as for the slow regime.

A more detailed study published in 2013 focused on the catalytic dehydrocoupling of $H_3B \cdot NH_3$ with **54**, **55** and [Ru(^{Me}PNP)(H)(PMe_3)] {^{Me}PNP=MeN($CH_2CH_2P^iPr_2$)$_2$} (**57**) [21]. The methylation of the pincer nitrogen atom in **57** prevents the bifunctional reactivity that is thought to be key in rationalising the high activities of these complexes. Accordingly, catalysis using **57** exhibited a rate of H_2 evolution two orders of magnitude lower than with **54** or **55**, confirming the importance of amine cooperativity in these systems.

In contrast to the previous results, in which **54** and **55** appeared to operate within the same catalytic cycle [30], on closer examination, differences were found between the two, suggesting different mechanisms for each [21]. Both catalysts demonstrated first-order kinetics for H_2 evolution on dehydrocoupling $H_3B \cdot NH_3$. On using the *N*-deuterated analogue $H_3B \cdot ND_3$, first-order kinetics were retained with **55**. However, the H_2 evolution became zero order with **54**, implying a change in the turnover-limiting step upon deuteration for this system. Additionally, some cross-linking of $[H_2BNH_2]_n$ was observed with **55**, which was not detected in $[H_2BNH_2]_n$ produced with **54**.

For catalysis with **55**, a combination of DFT (using a PMe_2-truncated model) and experimental methods led to a proposed mechanism for the formation of $[H_2BNH_2]_n$ from $H_3B \cdot NH_3$, depicted in Scheme 34.

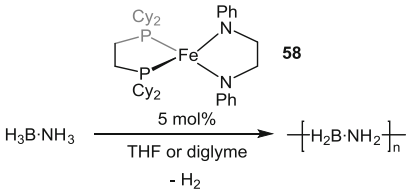

Scheme 35 Dehydrocoupling of $H_3B \cdot NH_3$ by **58**

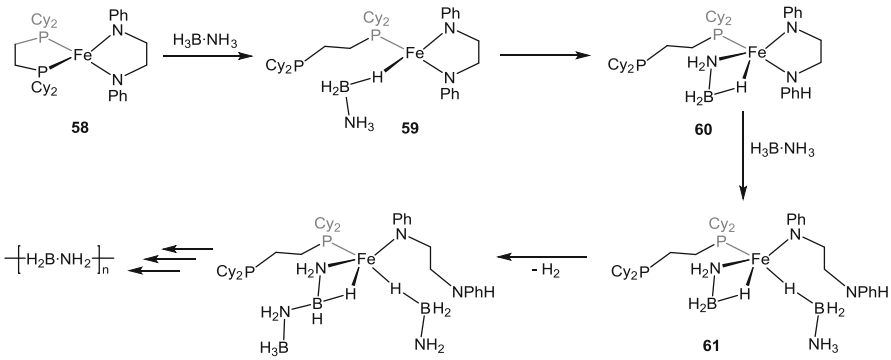

Scheme 36 A proposed mechanism for the dehydropolymerisation of $H_3B \cdot NH_3$ by **58**

The mechanism involves dehydrogenation of $H_3B \cdot NH_3$, via initial N–H activation, to form $H_2B{=}NH_2$ (Pathway A), which undergoes oligomerisation by catalytic insertion of $H_2B{=}NH_2$ into the N–H bond of the substrate (Pathway B). Experiments with $H_3B \cdot NMe_3$ and $Et_3B \cdot NH_3$ in the presence of 1 mol% **55** showed that "head-to-tail" coupling to yield $Et_3B \cdot NH_2BH_2 \cdot NMe_3$ did not occur, indicating that proton and hydride transfer from the same substrate molecule to the catalyst is required in this system, as suggested in the proposed mechanism.

Further mechanistic insight into dehydropolymerisation of amine–boranes was also obtained by Gordon and Baker et al. in the dehydrocoupling of $H_3B \cdot NH_3$ to selectively form $[H_2BNH_2]_n$ using $[Fe(PCy_2CH_2CH_2PCy_2)(NPhCH_2CH_2NPh)]$ (**58**) at 5 mol% loading (TOF ~80 h^{-1}) (Scheme 35) [68]. The catalyst could not be recycled; during catalysis, a black precipitate (presumed to be iron metal) was observed, indicating catalyst decomposition during dehydrocoupling. In situ NMR spectroscopy suggested de-coordination of one of the chelating phosphine arms during catalysis, possibly responsible for the observed induction period (ca. 2 min). Two mechanisms were proposed to account for experimental observations, one of which is shown in Scheme 36.

Initial dissociation of a phosphine arm enables coordination of $H_3B \cdot NH_3$ to form **59**. Protonation of one arm of the amido ligand by the amine–borane (affording a bound amidoborane, **60**) follows, and the resulting amino arm of the ligand can dissociate, allowing ligation of a second equivalent of $H_3B \cdot NH_3$ (**61**). From this, successive dehydrogenation and insertion steps yield $[H_2BNH_2]_n$. Throughout the proposed mechanism, no free $H_2B{=}NH_2$ is implicated, and

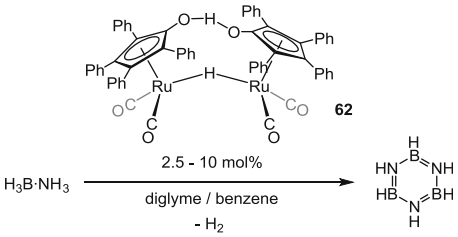

Scheme 37 Dehydrocoupling of $H_3B \cdot NH_3$ by **62**

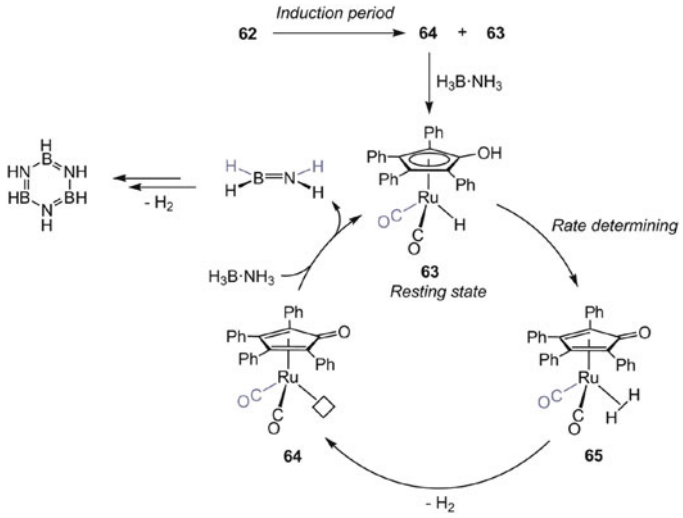

Scheme 38 Suggested catalytic cycle for the catalyst initiation and fast dehydrocoupling of $H_3B \cdot NH_3$

experimentally $H_2B{=}NH_2$ was neither detected directly nor with cyclohexene trapping. This is consistent with previous work by some of the authors [25] and others [17], suggesting that $H_2B{=}NH_2$ must remain bound to the metal to oligomerise (Sect. 2.2), although other work has suggested that cyclohexene trapping does not necessarily rule out the presence of free $H_2B{=}NH_2$ if the hydroboration is not kinetically competitive with oligomerisation [21, 28].

Williams also reported ligand cooperativity in the dehydrocoupling of $H_3B \cdot NH_3$ to yield borazine using Shvo's ruthenium catalyst, **62** (Scheme 37). The catalyst showed reasonable activity at 5 mol% **62** and 2 mol% EtOH (TOF ~18 h^{-1} for release of 2 equiv. H_2 at 70°C) [58]. H_2 release measurements (total 2 equiv.) produced a kinetic profile with three regimes evident: (*i*) initiation period, (*ii*) fast catalysis showing a zero-order decay of $[H_3B \cdot NH_3]$ and (*iii*) slow catalysis showing a first-order decay of $[H_3B \cdot NH_3]$. The induction period was attributed to the dissociation of **62** into **63** and **64** (Scheme 38). Fast dehydrogenation follows, in which H–H bond formation is the rate-determining step, similar to Fagnou's

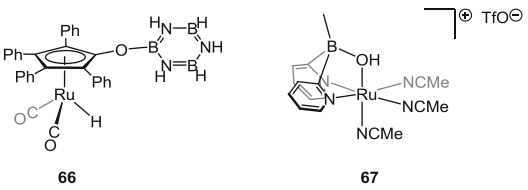

Fig. 14 Complexes **66** and **67**

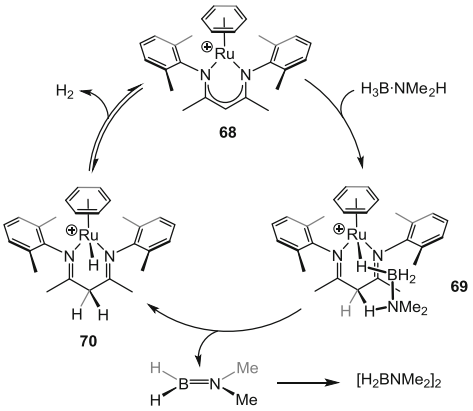

Scheme 39 Proposed mechanism for the initial dehydrogenation of $H_3B \cdot NMe_2H$ using **68**. $[OTf]^-$ anions not shown

mechanism [59], and **63** is the resting state observed during catalysis [58]. At high borazine concentrations, the third regime dominates. This is attributed to the hydroboration of **64** by borazine, to form **66** (Fig. 14). $H_3B \cdot NH_3$ is required to convert **66** back into **63**, which is the rate-limiting step in this slow regime, and, thus, the reaction becomes first order in $[H_3B \cdot NH_3]$ [117].

To avoid deactivation by borazine, the same group developed a Ruthenium catalyst with an oxygen atom already borylated, **67** (Fig. 12). Complex **67** catalysed the dehydropolymerisation of $H_3B \cdot NH_3$ to form a mixture of borazine and polyborazylene (2 mol%, 70°C, TOF ~25 h^{-1} for the release of 2 equiv. of H_2 in a tetraglyme slurry). Significantly for potential practical applications, the catalysis could be conducted under air and the catalyst could be reused; four successive runs in a single reactor produced similar rates and quantities of H_2 loss in each run (2.1–2.3 equiv.). To date, mechanistic details have not been unravelled, although a mechanism involving dual-site cooperativity is likely [118].

Phillips and co-workers recently reported the fast dehydrocoupling of $H_3B \cdot NH_3$ and $H_3B \cdot NMe_2H$ (TOF ~400 h^{-1} for $H_3B \cdot NMe_2H$ at 42°C in THF) using 0.5 mol% of the bifunctional Ru^{II} β-diketiminate complex, **68** (Scheme 39) [119]. Mechanistic studies focused on $H_3B \cdot NMe_2H$ as, under these reaction conditions, $H_3B \cdot NH_3$ can thermally release H_2 in the absence of a catalyst. The proposed mechanism for initial dehydrogenation is that of hydride coordination from BH_3 by the Ru^{II} centre, forming **69**. The acidic NMe_2H proton can then protonate the β-carbon position of the β-diketiminate ligand, resulting in **70**. Complex **68** had been previously shown to reversibly heterolytically cleave H_2 to yield **70** [120].

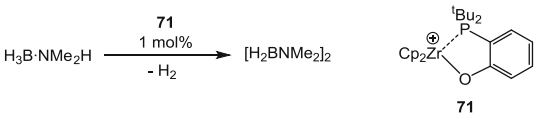

Scheme 40 Dehydrocoupling of $H_3B \cdot NMe_2H$ with **71**. $[B(C_6F_5)_4]^-$ anion not shown

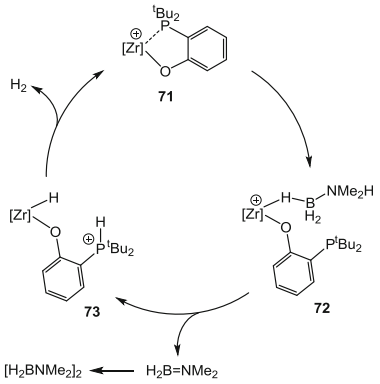

Scheme 41 Suggested mechanism for dehydrocoupling of $H_3B \cdot NMe_2H$ by **71**. [Zr]=Cp_2Zr. $[B(C_6F_5)_4]^-$ anions not shown

An induction period was observed in the dehydrocoupling, thought to be the slow initial formation of **70**, which is the active catalyst for subsequent dehydrogenations. An experiment performed using a THF solution that had been saturated with H_2 resulted in faster dehydrogenation and a reduced induction period compared with the N_2-flushed THF used as the normal reaction solvent, demonstrating the rate is dependent on the rate of formation of **70**.

Wass and co-workers reported a fast dehydrocoupling catalyst based upon a "frustrated" Lewis pair, but where the Lewis acid (typically a fluorinated aryl borane) was replaced with an electrophilic Zr^{IV} centre. The species $[Cp_2ZrOC_6H_4P^tBu_2][B(C_6F_5)_4]$ (**71**) dehydrocoupled $H_3B \cdot NMe_2H$ rapidly (1 mol% **71**, TOF ~600 h^{-1}), being the fastest reported group IV catalyst to our knowledge (Scheme 40) [121]. Wass' proposed mechanism (Scheme 41) is different from those of other group IV metallocene catalysts (Sect. 2.8.1). Following sigma coordination of $H_3B \cdot NMe_2H$ to the Zr^{IV} centre to form **72**, ligand-assisted dehydrogenation yields $H_2B{=}NMe_2$ and **73**. The loss of hydrogen from **73** is facile, regenerating **71**. The reaction using $[Cp_2ZrO^tBu][B(C_6F_5)_4]$ did not dehydrogenate $H_3B \cdot NMe_2H$, illustrating the importance of the phosphine in this cooperative system.

Ligand cooperativity in Ni(NHC) systems has been discussed in Sect. 2.8.3.

2.8.5 The Role of Solvent in Dehydrocoupling Using Late Transition Metals

Many dehydrocoupling reactions of amine–boranes are conducted in THF due to good solubility of $H_3B \cdot NMeH_2$ and $H_3B \cdot NH_3$ in this solvent [23]. A recent report by Conejero and López-Serrano, using [Pt(I^{t}Bu′)(I^{t}Bu)][BAr$^F{}_4$], **74** (Scheme 42) (I^{t}Bu = 1,3-di-*tert*-butylimidazol-2-ylidene, I^{t}Bu′=cyclometalated I^{t}Bu), showed that THF is intimately involved in the dehydrocoupling mechanism of $H_3B \cdot NMe_2H$ to form $[H_2BNMe_2]_2$ [122].

The suggested mechanism (Scheme 43), supported by DFT calculations (in which $H_3B \cdot NH_3$ was used as the model amine–borane), involves the initial reaction of **74** with $H_3B \cdot NMe_2H$ to form a sigma complex **75**. In the presence of NMe_2H (thought to arise from B–N cleavage of $H_3B \cdot NMe_2H$ [27, 32, 95]), complex **75** rearranges to form the neutral **76** with expulsion of the boronium cation $[(NMe_2H)_2BH_2]^+$. Calculations indicated that dehydrogenation of bound $H_3B \cdot NH_3$ to yield an aminoborane has a prohibitively high barrier of 42.5 kcal mol^{-1}. However, addition of a Lewis base such as THF or NMe_2H

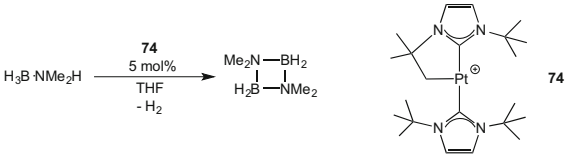

Scheme 42 Dehydrocoupling of $H_3B \cdot NMe_2H$ with **74**

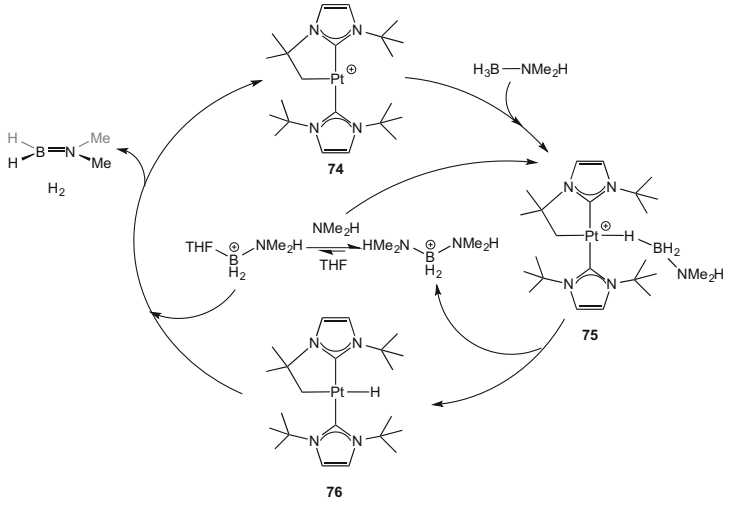

Scheme 43 Proposed catalytic cycle. $[BAr^F{}_4]^-$ not shown

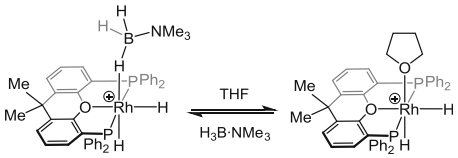

Scheme 44 Equilibrium between $[Rh(\kappa^3\text{-}_{P,O,P}\text{-Xantphos})(H)_2(\eta^1\text{-}H_3B \cdot NMe_3)][BAr^F{}_4]$ and $[Rh(\kappa^3\text{-}_{P,O,P}\text{-Xantphos})(H)_2(THF)][BAr^F{}_4]$. $[BAr^F{}_4]^-$ anions not shown

(Me_2O and NH_3 used as model analogues in the calculations) lowers the barrier to B–H activation. In THF solution, $[(NMe_2H)_2BH_2]^+$ and $[(NMe_2H)BH_2(THF)]^+$ are in equilibrium. The THF adduct reacts with **76** to reform **74** and $H_2B{=}NMe_2$ with H_2 loss. Stoichiometric experiments showed that $[(NMe_2H)_2BH_2]^+$ reacted slowly with **76**, leading to unidentified products, whereas $[(NMe_2H)BH_2(THF)]^+$ reacted rapidly, producing $H_2B{=}NMe_2$ and supporting the proposed cycle.

Many dehydrocoupling reactions involving cationic complexes have been studied in essentially non-coordinating solvents such as C_6H_5F or 1,2-$C_6H_4F_2$, enabling the observation of weakly sigma-bound intermediates [13, 66, 70]. Weller and co-workers have shown that sigma-bound amine–boranes can be displaced by excess THF (Scheme 44) [12].

As mentioned in Sect. 2.8.3, however, the formation of $[H_2BNMeH]_n$ using the cationic rhodium species **4** produced higher molecular weight material in THF than C_6H_5F, although the polymerisation took longer to reach completion. It was suggested that THF can bind to the Rh centre competitively with both amine–borane (slowing catalysis) and H_2 (hindering chain transfer). Solvent effects have also been noted by Manners and Weller in the off-metal dimerisation of $H_2B{=}NMe_2$, with the rate of dimerisation being accelerated in MeCN [19, 20].

2.9 *Generic Mechanisms for Dehydrocoupling of $H_3B \cdot NMe_2H$ Using Transition Metals*

In 2012, Weller and Lloyd-Jones conducted a thorough mechanistic study on the dehydrocoupling of $H_3B \cdot NMe_2H$ to form $[H_2BNMe_2]_2$ using the $\{Rh(PCy_3)_2\}^+$ fragment (Scheme 45) [13]. During catalysis (5 mol% [Rh], TOF 10 h^{-1}), both the aminoborane $H_2B{=}NMe_2$ and the linear diborazane $H_3B \cdot NMe_2BH_2 \cdot NMe_2H$ were observed by ^{11}B NMR spectroscopy. Several important observations were noted for this system. Addition of 2 equiv. of $H_3B \cdot NMe_2H$ to $\{Rh(PCy_3)_2\}^+$ led first to the Rh^I sigma complex $[Rh(PCy_3)_2(\eta^2\text{-}H_3B \cdot NMe_2H)][BAr^F{}_4]$, which then rapidly formed the Rh^{III} species $[Rh(PCy_3)_2(H)_2(\eta^2\text{-}H_3B \cdot NMe_2H)][BAr^F{}_4]$ with concomitant loss of $H_2B{=}NMe_2$ (Scheme 46). This species does not lose H_2 easily, implying the active catalyst is a Rh^{III} complex, operating at a constant oxidation state, after the initial dehydrogenation.

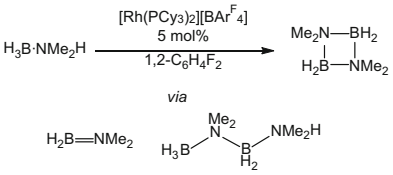

Scheme 45 Catalytic dehydrocoupling of $H_3B \cdot NMe_2H$ by $[Rh(PCy_3)_2L_n][BAr^F{}_4]$

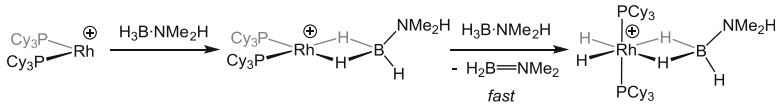

Scheme 46 Stoichiometric reactivity of $\{Rh(PCy_3)_2L_n\}^+$ with $H_3B \cdot NMe_2H$. $[BAr^F{}_4]^-$ not shown

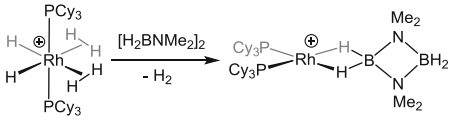

Scheme 47 Reduction from Rh^{III} to Rh^I by addition of $[H_2BNMe_2]_2$. $[BAr^F{}_4]^-$ not shown

However, addition of the product $[H_2BNMe_2]_2$ to the Rh^{III} species $[Rh(PCy_3)_2(H)_2(\eta^2\text{-}H_2)_2][BAr^F{}_4]$ resulted in the immediate formation of the Rh^I complex $[Rh(PCy_3)_2(\eta^2\text{-}(H_2BNMe_2)_2)][BAr^F{}_4]$, indicating that $[H_2BNMe_2]_2$ can drive the reductive elimination of H_2 to reform a Rh^I species (Scheme 47). Consistent with this, under catalytic conditions, $[H_2BNMe_2]_2$ was found to have an autocatalytic role in the dehydrocoupling catalysis by acting as a modifier to produce kinetically significant amounts of a Rh^I catalytically active species alongside the Rh^{III} species. Thus, the dehydrocoupling was shown to exist in both a constant oxidation state Rh^{III}/Rh^{III} cycle (slower) and a Rh^I/Rh^{III} cycle (faster).

Kinetic simulations indicated the presence of an additional catalyst present in constant (low) concentrations that promoted the first-order dehydrogenation of $H_3B \cdot NMe_2H$ to give $H_2B{=}NMe_2$. Due to a constant concentration of chloride ions in solution (arising from the catalyst preparation method), it was determined that the active catalyst was the neutral species $Rh(PCy_3)_2(H)_2Cl$, whose catalytic activity was separately examined (see Sect. 2.8.3) [32].

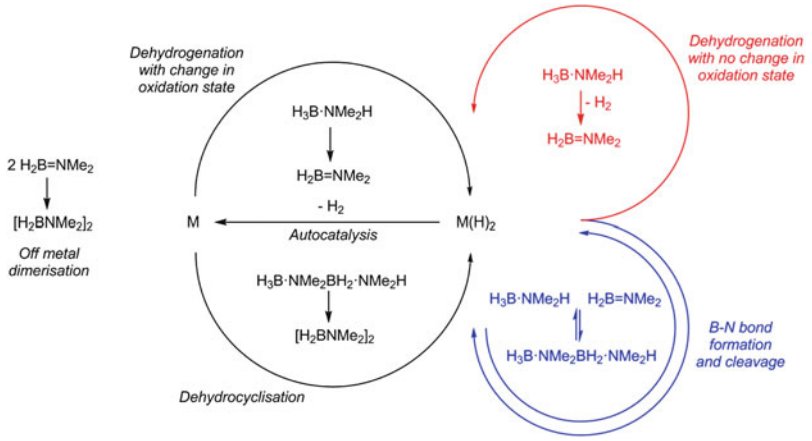

Scheme 48 General mechanistic cycle for the dehydrocoupling of $H_3B \cdot NMe_2H$. M=metal catalyst

The observations led to a generalised mechanistic scenario (Scheme 48) simplified into several parts: (1) dehydrogenation of $H_3B \cdot NMe_2H$ with a change in the oxidation state of the catalyst, (2) dehydrogenation of $H_3B \cdot NMe_2H$ with no change in the oxidation state of the catalyst, (3) the formation and cleavage of $H_3B \cdot NMe_2BH_2 \cdot NMe_2H$, (4) dehydrocyclisation of $H_3B \cdot NMe_2BH_2 \cdot NMe_2H$ and (5) the off-metal dimerisation of $H_2B{=}NMe_2$ to give $[H_2BNMe_2]_2$. This cycle, or parts thereof, is generally applicable to various homogeneous transition-metal-catalysed systems reported. For example, dehydrogenation with a change in oxidation state has been implicated for systems based upon Ti [69, 92], Re [86], Cr [98] and Rh [65]. Systems remaining in a constant oxidation state, however, include cationic Rh [66] and Ir [19, 70], as well as bifunctional Ru catalysts [21, 59]. The formation of $H_3B \cdot NMe_2BH_2 \cdot NMe_2H$ from $H_3B \cdot NMe_2H$ and $H_2B{=}NMe_2$ has been observed with Ti [69], Rh [66], Ir [19] and Ru [30] systems, which also catalyse the dehydrocyclisation of $H_3B \cdot NMe_2BH_2 \cdot NMe_2H$ to form $[H_2BNMe_2]_2$.

Manners and co-workers have suggested closely related, but alternative, schemes for the processes occurring in the dehydrogenation and dehydrocoupling of ammonia–borane and primary and secondary amine–boranes, as shown in Scheme 49 [5, 123].

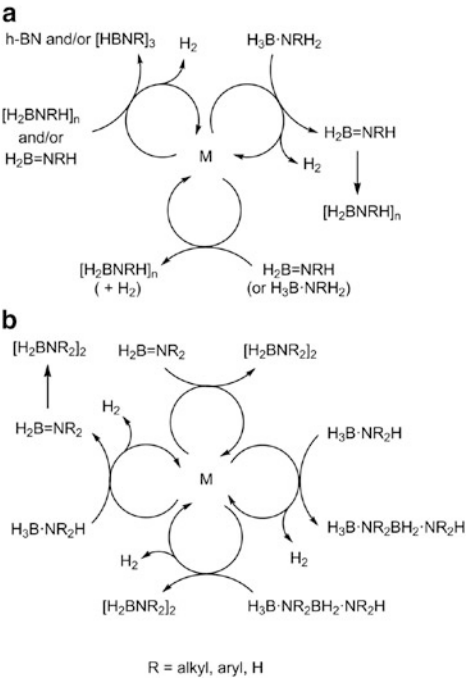

Scheme 49 (**a**) Generalised series of catalytic cycles summarising common transformations for primary amine–boranes and ammonia–borane. (**b**) A generalised series of catalytic cycles summarising common transformations for secondary amine–boranes. *M* metal catalyst

2.10 Main-Group Element-Catalysed Dehydrocoupling of Amine–Boranes

2.10.1 Main-Group Amidoboranes: Stoichiometric Studies

The use of amine–boranes as a means of chemical hydrogen storage prompted great interest in the dehydrogenation of these species. However, in the case of the parent ammonia–borane, which has the highest weight percentage of hydrogen, some of the dehydrocoupling products are insoluble and poorly characterised. A promising avenue of study was that of group 1 and 2 amidoboranes [124, 125]. Characterised as having the general formula $[M(NH_2 \cdot BH_3)_n]$ (M=group 1 or 2 metal; $n = 1$ for group 1, $n = 2$ for group 2), these simple amidoboranes were found to have a lower release temperature for 2 equiv. of dihydrogen than parent ammonia–borane (90°C for lithium and sodium amidoborane and 120–170°C for calcium bis(amidoborane) compared to 110–200°C for ammonia–borane). The dehydrogenation of the amidoboranes also proceeds more cleanly with little formation of borazine and other by-products observed for ammonia–borane. The structure of the calcium analogue $[Ca(NH_2 \cdot BH_3)_2(THF)_2]$ was determined by X-ray crystallography, and the molecules were found to form long chains with intermolecular sigma interactions between the B–H bonds and the calcium centres of adjacent molecules. The

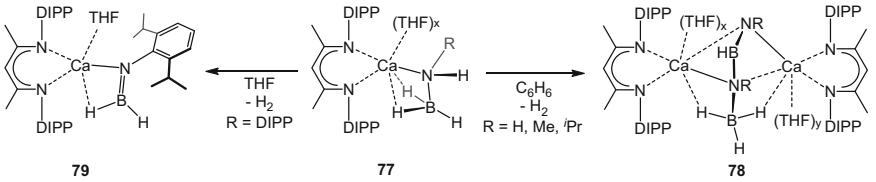

Scheme 50 Dehydrogenation of [(DIPP-nacnac)Ca(NRH · BH_3)$(THF)_2$] (**77**). DIPP=2,6-di(isopropyl)phenyl

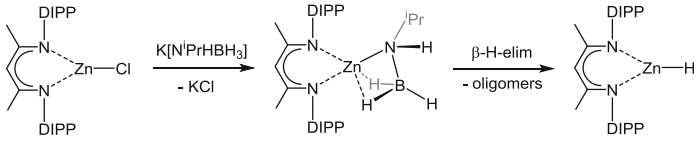

Scheme 51 Formation of [(DIPP-nacnac)ZnH]. DIPP=2,6-di(isopropyl)phenyl

THF solvent could be removed under vacuum at room temperature to form [Ca$(NH_2 \cdot BH_3)_2$] [125].

The first example of a monomeric calcium amidoborane was reported by Harder et al. who used the bulky β-diketiminate ligand {(2,6-$^{i}Pr_2C_6H_3$)NC(Me)C(H)C(Me)N(2,6-$^{i}Pr_2C_6H_3$)=DIPP-nacnac} to stabilise the calcium centre. Reaction of the dimeric calcium hydride starting material [(DIPP-nacnac)CaH(THF)]$_2$, with ammonia–borane in a mixture of toluene and THF, led to the elimination of dihydrogen and formation of the amidoborane complex [(DIPP-nacnac)Ca$(NH_2 \cdot BH_3)(THF)_2$] (**77**), Scheme 50. In THF solution, this complex was stable, even at elevated temperatures, but in benzene solution, hydrogen loss was observed and dimerisation occurred. The product was the dinuclear species [{(DIPP-nacnac)Ca(THF)}$_2$(HNBHNH · BH_3)] (**78**) with a dianionic $(HNBHNH \cdot BH_3)^{2-}$ fragment bridging the calcium centres [126]. If a bulky substituent was attached to the nitrogen centre of the amine–borane (e.g. DIPP), a similar monomeric amidoborane complex was formed initially. This complex lost dihydrogen, but did not dimerise to form a dinuclear species and remained mononuclear with a borylamide ligand at the calcium centre (**79**), being a deprotonated analogue of an aminoborane (Scheme 50) [127].

This ligand system was also used in an attempt to form a zinc amidoborane complex. The reaction of [(DIPP-nacnac)ZnCl] with the amidoborane salt K[$H_3B \cdot N^{i}PrH$] did not give the amidoborane complex as expected, but a hydride species was formed, [(DIPP-nacnac)ZnH], along with oligomeric aminoborane species. The authors postulated that an amidoborane complex did form but underwent rapid β-hydride elimination of a B–H bond to form the zinc hydride and free, reactive aminoborane which quickly formed oligomers (Scheme 51) [128]. Although this reaction was not catalytic, it did suggest that main-group metals could be used to dehydrogenate amine–boranes.

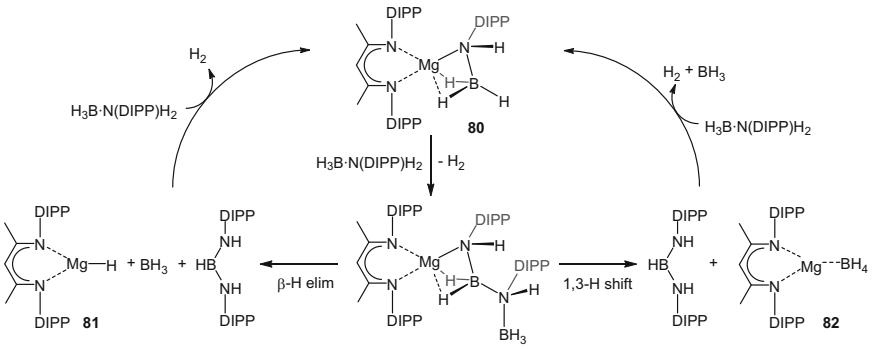

Scheme 52 Suggested mechanism for the dehydrocoupling of $H_3B \cdot N(DIPP)H_2$ to form bis (amine)borane and BH_3. DIPP=2,6-di(isopropyl)phenyl

2.10.2 Group 2 Metal-Catalysed Dehydrocoupling of Amine–Boranes

The first catalytic use of a main-group metal for the dehydrogenation of an amine–borane also came from the group of Harder who used the same bulky β-diketiminate ligand DIPP-nacnac on a magnesium centre to dehydrocouple $H_3B \cdot N(DIPP)H_2$ to form a diaminoborane $HB\{N(DIPP)H\}_2$ and BH_3 (detected as B_2H_6). The authors were able to improve the atom efficiency of the system by using a 2:1 ratio of $N(DIPP)H_2$ and $H_3B \cdot SMe_2$ as the substrates and commercially available Mg^nBu_2 (2.5 mol%) as the precatalyst. Heating this mixture to 60°C for 14 h led to complete conversion to the diaminoborane product [129].

The first stage of the reaction involves the formation of the amidoborane complex **80**, Scheme 52. The authors then propose that B–N coupling occurs at the metal centre, followed by either a β-hydride elimination to form a magnesium hydride species **81** or a 1,3-hydride shift from one boron centre to the other to form a magnesium borohydride species **82**. Evidence for this latter mechanism was obtained by isolation of the $[(DIPP\text{-}nacnac)Mg(BH_4)]_2$ species as a product of the reaction, although the first mechanism could not be ruled out as a reactive Mg–H bond could react with the BH_3 released to form a borohydride species. In a follow-up report, the authors suggested that the β-hydride elimination mechanism was the most likely to occur with the formation of the metal hydride and aminoborane. The reactivity of these intermediates then depends on the metal and the nitrogen substituents of the aminoborane [130].

A more general route to a variety of diaminoboranes, including unsymmetrical ones, was reported by Hill and co-workers. Using the group 2 metal catalysts $[M\{N(SiMe_3)_2\}_2]$ (M = Mg, Ca), a mixture of primary and secondary amines and amine–boranes in a 1:1 ratio could be dehydrocoupled to form the $[RR'NBHNR''R''']$ (R, R′, R″, R‴=H, alkyl or aryl) species with little or no formation of the symmetrical products. The mechanism of formation of these species is proposed to proceed via the formation of an amidoborane complex which undergoes β-hydride elimination to give an aminoborane and a metal hydride. The free amine then reacts with the

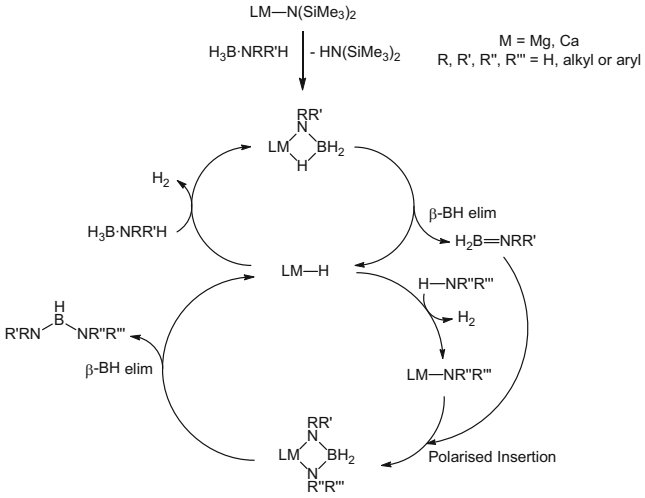

Scheme 53 Suggested mechanism for the formation of unsymmetrical bis(amine)borane from $H_3B \cdot NRR'H$ and $HNR''R'''$

metal hydride releasing H_2 and the aminoborane inserts into the M–NRR′ bond. A further β-hydride elimination regenerates the metal hydride and releases the diaminoborane product (Scheme 53) [131].

The first example of a main-group catalyst which formed a product with an equal B:N ratio was also from the group of Hill [132]. Stoichiometric reactions between either Mg^nBu_2 or $[Mg\{CH(SiMe_3)_2\}_2(THF)_2]$ and 4 equiv. of $H_3B \cdot NMe_2H$ produced H_2 and $[Mg(NMe_2BH_2NMe_2BH_3)_2(THF)]$ in which the amine–borane units have formed anionic linear diborazane coordinated to the Mg centre through an amide bond and an η^2-agostic interaction from the terminal BH_3. Heating this species to 60°C led to the formation of the cyclic $[H_2BNMe_2]_2$ dimer; however, the corresponding metal species was not able to be identified. In order to attempt to create a soluble, stable metal species, the same bulky β-diketiminate ligand used by Harder et al. [129] was employed to synthesise [(DIPP-nacnac)Mg^nBu]. Reaction of this complex with 2 equiv. of $H_3B \cdot NMe_2H$ again produced hydrogen, and the product with bound linear diborazane was isolated [(DIPP-nacnac)Mg$(NMe_2BH_2NMe_2BH_3)$]. Heating this species to 60°C resulted in a slower reaction, but the cyclic $[H_2BNMe_2]_2$ dimer was again observed and the metal–ligand species formed could be identified as [(DIPP-nacnac)$MgH(THF)_2$]. The formation of the metal hydride means reaction with a further 2 equiv. of amine–borane could again form the bound linear diborazane species, and the reaction could turn over in a catalytic sense. This hypothesis was tested by heating 5 mol% of $[Mg\{CH(SiMe_3)_2\}_2(THF)_2]$ with $H_3B \cdot NMe_2H$. Although the reaction was slow, taking 72 h for 80% conversion, $[H_2BNMe_2]_2$ was produced along with a small amount of the diaminoborane $HB(NMe_2)_2$. The proposed reaction mechanism is detailed in Scheme 54.

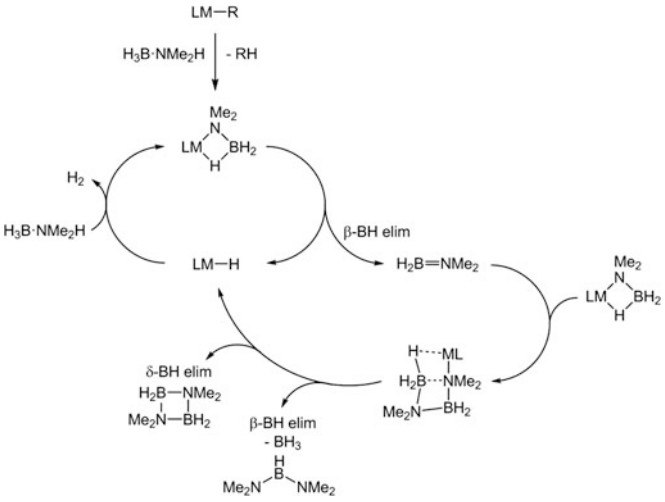

Scheme 54 Proposed mechanism of group 2-catalysed dehydrocoupling of $H_3B \cdot NMe_2H$

Hill and co-workers also employed a calcium β-diketiminate ligand system to dehydrocouple the primary amine–borane $H_3B \cdot N^tBuH_2$. 5 mol% of [(DIPP-nacnac)Ca{N(SiMe$_3$)$_2$}(THF)] was heated to 60°C in the presence of the substrate to form a mixture of boron-containing compounds. After 24 h, 68% of the $H_3B \cdot N^tBuH_2$ remained unreacted, and the products were found to be $[H_2BN^tBuH]_2$ (5%), $H_2B{=}N^tBuH$ (1%), $HB(N^tBuH)_2$ (13%), $H_3B \cdot N^tBuHBH_2$ (7%) and $[Ca(BH_4)_2]$ (6%). Heating of this reaction mixture for a further 5 days led to the formation of the borazine product $[HBN^tBu]_3$ (20%) and an increased amount of $[H_2BN^tBuH]_2$ (45%) although 14% of the starting substrate remained unreacted [133].

Sicilia and co-workers performed a computational DFT analysis on the group II metal-β-diketiminate-catalysed dehydrocoupling of secondary amine–boranes [134]. Using magnesium as the metal, they found that the calculated mechanism was broadly the same as that proposed by Hill et al. [132] (Scheme 54) in which the amidoborane undergoes β-hydride elimination to form the metal hydride and free aminoborane. The aminoborane inserts into the M–N bond of a metal-bound amidoborane to form the bound diborazane. The rate-determining step of the reaction was found computationally to be the δ-hydride elimination to form $[H_2BNMe_2]_2$. In contrast, when a DFT analysis was carried out on the analogous calcium system, the β-hydride elimination from the amidoborane species was not found to occur. In order for dehydrogenation to take place, a further equivalent of amine–borane must also coordinate to the metal centre, and the interaction of the N–H of the bound amine–borane with the B–H of the amidoborane releases H_2 and aminoborane, regenerating the amidoborane. This difference in mechanism was ascribed to the larger ionic radius of the calcium ion and the calculated relative instability of the calcium hydride species compared to the amidoborane complex.

2.10.3 Group 3 Metal-Catalysed Dehydrocoupling of Amine–Boranes

Hypothesising that an increase in charge density at the metal centre would increase the dehydrocoupling activity, Hill and co-workers used group 3 metals as catalysts for the dehydrocoupling of amine–boranes. Reaction of 3 mol% of $[Y\{N(SiMe_3)_2\}_3]$ with $H_3B \cdot NMe_2H$ at 60°C led to the complete consumption of the substrate and formation of $[H_2BNMe_2]_2$ dimer (90%) and $HB(NMe_2)_2$ (10%) in 12 h. The first stage of the reaction was observed to be the protonation of the amide ligands with the formation of amidoborane ligands as seen with the group 2 metals. Use of the more reactive scandium starting material $[Sc\{N(SiHMe_2)_2\}_3(THF)_2]$ (3 mol%) provided a much faster reaction with complete consumption of the amine–borane and near quantitative conversion to $[H_2BNMe_2]_2$ in 1 h at 60°C. In an attempt to elucidate the active species, when 4 equiv. of $H_3B \cdot NMe_2H$ was reacted with $[Sc\{N(SiHMe_2)_2\}_3(THF)_2]$, the dehydrocoupling product $[Sc\{N(SiHMe_2)_2\}(NMe_2BH_2NMe_2BH_3)_2]$ (**83**) was isolated (Scheme 55). The linear diborazane species coordinates in a similar fashion to the group 2 metal complexes with a metal–amido bond from the deprotonated nitrogen centre and a η^2-B-agostic interaction from the terminal BH_3 [135].

The increased activity of the rare-earth metals in oxidation state (III) was further exploited by Chen et al. who used an yttrium complex with two unusual 1-methyl boratabenzene ligands to catalyse the dehydrocoupling of a secondary amine–borane [136]. $[(MeBC_5H_5)_2Y\{CH(SiMe_3)_2\}]$ (0.5 mol%) was used to dehydrocouple $H_3B \cdot NMe_2H$ at 50°C with the reaction reaching completion in ca. 12 min (Scheme 56). The products of the reaction observed after this were $[H_2BNMe_2]_2$ (98%) and a small portion of as yet undimerised aminoborane $H_2B{=}NMe_2$ (2%). A turnover frequency of 1,015 h^{-1} is by far the largest observed for the main-group catalysts and comparable with some of the best transition metal catalysts. The reaction using the lutetium analogue of this system reached completion in 29 min with a similar product distribution.

The extremely high activity of this system was ascribed to either the electron-withdrawing nature of the ligand or a possible interaction between the electron-

Scheme 55 Formation of $[Sc\{N(SiHMe_2)_2\}(NMe_2BH_2NMe_2BH_3)_2]$ (**83**)

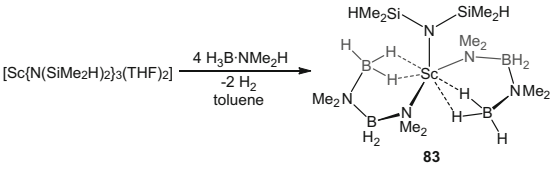

Scheme 56 Catalytic dehydrocoupling of $H_3B \cdot NMe_2H$ using $[(MeBC_5H_5)_2Y\{CH(SiMe_3)_2\}]$

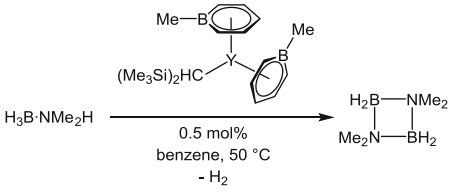

Scheme 57 Catalytic dehydrocoupling of $H_3B \cdot NMe_2H$ using $[\{(1,7\text{-}Me_2TACD)LaH\}_4]$

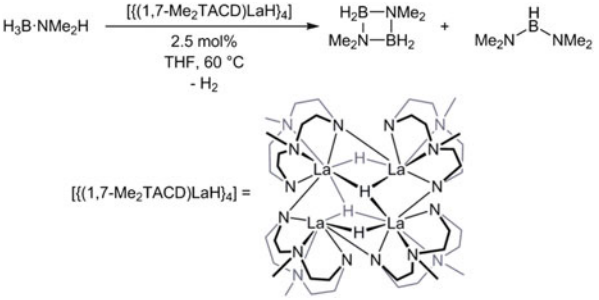

Scheme 58 Formation of $[AlH\{H_2B(NMe_2)_2\}_2]$

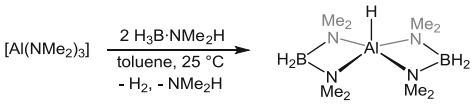

deficient boron centre of the 1-methyl boratabenzene ligand and the hydridic B–H bonds of the substrate. An analogous complex with an electron-donating substituent (NEt_2) on the boratabenzene $[(Et_2NBC_5H_5)_2Y\{CH(SiMe_3)_2\}]$ proved to be much less active in catalysis indicating either the electron-withdrawing nature of the ligand or the Lewis acidic centre was important for high activity. While the authors were unable to elucidate the mechanism of the reaction, they did observe free diborazane $H_3B \cdot NMe_2BH_2 \cdot NMe_2H$ as an intermediate in the reaction mixture, suggesting the mechanism is different than those reported by Harder and Hill in which free linear diborazane was never observed [130, 137].

Rare-earth metal catalysts were used by Okuda et al. for which the hydride tetramers $[\{(1,7\text{-}Me_2TACD)MH\}_4]$ (M = La, Y; 1,7-Me_2TACD = 1,7-dimethyl-1,4,7,10-tetraazacyclododecane) were used to catalyse the dehydrocoupling of $H_3B \cdot NMe_2H$ (2.5 mol%, 60°C, THF), with the lanthanum complex giving full conversion to $[H_2BNMe_2]_2$ (79%) and diaminoborane (21%) in 2 h, Scheme 57. The yttrium analogue took significantly longer with 95% conversion reached after 48 h to form a similar product ratio. Stoichiometric reactivity of $[\{(1,7\text{-}Me_2TACD)LaH\}_4]$ demonstrated the non-innocent behaviour of the ligand in reactivity with the secondary amine–borane. The basic amido-groups of the 1,7-Me_2TACD ligand were shown to deprotonate the acidic amine protons of the amine–borane to form coordinated amidoborane species. The lone pair of these amido-groups was also able to provide stabilisation for the boron centre of a coordinated aminoborane by acting as a Lewis base [138].

2.10.4 P-Block-Catalysed Dehydrocoupling of Amine–Boranes

Wright et al. reported that the reaction of $[Al(NMe_2)_3]$ with $H_3B \cdot NMe_2H$ led to the formation of $[AlH\{H_2B(NMe_2)_2\}_2]$ (Scheme 58) by formation of an amidoborane complex and migration of the NMe_2 amido ligands to the boron centre. This complex (at 5 mol%) was able to catalyse the dehydrocoupling of $H_3B \cdot NMe_2H$

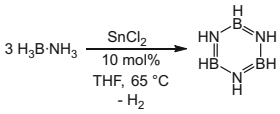

Scheme 59 $SnCl_2$-catalysed dehydrocoupling of $H_3B \cdot NH_3$ to give borazine (87%)

at 50°C to give $[H_2BNMe_2]_2$ and $HB(NMe_2)_2$ in a 6:1 molar ratio after 48 h [139]. In a follow-up report, $[Al(N^iPr_2)_3]$ was used to catalytically form the aminoborane $H_2B{=}N^iPr_2$ from the corresponding secondary amine–borane (10 mol%, 60°C, 2 h). As with the system reported by Okuda et al., the amido ligands of the starting material were found to be non-innocent, and if $[Al(NMe_2)_3]$ was used instead, by-products containing the NMe_2 moiety were observed. Extending this investigation to a primary amine–borane, the precatalyst $[Al(NMe_2)_3]$ was able to slowly dehydrocouple $H_3B \cdot N^tBuH_2$ to form first the cyclic trimer borazane $[H_2BN^tBuH]_3$ which was then further dehydrogenated to the borazine product $[HBN^tBu]_3$. Because the borazine can be observed early in the reaction, this suggests the rate of formation of borazine from borazane is comparable to the rate of initial dehydrocoupling to form the borazane from the monomers. However, overall this reaction was slow with only 30% conversion of the amine–borane after 4 days at 20°C [140]. Wright et al. have also found that Li$[AlH_4]$ can be used as a catalyst to dehydrocouple $H_3B \cdot NMe_2H$ to give $[H_2BNMe_2]_2$ along with $HB(NMe_2)_2$ as a minor product [141]. Stoichiometric reactions of amine–boranes with aluminium species have revealed possible reaction intermediates although the mechanism of the dehydrocoupling has not been unambiguously determined [139–142].

The group IV metal tin, in both II and IV oxidation states, was utilised by Waterman et al. to catalyse the dehydrocoupling of $H_3B \cdot NMe_2H$, $H_3B \cdot N^tBuH_2$ and $H_3B \cdot NH_3$. The majority of the catalytic reactions occurred slowly with most taking at least 24 h and producing a range of BN-containing products. The best performing was the $SnCl_2$-catalysed (10 mol%) dehydrocoupling of $H_3B \cdot NH_3$ to borazine (87%) in 1 h at 65°C (Scheme 59). Attempts to identify the active species in catalysis were not successful as no tin-containing intermediates could be characterised or isolated. NMR spectroscopic investigations could not determine whether the active species was a Sn^{II} or Sn^{IV} complex, although several different active species could be present. It was determined that the likely method of catalyst deactivation was by reduction to Sn^0 [143].

Sneddon has reported that Verkade's base (VB) acts as an initiator for base-promoted anionic dehydropolymerisation of $H_3B \cdot NH_3$ to form anionic aminoborane chain growth products, such as the structurally characterised $[VBH]^+[H_3BNH_2BH_2NH_2BH_3]^-$ [9]. The mechanism proposed for this dehydrocoupling invokes initial deprotonation of $H_3B \cdot NH_3$ by VB to form $[VBH]^+[BH_3NH_2]^-$, which then reacts with further $H_3B \cdot NH_3$ to form the borane-capped $[VBH]^+[BH_3NH_2BH_3]^-$ and NH_3. Subsequent, sequential, dehydrocoupling affords the longer-chain oligomers. Such steps are suggested to

be facilitated by N–H···H–B dihydrogen bonding as informed by a solid-state structural analysis. This result builds upon earlier studies in which proton sponge was used as the base initiator [36], as well as work by Girolami and co-workers that reported mild thermal conversion of $Na[NH_2BH_3]$ leads to $NaNH_2$ and $Na[NH_2(BH_3)_2]$ [144]. By contrast, Baker and Dixon have reported that the strong Lewis acid, $B(C_6F_5)_3$, or Brønsted acid, $HOSO_2CF_3$, promotes dehydrocoupling of amine–borane by a *hydride* abstraction pathway to form a boronium cation [102]. This is not dissimilar to the mechanism suggested for the Pt–catalysed dehydrocoupling of $H_3B \cdot NMe_2H$ (Scheme 43).

2.10.5 Frustrated Lewis Pair Dehydrogenation of Amine–Boranes

Since the discovery that frustrated Lewis pairs can activate dihydrogen, interest has focussed on the activation of other small molecules [145, 146]. The abstraction of dihydrogen from amine–boranes, particularly if it could be performed catalytically, would provide an alternative method to the traditional metal-based catalysis. The first to develop the dehydrogenation of $H_3B \cdot NMe_2H$ using frustrated Lewis pairs were Miller and Bercaw, who used a stoichiometric combination of P^tBu_3 and $B(C_6F_5)_3$ to ultimately form $[H_2BNMe_2]_2$ along with trace amounts of other BN-containing products. However, this reaction could not be carried out catalytically, and heating the reaction mixture in an attempt to release hydrogen gas from $[HP^tBu_3][HB(C_6F_5)_3]$ and regenerate the frustrated Lewis pair was unsuccessful. Ammonia–borane could also be dehydrocoupled by a stoichiometric amount of these reagents to give polyaminoborane $[H_2BNH_2]_n$ and $[HP^tBu_3][HB(C_6F_5)_3]$. Addition of further P^tBu_3 and $B(C_6F_5)_3$ did not appear to result in further dehydrogenation to form borazine or other products. The authors suggested the mechanism of dehydrogenation was likely to proceed via hydride abstraction by $B(C_6F_5)_3$, followed by rapid deprotonation by P^tBu_3 to form the aminoborane. This then undergoes rapid oligomerisation to form the products [147]. The group of Manners used a variety of less expensive frustrated Lewis pairs to dehydrocouple $H_3B \cdot NMe_2H$, with a combination of $[Me_3SiO_3SCF_3]$ and 2,2,6,6-tetramethylpiperidine performing best in forming $[H_2BNMe_2]_2$, with only traces of side products observed. The reaction could only be performed by a stoichiometric amount of Lewis pair, and therefore the reaction was not catalytic. Attempts to dehydrogenate the primary amine–borane $H_3B \cdot NMeH_2$ did not result in readily characterised products [148].

An early example of use of a frustrated Lewis pair to *catalytically* dehydrocouple an amine–borane was reported by Uhl et al. who used a compound containing both a Lewis basic bulky phosphine and a Lewis acidic aluminium centre (Scheme 60). Stoichiometric reaction between this compound and ammonia–borane led to the dehydrogenation and formation of the aminoborane adduct. However, this final complex was thermally stable and the aminoborane could not be liberated to regenerate the original Lewis pair. Computational analysis of this reaction gave a mechanism contrasting that suggested by Miller and Manners where the first step of the reaction is now deprotonation of the N–H by the phosphine

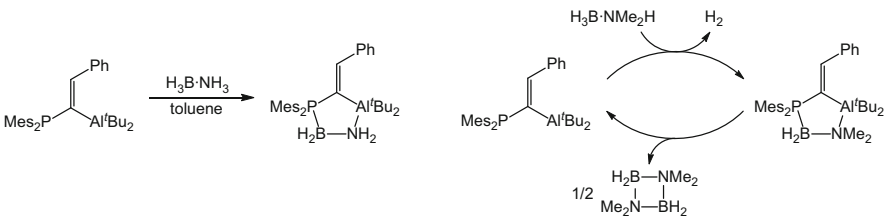

Scheme 60 Reaction of the FLP with $H_3B \cdot NH_3$ (*top*) and catalytic dehydrocoupling of $H_3B \cdot NMe_2H$ (*bottom*)

centre and formation of an Al–N bond. Rearrangement, followed by loss of H_2 from the complex, gives the aminoborane and the 5-membered cyclic product quickly forms. The forced proximity of the Lewis acid and base in this compound may be the cause of this alternative mechanism. When the secondary amine–borane $H_3B \cdot NMe_2H$ was used, dihydrogen was again produced and the five-membered cyclic species was formed, but this was found to only be stable below −30°C. Above this temperature, the aminoborane $H_2B{=}NMe_2$ is released, which quickly dimerises to form $[H_2BNMe_2]_2$, and the frustrated Lewis pair catalyst is regenerated. A melt reaction of $H_3B \cdot NMe_2H$ (45°C then 90°C) with 9.3 mol% of catalyst produced $[H_2BNMe_2]_2$ in 71% isolated yield after 45 min. A lower catalyst loading (0.4 mol%) gave 77% $[H_2BNMe_2]_2$ in 44 h under similar conditions [149].

3 Dehydrocoupling of Phosphine–Boranes

3.1 Transition-Metal-Catalysed Dehydrocoupling of Phosphine–Boranes

Phosphine–boranes were first found to undergo thermal dehydrocoupling in the 1950s when monomers were heated to 150°C and released hydrogen to form a mixture of cyclic trimer and tetramers [150]. Some polymerisation was reported at higher temperature but the products were ill-defined (Scheme 61) [151].

The breakthrough in *catalytic* dehydrocoupling came at the turn of the century when the group of Manners reported dehydrocoupling of both secondary and primary phosphine–boranes to give a variety of products. The precatalysts used were initially simple rhodium(I) species $[Rh(1,5\text{-cod})(\mu\text{-Cl})]_2$ or the salt $[Rh(1,5\text{-cod})_2][O_3SCF_3]$. The secondary phosphine–borane $H_3B \cdot PPh_2H$ was found to selectively form the linear diboraphosphine species $[H_3B \cdot PPh_2BH_2 \cdot PPh_2H]$ at 90°C in the presence of 0.3 mol% of the rhodium(I) precatalyst in the absence of solvent (melt conditions) after 14 h. Heating a similar reaction mixture to 120°C for 15 h gave cyclic trimer and tetramers as the sole products (Scheme 62) [152, 153]. Analysis of this reaction mixture after 4 h showed complete consumption of the $H_3B \cdot PPh_2H$

Scheme 61 Thermal dehydrocoupling of dimethyl phosphine–borane

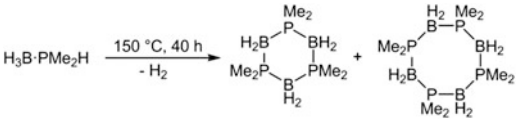

Scheme 62 Rhodium (I)-catalysed dehydrocoupling of secondary phosphine–borane

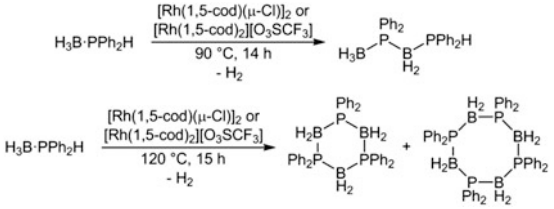

Scheme 63 Catalytic formation of polyphosphinoboranes

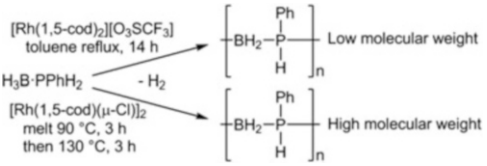

starting material and a mixture of diboraphosphine, $H_3B \cdot PPh_2BH_2 \cdot PPh_2H$, and the cyclic species. It was suggested that $H_3B \cdot PPh_2BH_2 \cdot PPh_2H$ is an intermediate in the formation of the cyclic oligomers.

When the primary phosphine–borane $H_3B \cdot PPhH_2$ was used, 0.3 mol% of $[Rh(1,5\text{-cod})_2][O_3SCF_3]$ in refluxing toluene gave an air- and moisture-stable, off-white solid product found to be low molecular weight polyphenylphosphinoborane ($M_w = 5{,}600$). If melt conditions were used with $[Rh(1,5\text{-cod})(\mu\text{-Cl})]_2$ as the catalyst, a similar product could be made with a higher molecular weight ($M_w = 31{,}000$) (Scheme 63 and Fig. 15) [152].

In a follow-up report, Manners et al. screened a range of precatalysts for the dehydrocoupling of $H_3B \cdot PPh_2H$. In addition to the species tested above, the best performing precatalysts under melt conditions were found to be either Rh^I or Rh^{III} compounds, with species containing other metals (Ir, Pd, Pt) giving lower conversions and slower turnover. The scope of the polymerisation of primary phosphine–boranes was also expanded to the alkyl-substituted $H_3B \cdot P^tBuH_2$, which was dehydrocoupled in 13 h at 120°C [153].

The alkyl-substituted secondary phosphine–borane $H_3B \cdot P^tBu_2H$ could be dehydrocoupled by similar rhodium-based precatalysts under melt conditions at elevated temperatures. Full conversion of the phosphine–borane was not achieved for any of the catalysts although the major product formed was the diboraphosphine, $H_3B \cdot P^tBu_2BH_2 \cdot P^tBu_2H$. Other products were also observed including in some cases the chloride-terminated diboraphosphine ($ClH_2B \cdot P^tBu_2BH_2 \cdot P^tBu_2H$) with the chloride provided by the precatalyst. One of the best catalysts was found to be $[Rh(1,5\text{-cod})(\mu\text{-Cl})]_2$ which had also been used

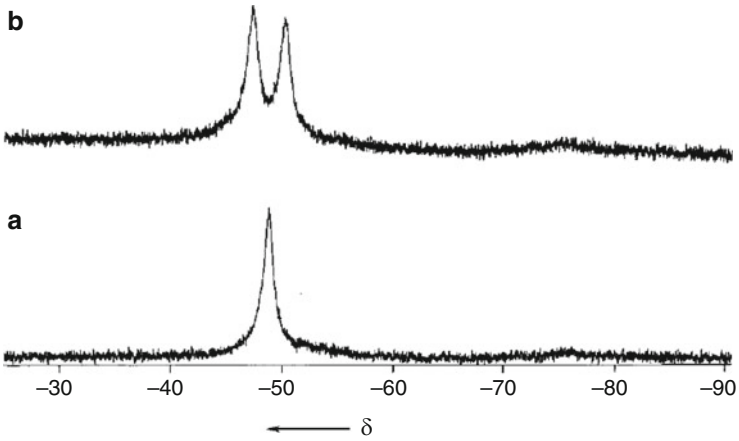

Fig. 15 ^{31}P NMR spectrum of $[H_2BPPhH]_n$ in $CDCl_3$ (121 MHz): (**a**) ^{1}H-decoupled and (**b**) ^{1}H-coupled, $J_{PH} = 360$ Hz. Reprinted (adapted) with permission from Dorn et al. [153]. Copyright 2000, American Chemical Society

for the previous systems [154]. Another report from Manners and co-workers focussed on the formation of polymers from the dehydrocoupling of primary phosphine–boranes; aryl-substituted phosphine–boranes $H_3B \cdot P(p\text{-}^n Bu\text{-}C_6H_4)H_2$ and $H_3B \cdot P(p\text{-}(C_{12}H_{25})\text{-}C_6H_4)H_2$ were polymerised by $[Rh(1,5\text{-cod})(\mu\text{-Cl})]_2$ under melt conditions [155].

3.2 *Determination of the Active Catalytic Species: Hetero- or Homogeneous*

In all of these reports from the group of Manners, the active catalytic species and mechanism of polymerisation were not investigated in detail. While in general rhodium-based precatalysts under melt conditions performed best, precatalysts with different oxidation states and ligands could all give catalytic turnover for dehydrocoupling. Since the formation of rhodium nanoparticles had been found to be an important step in the catalytic dehydrocoupling of amine–boranes, Manners et al. investigated whether the phosphine–borane catalysis operated in a hetero- or homogeneous mode. Addition of 10 mol% of $[Rh(1,5\text{-cod})(\mu\text{-Cl})]_2$ to a toluene solution of $H_3B \cdot PPh_2H$ at 90°C resulted in a colour change from orange to red, but no evidence of black material was observed, which is often characteristic of nanoparticle formation [156]. In addition to this, no induction period was observed, and filtration and mercury poisoning experiments also suggested the catalyst was a heterogeneous species. Similar results were found for the ion-separated precatalyst $[Rh(1,5\text{-cod})_2][O_3SCF_3]$ (Fig. 16).

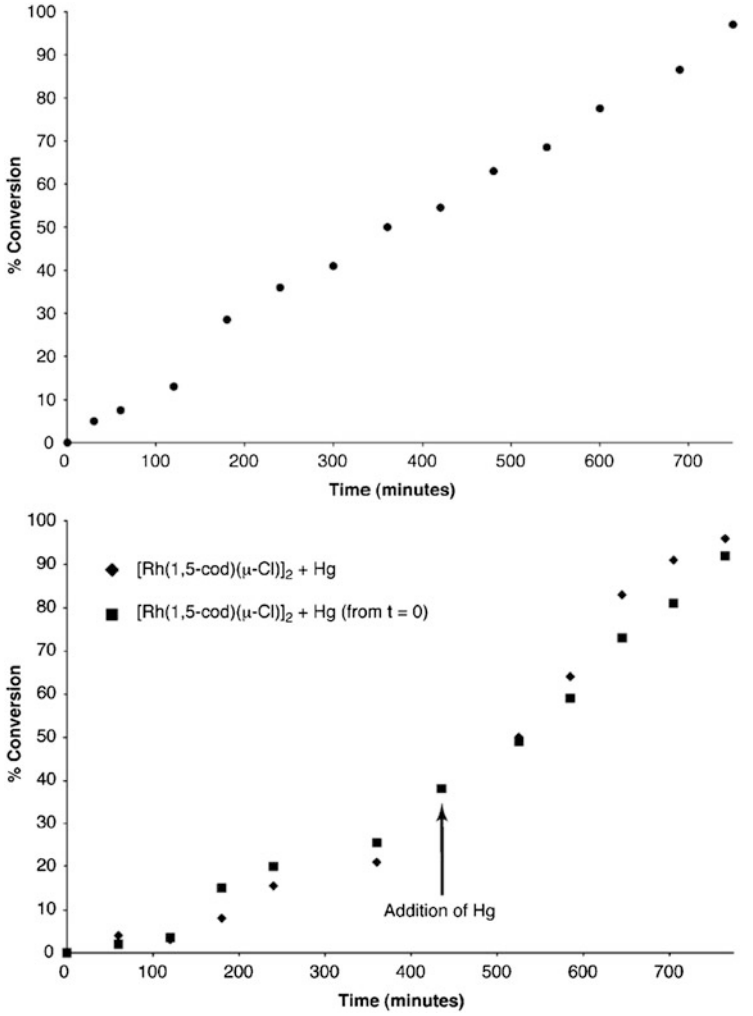

Fig. 16 *Top*: graph of % conversion vs. time for the catalytic dehydrocoupling of $H_3B \cdot PPh_2H$ using $[Rh(1,5\text{-cod})(\mu\text{-Cl})]_2$ (ca. 10 mol% Rh, toluene, 90°C). *Bottom*: graph of % conversion vs. time for the catalytic dehydrocoupling of $H_3B \cdot PPh_2H$ using $[Rh(1,5\text{-cod})(\mu\text{-Cl})]_2$ (ca. 10 mol % Rh, toluene, 90°C). At ca. 35% conversion, excess Hg was added to the reaction mixture (curve *filled diamond*). The dehydrocoupling reaction was initiated in the presence of excess Hg (curve *filled square*). Reprinted (adapted) with permission from Jaska and Manners [39]. Copyright 2004, American Chemical Society

Dehydrocoupling was attempted using the heterogeneous Rh/Al_2O_3 (5 wt% Rh) precatalyst and, interestingly, catalysis was found to occur. However, filtration of the solution showed the soluble portion to be orange, suggesting some rhodium had leached into the solution to form a homogeneous catalytically active species. Addition of further $H_3B \cdot PPh_2H$ to both soluble and insoluble portions showed

them to be active and inactive, respectively, confirming the homogeneous nature of the catalyst. While the authors were unable to identify the true catalytic species, they were able to speculate that the phosphine–boranes were not reducing enough to form Rh^0 from the Rh^I precatalyst. In addition to this, the relative weakness of the P–B bond (compared to the N–B bond in amine–boranes) allowed dissociation and formation of free phosphine which could act as ligands for solubilising heterogeneous species. However, an excess of free phosphine could act as a catalyst poison, and they suggest higher temperatures required for phosphine–borane dehydrocoupling might be needed to create a vacant site at the metal centre, which is often required in polymerisation catalysis [39].

3.3 *Sigma Complexes and B-Agostic Interactions of Phosphine–Boranes*

An important step in the dehydrocoupling of amine–boranes is thought to be the formation of σ-complexes where the metal centre interacts with the H–B bond of the borane moiety (Sect. 2.7.1). Similarly, in phosphine–borane dehydrocoupling, the creation of a vacant site at the metal centre to which the phosphine–borane can bind, or displacement of a ligand by a phosphine–borane, is likely to be an important step [39]. The initial interaction between the metal centre and the substrate is likely through formation of a σ-complex with the hydridic B–H bonds. A number of phosphine–borane σ-complexes and B-agostic interactions (where the phosphine–borane is further tethered to the metal centre) have been reported in the literature. An early example of a σ-complex was reported in 1984 in which zinc is complexed with diphosphine–diborane(4), $[ZnCl_2\{B_2H_4 \cdot (PMe_3)_2\}]$ [157], and a phosphidoborane complex with a β-B-agostic interaction $[CpMo(CO)_2(P\{N(SiMe_3)_2\}Ph \cdot BH_3)]$ was published 2 years later [158]. The first σ-complex with a monomeric phosphine–borane was synthesised by the photolysis of $[M(CO)_6]$ (M=Cr, Mo, W) in the presence of $H_3B \cdot PR_3$ (R=Me, Ph) to form the η^1-complexes $[M(CO)_5(H_3B \cdot PR_3)]$ [61]. There are a number of reports of similar compounds [159–161] including examples of η^2-B-agostic interactions in rhodium complexes [162–164].

An interesting observation came from Whittlesey et al. who reported that reaction of $[RuH(Xantphos)(PPh_3)(OH_2)][BAr^F{}_4]$ with amine–boranes produced σ-complexes by displacement of the water ligand, but reaction with the phosphine–borane $H_3B \cdot PPh_2H$ gave only the P–B cleavage product $[RuH(Xantphos)(PPh_2H)_2][BAr^F{}_4]$. This shows the relative weakness of the P–B bond compared to the N–B bond in amine–boranes and suggests P–B cleavage is likely to play a role in metal-catalysed dehydrocoupling of phosphine–boranes [63].

In 2013, Weller et al. described an attempt to form a σ-complex from the reaction between $[RhCl(PPh_3)_3]$ and $Na[BAr^F{}_4]$ in the presence of a secondary phosphine–borane $H_3B \cdot PPh_2H$. However, this reaction led to dehydrocoupling and

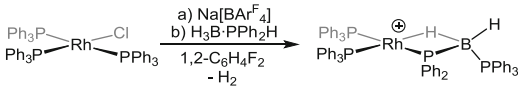

Scheme 64 Formation of $[Rh(PPh_3)_2(PPh_2BH_2 \cdot PPh_3)][BAr^F{}_4]$ from the dehydrogenation of $H_3B \cdot PPh_2H$. $[BAr^F{}_4]^-$ anion not shown

the formation of the complex $[Rh(PPh_3)_2(PPh_2BH_2 \cdot PPh_3)][BAr^F{}_4]$ (Scheme 64). One triphenylphosphine ligand has migrated to the boron centre, and a B–H bond has formed a β-B-agostic interaction with the rhodium centre. While the mechanism of this transformation was not determined, it was postulated that the reaction could occur either via P–H activation, B–H activation or the formation of a transient phosphinoborane intermediate $H_2B=PPh_2$ at the metal centre [165]. In contrast, aminoboranes have been shown to be crucial, if often short-lived, intermediates in the metal-catalysed dehydrocoupling of amine–boranes (vide supra); however, free phosphinoboranes have yet to be observed during phosphine–borane dehydrocoupling.

There are examples of group X phosphidoborane complexes that have been synthesised by the reaction of a metal fragment with $H_3B \cdot PR_2H$ and oxidative addition of the P–H bond [166, 167]. These examples, however, are not active in dehydrocoupling either stoichiometric or catalytic, although, as will be shown in Sect. 3.6, such motifs can be strongly implicated in the dehydrocoupling process with different metal–ligand fragments.

3.4 Stabilised Phosphinoboranes

Although not directly observed during dehydrocoupling, there are phosphinoboranes which have been synthesised that rely on stabilisation by the presence of bulky substituents or by coordination of a Lewis acid or Lewis base. Those with large substituents do not oligomerise due to the steric crowding of the phosphorus and boron centres [168]. However, those with Lewis acid or base stabilisation can undergo further reaction [169, 170]. The Lewis base-stabilised unsubstituted phosphinoborane $Me_3N \cdot H_2BPH_2$ was synthesised by Scheer et al. and was found to oligomerise in the presence of $[Cp_2Ti(\eta_2Me_3SiCCSiMe_3)]$, with different products observed depending on the temperature and stoichiometry. The first step of the reaction is the coordination of the stabilised phosphinoborane through the lone pair at the phosphorus centre to form $[Cp_2Ti(\eta_2Me_3SiCCSiMe_3)(PH_2BH_2 \cdot NMe_3)]$ (**84**) (Scheme 65). This complex is only stable below −80°C in solution, and above this temperature alkyne dissociates and oligomerisation occurs in both head-to-tail and head-to-head fashion, along with some Lewis base dissociation. The complexes formed are oligomeric chains of 3 (**85**), 4 (**86**) and 6 (**87**) phosphinoborane monomers stabilised by the coordination of the $[Cp_2Ti]$ fragment [171].

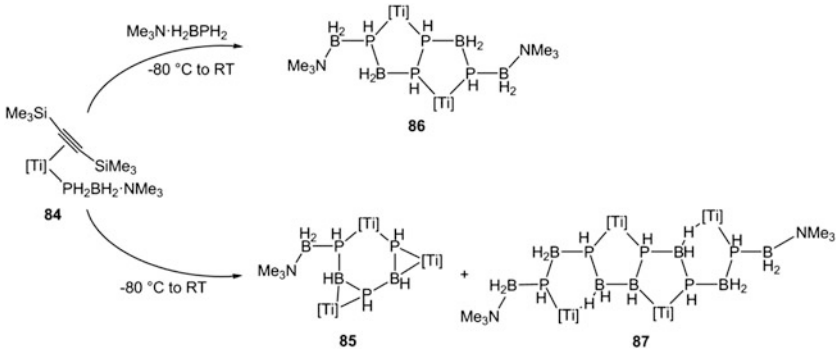

Scheme 65 [Cp_2Ti]-catalysed oligomerisation of $Me_3N \cdot H_2BPH_2$. [Ti]=Cp_2Ti

3.5 Group 8 Metal-Catalysed Dehydrocoupling of Phosphine–Boranes

Complexes based on group 8 metals were first used in 2008 as precatalysts for dehydrocoupling, when Manners et al. reported the use of [$CpM(CO)_2(PPh_2 \cdot BH_3)$] (M=Fe, Ru) to form diboraphosphine, $H_3B \cdot PPh_2BH_2 \cdot PPh_2H$, from the secondary phosphine–borane $H_3B \cdot PPh_2H$ under both melt conditions and in solution. The phosphidoborane precatalyst complexes were synthesised by a reaction of [CpMI $(CO)_2$] (M=Fe, Ru) with $(H_3B \cdot PPh_2)Li$. In toluene solution at 110°C, the Fe complex performed poorly only converting 50% of $H_3B \cdot PPh_2H$ at 25 mol% catalyst loading. However, under melt conditions (120°C), the iron and ruthenium complexes were able to convert 65 and 60% of the starting material to linear diboraphosphine, respectively (1.5 mol%, 15 h). Under the same melt conditions, $Fe_2(CO)_9$ was also found to catalyse the dehydrocoupling of $H_3B \cdot PPh_2H$ to form the same product (80% conversion in 15 h). The authors postulated that the loss of a carbonyl ligand at high temperatures allowed dehydrocoupling to occur in the vacant coordination site created [172]. This is closely related to the mechanism proposed for amine–borane dehydrocoupling using the same metal–ligand system (Scheme 30).

3.6 Mechanistic Investigations into the Rhodium-Catalysed Dehydrocoupling of Secondary Phosphine–Boranes

The first detailed investigation into the mechanism of the rhodium-catalysed dehydrocoupling of phosphine–boranes was reported by Huertos and Weller in 2012. The precatalyst used was $[Rh(1,5\text{-cod})_2][BAr^F{}_4]$ similar to the $[Rh(1,5\text{-cod})_2]$ $[O_3SCF_3]$ complex used previously by Manners and co-workers [7]. Heating 5 mol % of the precatalyst with $H_3B \cdot P^tBu_2H$ under melt conditions (140°C) for 20 h led

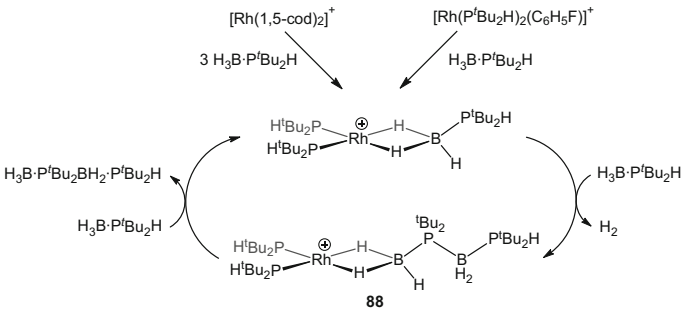

Scheme 66 Proposed mechanism for rhodium-catalysed formation of linear diboraphosphine from $H_3B \cdot P^tBu_2H$. $[BAr^F{}_4]^-$ omitted for clarity

to the formation of $H_3B \cdot P^tBu_2BH_2 \cdot P^tBu_2H$ (65%) along with a bis(phosphine) boronium salt $[H_2B(P^tBu_2H)_2][BH_4]$ (10%) as a side product from P–B cleavage. Interrogation of the melt reaction by addition of 1,2-difluorobenzene solvent and analysis by ^{31}P NMR spectroscopy and ESI mass spectrometry revealed the organometallic species present to be $[Rh(P^tBu_2H)_2(\eta^2\text{-}H_3B \cdot P^tBu_2BH_2 \cdot P^tBu_2H)]^+$ (**88**) and $[Rh(P^tBu_2H)_2(\eta^6\text{-}C_6H_4F_2)]^+$. The secondary phosphine ligands at the rhodium centre originate from the phosphine–borane having undergone P–B cleavage, and the rest of the coordination sphere of the Rh^I centre is filled by a solvent molecule or the σ-bound phosphine–borane or diboraphosphine. These observations suggested that the $[Rh(P^tBu_2H)_2]^+$ fragment was the active species in the catalysis. $[Rh(P^tBu_2H)_2(\eta^6\text{-}C_6H_5F)][BAr^F{}_4]$ was independently synthesised and was found to catalyse the dehydrocoupling of $H_3B \cdot P^tBu_2H$ under melt conditions to form the same intermediates and final products as $[Rh(1,5\text{-cod})_2][BAr^F{}_4]$. This provided further evidence that the $[Rh(P^tBu_2H)_2]^+$ fragment is the active catalyst, and a simple mechanism was postulated (Scheme 66) [173].

In an attempt to find a more stable catalytic fragment, $[Rh(P^iBu_3)_2(\eta^6\text{-}C_6H_5F)][BAr^F{}_4]$, which had been shown to be an effective dehydrocoupling catalyst for amine–boranes, was used as a precatalyst for the dimerisation of $H_3B \cdot P^tBu_2H$. However, analysis of the reaction mixture found a mixture of organometallic species with the tri-*i*-butylphosphine ligand replaced on the rhodium centre by P^tBu_2H ligands, presumably from P–B cleavage of the substrate. In a further development of this system, Huertos and Weller were able to form a more stable catalytic fragment by replacement of the monodentate phosphine ligands with a chelating phosphine ligand 1,3-bis(diphenylphosphino)propane ($Ph_2PCH_2CH_2CH_2PPh_2$, dppp) [174]. Under the harsh melt conditions required for catalysis to occur, the chelating ligand was not displaced by any free phosphine formed from P–B cleavage of the substrate, allowing further investigation into the $[Rh(dppp)]^+$ fragment as the active catalytic species. A stoichiometric reaction between the precatalyst $[Rh(dppp)(\eta^6\text{-}C_6H_5F)][BAr^F{}_4]$ and $H_3B \cdot P^tBu_2H$ led to the formation of the σ-complex $[Rh(dppp)(\eta^2\text{-}H_3B \cdot P^tBu_2H)][BAr^F{}_4]$ by displacement of the labile fluorobenzene ligand (Scheme 67). In the presence of another

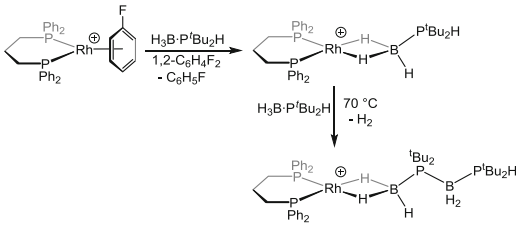

Scheme 67 Formation of $[Rh(dppp)(\eta^2\text{-}H_3B \cdot P^tBu_2H)]^+$ and dehydrocoupling. $[BAr^F{}_4]^-$ omitted for clarity

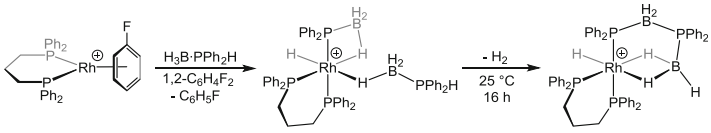

Scheme 68 Formation of $[RhH(dppp)(PPh_2 \cdot BH_3)(\eta^1\text{-}H_3B \cdot PPh_2H)]^+$ and dehydrocoupling. $[BAr^F{}_4]^-$ omitted for clarity

equivalent of $H_3B \cdot P^tBu_2H$, the complex was found to undergo dehydrocoupling at 70°C in 1,2-difluorobenzene to form the σ-bound linear diboraphosphine product $[Rh(dppp)(H_3B \cdot P^tBu_2BH_2 \cdot P^tBu_2H)]^+$ although the reaction produced several side products.

Extending the study to $H_3B \cdot PPh_2H$ resulted in quite different complexes being isolated from these stoichiometric studies. Reaction of $[Rh(dppp)(\eta^6\text{-}C_6H_5F)][BAr^F{}_4]$ with 2 equiv. of $H_3B \cdot PPh_2H$ in 1,2-difluorobenzene gave a Rh^{III} complex in which one phosphine–borane unit had undergone P–H activation to form a rhodium hydride and a β-B-agostic phosphidoborane, and the second molecule was σ-bound through one hydrogen atom of the borane moiety. The two phosphine–borane units on this complex were found to cleanly dehydrocouple in a first-order process at room temperature to form a linear diboraphosphine product which is also P–H activated, and the remainder of the Rh^{III} coordination sphere is filled by two β-B-agostic interactions from the terminal BH_3 moiety (Scheme 68, Fig. 17). These data, when combined with H/D labelling experiments, allowed the rate-determining step for dehydrocoupling to be suggested to lie in the second B–H activation and ligand reorganisation step(s). In catalysis, the turnover-limiting step, however, is the substitution of the chelating linear diboraphosphine by another molecule of $H_3B \cdot PPh_2H$ (Scheme 69).

The substituents at the phosphorus position of the phosphine–borane unit were found to have an effect on the reactivity both stoichiometrically and in catalysis. The phosphine–borane with the bulky, electron-donating *t*-butyl substituent was found to dehydrocouple slowly (16 h at 140°C, 60% conversion), and complexes with this ligand were observed in the Rh^I oxidation state. Contrastingly, when the phosphine–borane with the electron-withdrawing phenyl substituent was used, dehydrocoupling proceeded faster (4 h at 90°C) while Rh^{III} complexes were

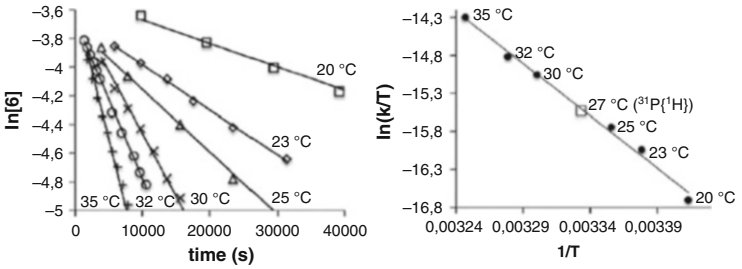

Fig. 17 First-order plots and Eyring analysis of dehydrocoupling of $[RhH(dppp)(PPh_2 \cdot BH_3)(\eta^1\text{-}H_3B \cdot PPh_2H)][BAr^F{}_4]$ to $[RhH(dppp)(PPh_2 \cdot BH_2PPh_2 \cdot BH_3)][BAr^F{}_4]$. Reprinted (adapted) with permission from Huertos and Weller [174]. Copyright 2014, Royal Society of Chemistry

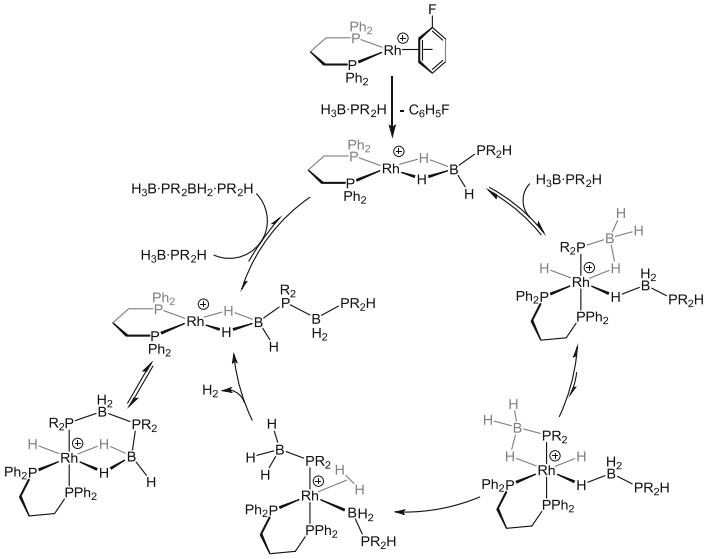

Scheme 69 Detailed mechanism for the dehydrocoupling of secondary phosphine–borane by the $[Rh(dppp)]^+$ fragment. $[BAr^F{}_4]^-$ omitted for clarity

favoured. The difference in oxidation state of the rhodium centre in these cases is likely due to the acidity of the P–H bond. When electron-withdrawing substituents are present on phosphorus, the P–H bond more readily undergoes P–H oxidative addition, making Rh^{III} species favoured [174].

In a follow-up report, secondary phosphine–boranes bearing fluorinated substituents $H_3B \cdot P(p\text{-}F_3C\text{-}C_6H_4)_2H$ and $H_3B \cdot P(m\text{-}(F_3C)_2C_6H_3)_2H$ were found to dehydrocouple at a faster rate than $H_3B \cdot PPh_2H$ using the same $[Rh(dppp)]^+$ system [175]. However, stoichiometric reactions showed that the weakening of the P–B bond by the presence of the electron-withdrawing groups caused P–B bond cleavage and hence catalyst deactivation by the formation of $[Rh(dppp)(PR_2H)_2]^+$. The

faster dehydrocoupling of fluorinated phosphine–boranes is in agreement with Manners et al. who found that these substrates could be catalytically dehydrocoupled at lower temperature than the non-fluorinated aryl analogues (vide infra). Conversely, the presence of an electron-donating group $H_3B \cdot P(p\text{-}MeO\text{-}C_6H_4)_2H$ at the phosphorus centre was found to reduce the rate of dehydrocoupling. However, the increased strength of the P–B bond meant cleavage and hence catalyst deactivation was largely avoided. Fluorinated phosphine–boranes can be also catalytically dehydrocoupled using different catalyst systems. The secondary phosphine–borane $H_3B \cdot P(p\text{-}F_3C\text{-}C_6H_4)_2H$ was converted to the corresponding linear diboraphosphine product by heating with [Rh(1,5-cod)(μ-Cl)]$_2$ (2 mol% based on Rh) to 60°C for 15 h under melt conditions [176]. The cyclic trimer and tetramer species observed for the high-temperature dehydrocoupling of $H_3B \cdot PPh_2H$ were also formed at lower temperature (100°C, 15 h). The fluorinated primary phosphine–borane $H_3B \cdot P(p\text{-}F_3C\text{-}C_6H_4)H_2$ was found to form high molecular weight polymer under similar conditions, [Rh(1,5-cod)(μ-Cl)]$_2$ precatalyst (2.5 mol% based on Rh), 60°C, 9 h in melt conditions. The lowering of the reaction temperature was ascribed to the increased acidity of the P–H bond due to the electron-withdrawing substituents and therefore its ability to react more readily with the hydridic B–H bonds to dehydrocouple.

3.7 *Mechanistic Investigation into the Rhodium-Catalysed Dehydrocoupling of Primary Phosphine–Boranes*

The mechanism of dehydrocoupling of primary phosphine–boranes using [Rh(dppp)(η^6-C_6H_5F)][$BAr^F{}_4$] has also been reported. $H_3B \cdot PCyH_2$ was used as the substrate, and under stoichiometric conditions, it reacted in a similar way to $H_3B \cdot PPh_2H$ with the formation of a Rh^{III} complex with a hydride, a phosphidoborane and a σ-bound η^1-$H_3B \cdot PCyH_2$ (Scheme 70). This complex was found to exist as an approximately 1:1 mixture of two diastereoisomers (**89a** and **89b**) due to the P–H activation at the prochiral phosphorus centre. As with the secondary aryl phosphine–boranes, this complex underwent dehydrocoupling, although faster than the secondary analogues, being complete in 1 h at room temperature. The dehydrocoupled complex formed was again equivalent to the $H_3B \cdot PPh_2H$ reaction with the linear diboraphosphine having undergone P–H activation and chelating via 2 β-B-agostic bonds from the terminal borane moiety. The complex is formed as a mixture of two, unresolved, diatereoisomer (**90a** and **90b**) because of P–H activation at the prochiral phosphorus centre although the diastereomers are present as a 6:1 mixture with one thermodynamically favoured. This complex can also be synthesised by the reaction of the preformed linear diboraphosphine with [Rh(dppp)(η^6-C_6H_5F)][$BAr^F{}_4$], which initially forms a kinetic 1:1 diastereomeric mixture and over 18 h reaches the 6:1 ratio observed from dehydrocoupling. This provides evidence for the mechanism proposed in

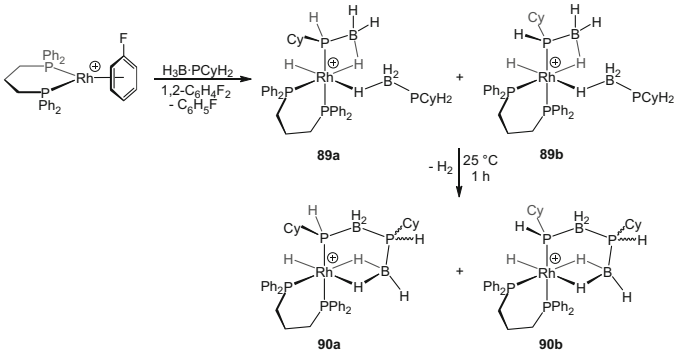

Scheme 70 Reaction of $[Rh(dppp)(\eta^6\text{-}C_6H_5F)][BAr^F{}_4]$ with primary phosphine–borane $H_3B \cdot PCyH_2$. $[BAr^F{}_4]^-$ omitted for clarity

Scheme 69 in which the Rh^I σ-bound linear diboraphosphine complex is in equilibrium with the P–H-activated Rh^{III} octahedral complex as such a process would allow interconversion of the Rh^{III} diastereomers. Such a diastereomeric bias may afford some control of polymer tacticity in dehydropolymerisation reactions [175]. Interestingly, the use of a chiral chelating phosphine ligand on rhodium resulted in a further bias towards one diastereoisomer, but the absolute configuration was not determined.

The $[Rh(dppp)]^+$ fragment performed competently as a catalyst for the polymerisation of the more reactive primary phosphine–borane $H_3B \cdot PPhH_2$ under melt conditions. Heating 5 mol% of precatalyst $[Rh(dppp)(\eta^6\text{-}C_6H_5F)][BAr^F{}_4]$ with neat $H_3B \cdot PPhH_2$ to 90°C for 4 h led to a peak in the ^{31}P NMR spectrum matching previous literature reports for polyphenylphosphinoborane along with minor signals thought to be short-chain oligomers and cyclic species [153].

An expansion of the scope of dehydrocoupling of primary phosphine–boranes was reported in 2014 when ferrocenylphosphine–boranes were dehydrocoupled to form polymeric material. Using the catalytic system developed by Manners et al., $H_3B \cdot P\{(CH_2)_xFc\}H_2$ (Fc = ferrocenyl, $x = 0$ or 1) was dehydrocoupled using 0.6 mol% $[Rh(1,5\text{-cod})(\mu\text{-Cl})]_2$ (based on Rh) with the products characterised by NMR spectroscopy (Fig. 18). Low molecular weight polymer was formed when the reaction was carried out in toluene solution (110°C), but in melt conditions, higher molecular weights could be obtained (Scheme 71) [177].

The same group reported the dehydrocoupling of secondary phosphine–boranes bearing ferrocenyl substituents. The $H_3B \cdot P^tBu(Fc)H$ substrate could be dehydrocoupled to form the linear diboraphosphine under melt conditions (160°C) using $[Rh(1,5\text{-cod})(\mu\text{-Cl})]_2$ as the catalyst. The product was found to be a mixture of $H_3B \cdot P^tBu(Fc)H_2B \cdot P^tBu(Fc)H$ and $ClH_2B \cdot P^tBu(Fc)H_2B \cdot P^tBu(Fc)H$ (Scheme 72), which is a similar observation to that made by Manners et al. in the dimerisation of $H_3B \cdot P^tBu_2H$ where the terminal chloride was thought to originate from the precatalyst [154]. Interestingly, the authors were able to couple two different phosphine–boranes to form a mixed diboraphosphine, the first time this

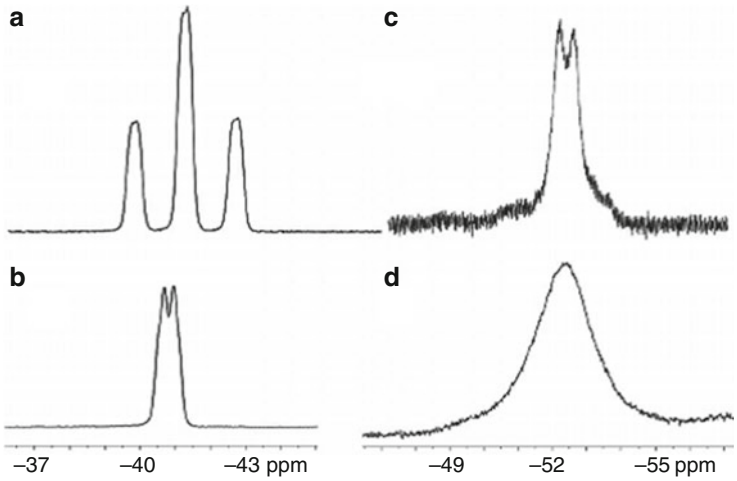

Fig. 18 ^{31}P NMR spectra of monomer $H_3B \cdot P(CH_2Fc)H_2$ (**a**, **b**) and polymer $[H_2BP(CH_2Fc)H]_n$ (**c**, **d**) in $CDCl_3$ (161.9 MHz): (**a**) ^{1}H-coupled, $^1J_{PH} = 358$ Hz; (**b**) ^{1}H-decoupled; (**c**) ^{1}H-coupled, $^1J_{PH} = 352$ Hz; (**d**) ^{1}H-decoupled. Reprinted (adapted) with permission from Pandey et al. [177]. Copyright 2014, John Wiley and Sons

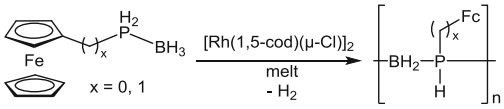

Scheme 71 Rh^{I}-catalysed dehydrocoupling of primary ferrocenyl phosphine–boranes

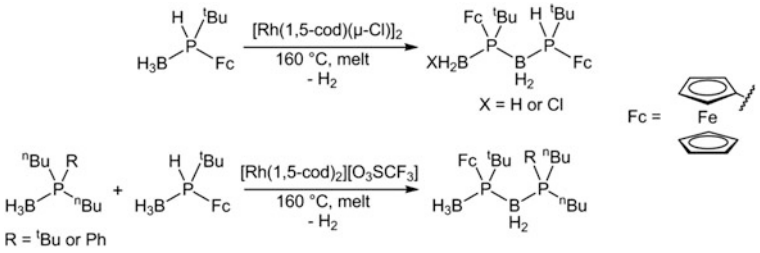

Scheme 72 Catalytic dehydrocoupling of secondary phosphine–boranes bearing ferrocenyl substituents

had been achieved. If a mixture of $H_3B \cdot P^tBu(Fc)H$ and a slight excess of either $H_3B \cdot P^tBu(^nBu)_2$ or $H_3B \cdot PPh(^nBu)_2$ was heated under melt conditions (160°C) with a $[Rh(1,5\text{-cod})_2][O_3SCF_3]$ precatalyst (4 mol%), the linear diboraphosphines could be synthesised in moderate isolated yield with the tertiary phosphine in the terminal position due to its lack of P–H functionality (Scheme 72) [178].

3.8 *Lewis Acid-Catalysed Dehydrocoupling of Phosphine–Boranes*

In 2003 came the first report of a non-transition-metal-catalysed dehydrocoupling of primary phosphine–boranes. The strong Lewis acid $B(C_6F_5)_3$ was used as the catalyst, and heating a solution of $H_3B \cdot PPhH_2$ to 90°C in toluene (0.5 mol% catalyst) for 3 h resulted in short oligomers and cyclic species characterised by ^{31}P NMR spectroscopy and size-exclusion chromatography. Alternatively, a longer reaction time at a lower temperature (3 days at 20°C) resulted in high molecular weight polymeric material. This catalyst was also found to dehydropolymerise $H_3B \cdot PH_3$ (formed from bubbling PH_3 and B_2H_6 through dichloromethane) to form oligomers at 70°C and polymer at 90°C (Scheme 73). The mechanism of polymerisation was thought to involve an initial exchange reaction of the strong Lewis acid with the BH_3 of one phosphine–borane to form $(C_6F_5)_3B \cdot PPhH_2$. The coordination of the electron-withdrawing group thus increased the acidity of the P–H bond, allowing reaction with the hydridic B–H bond on another phosphine–borane. This argument is similar to that made by Manners et al. for the reason that phosphine–boranes with fluorinated substituents dehydrocouple at lower temperatures than simple aryl phosphine–boranes [179].

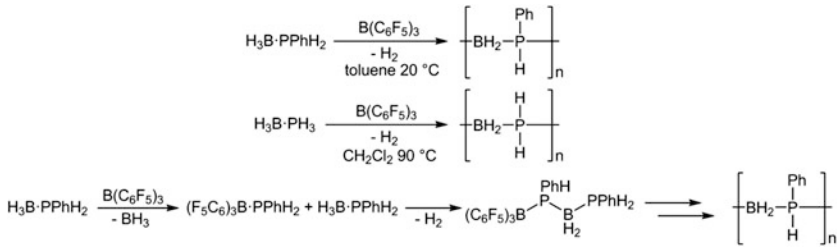

Scheme 73 Formation of polyphosphinoboranes using Lewis acid $B(C_6F_5)_3$ as a precatalyst along with a suggested mechanism

4 Future Prospects

It is clear from this review that the mechanistic studies into the dehydrocoupling of amine–boranes and phosphine–boranes have seen a rapid development over the last 5 years, with many systems studied, using catalysts based on metals from across the whole periodic table. The primary driver for this intense research has been the development of catalysts that might offer significant benefits with regard to the kinetics of hydrogen release, for potential use when this gaseous product is linked with a fuel cell. Although it is unlikely that any of these sometimes elegant and well-defined molecular systems would be capable of delivering a truly practicable system for long-term commercial use (i.e. with the constraints of total system weight, cost, extended recyclability, stability, operating conditions), although notable examples do exist of systems that show promise [118], this overarching goal has provided a focus for the elucidation of the mechanism of dehydrocoupling. More likely is that any commercial catalyst will be based around heterogeneous systems that utilise relatively cheap metal–ligand precursors, such as first-row transition metals [47]. Attention is now turning to the use of molecular, single-site catalysts for the closely related dehydropolymerisation of amine–boranes. In this process, the end product of value is the aminoborane, rather than the hydrogen released. It is probable that many of the major developments will likely arise from this area in the near future, as polyaminoboranes (and their closely related polyphosphinoboranes) have an essentially untapped potential with regard to their use as high-performance polymeric materials, as pre-ceramics or as precursors to extended B–N materials, such as white graphene.

Although complex and nuanced, with different catalysts and amine–borane starting materials offering a variety of final products, intermediates and observed catalyst resting states, a number of mechanistic scenarios are now becoming apparent for dehydrocoupling. The intermediate role of aminoboranes is now becoming clear, but whether such species remain associated with the metal centre once formed or are released into solution is still to be completely resolved. This is important as free aminoborane oligomerises to form cyclic products (i.e. borazines), whereas if B–N bond formation at the metal centre is fast, then polymerisation can occur. In some systems aminoborane formation and B–N bond-forming reactions may be closely correlated. Likewise, the propagating species in dehydropolymerisation and dehydrooligomerisation still remain to be fully resolved. Given the regular occurrence of amidoboranes (and phosphidoboranes) with supporting β-B-agostic interactions in many of these mechanistic studies, such species are perhaps likely candidates as key intermediates. If the current pace of discovery continues over the next 5 years, it is likely that the resulting mechanistic insight will lead to the production of catalysts that can dehydrocouple amine–boranes and phosphine–boranes “to order”, to provide high-value bespoke materials such as polyaminoboranes or pre-ceramics in an atom-efficient process, recognising that hydrogen is the only by-product. Indeed, linking such bond-forming processes with hydrogen transfer reactions might prove profitable if it generates two products of value with true 100% atom economy [86]. As recently enunciated [5], the formation

of main-group element–element bonds using catalytic techniques lags behind those developed for carbon–carbon bond-forming reactions that are so important for the synthesis of state-of-the-art organic molecules and macromolecules. The development of robust, and scalable, catalysts for amine–borane and phosphine–borane dehydrocoupling is thus one promising area to develop with regard to opening up the field to all those interested in main-group element–element bond-forming reactions: whether ultimately more interested in the release of gaseous hydrogen from such processes or the products and functional materials that arise directly from such events. Either way, it will certainly be interesting to see how the field develops.

The key intermediate in the dehydrocoupling of $H_3B \cdot NH_3$, B-(cyclotriborazanyl)amine–borane has been synthesized using a Cp_2ZrCl catalyst, allowing for its structural characterization [180].

The kinetics of $H_3B \cdot NH_3$ dehydrogenation using a Os dihydride catalyst have been studied, and show a zero order dependence on amine borane. Calculations suggest a mechanism in which H_2 loss from the catalyst is turnover limiting [181].

Acknowledgment The authors would like to thank EPRSC for the support (EP/J02127X/1).

References

1. Staubitz A, Robertson APM, Sloan ME, Manners I (2010) Chem Rev 110:4023
2. Huang Z, Autrey T (2012) Energy Environ Sci 5:9257
3. Hügle T, Hartl M, Lentz D (2011) Chem Eur J 17:10184
4. Staubitz A, Robertson APM, Manners I (2010) Chem Rev 110:4079
5. Leitao EM, Jurca T, Manners I (2013) Nat Chem 5:817
6. Liu Z, Song L, Zhao S, Huang J, Ma L, Zhang J, Lou J, Ajayan PM (2011) Nano Lett 11:2032
7. Clark TJ, Lee K, Manners I (2006) Chem Eur J 12:8634
8. Stephens FH, Pons V, Tom Baker R (2007) Dalton Trans 25:2613
9. Ewing WC, Marchione A, Himmelberger DW, Carroll PJ, Sneddon LG (2011) J Am Chem Soc 133:17093
10. Waterman R (2013) Chem Soc Rev 42:5629
11. Alcaraz G, Sabo-Etienne S (2010) Angew Chem Int Ed 49:7170
12. Johnson HC, Leitao EM, Whittell GR, Manners I, Lloyd-Jones GC, Weller AS (2014) J Am Chem Soc 136:9078
13. Sewell LJ, Lloyd-Jones GC, Weller AS (2012) J Am Chem Soc 134:3598
14. Staubitz A, Soto AP, Manners I (2008) Angew Chem Int Ed 47:6212
15. Jaska CA, Temple K, Lough AJ, Manners I (2003) J Am Chem Soc 125:9424
16. Pasumansky L, Haddenham D, Clary JW, Fisher GB, Goralski CT, Singaram B (2008) J Org Chem 73:1898
17. Johnson HC, Weller AS (2012) J Organomet Chem 721:17
18. Garcia-Vivo D, Huergo E, Ruiz MA, Travieso-Puente R (2013) Eur J Inorg Chem 4998
19. Stevens CJ, Dallanegra R, Chaplin AB, Weller AS, Macgregor SA, Ward B, McKay D, Alcaraz G, Sabo-Etienne S (2011) Chem Eur J 17:3011
20. Leitao EM, Stubbs NE, Robertson APM, Helten H, Cox RJ, Lloyd-Jones GC, Manners I (2012) J Am Chem Soc 134:16805
21. Marziale AN, Friedrich A, Klopsch I, Drees M, Celinski VR, Günne J, Schneider S (2013) J Am Chem Soc 135:13342
22. Robertson APM, Suter R, Chabanne L, Whittell GR, Manners I (2011) Inorg Chem 50:12680

23. Staubitz A, Sloan ME, Robertson APM, Friedrich A, Schneider S, Gates PJ, Günne J, Manners I (2010) J Am Chem Soc 132:13332
24. Alcaraz G, Vendier L, Clot E, Sabo-Etienne S (2010) Angew Chem Int Ed 49:918
25. Pons V, Baker RT, Szymczak NK, Heldebrant DJ, Linehan JC, Matus MH, Grant DJ, Dixon DA (2008) Chem Commun 6597
26. Jaska CA, Temple K, Lough AJ, Manners I (2001) Chem Commun 962
27. Denney MC, Pons V, Hebden TJ, Heinekey DM, Goldberg KI (2006) J Am Chem Soc 128:12048
28. Robertson APM, Leitao EM, Jurca T, Haddow MF, Helten H, Lloyd-Jones GC, Manners I (2013) J Am Chem Soc 135:12670
29. Bhunya S, Malakar T, Paul A (2014) Chem Commun 50:5919
30. Friedrich A, Drees M, Schneider S (2009) Chem Eur J 15:10339
31. Dallanegra R, Chaplin AB, Tsim J, Weller AS (2010) Chem Commun 46:3092
32. Sewell LJ, Huertos MA, Dickinson ME, Weller AS, Lloyd-Jones GC (2013) Inorg Chem 52:4509
33. Johnson HC, Robertson APM, Chaplin AB, Sewell LJ, Thompson AL, Haddow MF, Manners I, Weller AS (2011) J Am Chem Soc 133:11076
34. Chen X, Zhao J-C, Shore SG (2010) J Am Chem Soc 132:10658
35. Ewing WC, Carroll PJ, Sneddon LG (2013) Inorg Chem 52:10690
36. Himmelberger DW, Yoon CW, Bluhm ME, Carroll PJ, Sneddon LG (2009) J Am Chem Soc 131:14101
37. Green IG, Johnson KM, Roberts BP (1989) J Chem Soc Perkin Trans 2:1963
38. Widegren JA, Finke RG (2003) J Mol Catal A Chem 198:317
39. Jaska CA, Manners I (2004) J Am Chem Soc 126:9776
40. Chen YS, Fulton JL, Linehan JC, Autrey T (2005) J Am Chem Soc 127:3254
41. Sonnenberg JF, Morris RH (2013) ACS Catal 3:1092
42. Duman S, Ozkar S (2013) Int J Hydrog Energy 38:10000
43. Zahmakiran M, Philippot K, Ozkar S, Chaudret B (2012) Dalton Trans 41:590
44. Zahmakiran M, Ozkar S (2009) Inorg Chem 48:8955
45. Zahmakiran M, Ayvali T, Philippot K (2012) Langmuir 28:4908
46. He T, Wang JH, Wu GT, Kim H, Proffen T, Wu AA, Li W, Liu T, Xiong ZT, Wu CZ, Chu HL, Guo JP, Autrey T, Zhang T, Chen P (2010) Chem Eur J 16:12814
47. Luo W, Campbell PG, Zakharov LN, Liu SY (2011) J Am Chem Soc 133:19326
48. Luo W, Neiner D, Karkamkar A, Parab K, Garner Iii EB, Dixon DA, Matson D, Autrey T, Liu S-Y (2013) Dalton Trans 42:611
49. Campbell PG, Ishibashi JSA, Zakharov LN, Liu S-Y (2014) Aust J Chem 67:521
50. Vance JR, Robertson APM, Lee K, Manners I (2011) Chem Eur J 17:4099
51. Vance JR, Schafer A, Robertson APM, Lee K, Turner J, Whittell GR, Manners I (2014) J Am Chem Soc 136:3048
52. Bluhm ME, Bradley MG, Butterick R, Kusari U, Sneddon LG (2006) J Am Chem Soc 128:7748
53. Himmelberger DW, Alden LR, Bluhm ME, Sneddon LG (2009) Inorg Chem 48:9883
54. Wright WRH, Berkeley ER, Alden LR, Baker RT, Sneddon LG (2011) Chem Commun 47:3177
55. Mal SS, Stephens FH, Baker RT (2011) Chem Commun 47:2922
56. Boulho C, Djukic J-P (2010) Dalton Trans 39:8893
57. Kass M, Friedrich A, Drees M, Schneider S (2009) Angew Chem Int Ed 48:905
58. Conley BL, Williams TJ (2010) Chem Commun 46:4815
59. Blaquiere N, Diallo-Garcia S, Gorelsky SI, Black DA, Fagnou K (2008) J Am Chem Soc 130:14034
60. Kubas GJ (2001) Metal dihydrogen and σ-bond complexes. Kluwer, New York
61. Shimoi M, Nagai S, Ichikawa M, Kawano Y, Katoh K, Uruichi M, Ogino H (1999) J Am Chem Soc 121:11704
62. Johnson HC, McMullin CL, Pike SD, Macgregor SA, Weller AS (2013) Angew Chem Int Ed 52:9776

63. Ledger AEW, Ellul CE, Mahon MF, Williams JMJ, Whittlesey MK (2011) Chem Eur J 17:8704
64. Tang CY, Thompson AL, Aldridge S (2010) J Am Chem Soc 132:10578
65. Dallanegra R, Robertson APM, Chaplin AB, Manners I, Weller AS (2011) Chem Commun 47:3763
66. Douglas TM, Chaplin AB, Weller AS, Yang XZ, Hall MB (2009) J Am Chem Soc 131:15440
67. Chaplin AB, Weller AS (2011) Acta Cryst Sect C Cryst Struct Commun 67:M355
68. Baker RT, Gordon JC, Hamilton CW, Henson NJ, Lin PH, Maguire S, Murugesu M, Scott BL, Smythe NC (2012) J Am Chem Soc 134:5598
69. Sloan ME, Staubitz A, Clark TJ, Russell CA, Lloyd-Jones GC, Manners I (2010) J Am Chem Soc 132:3831
70. Kumar A, Johnson HC, Hooper TN, Weller AS, Algarra AG, Macgregor SA (2014) Chem Sci 5:2546
71. Chaplin AB, Weller AS (2010) Angew Chem Int Ed 49:581
72. Dallanegra R, Chaplin AB, Weller AS (2009) Angew Chem Int Ed 48:6875
73. Corcoran EW, Sneddon LG (1984) J Am Chem Soc 106:7793
74. Corcoran EW, Sneddon LG (1985) J Am Chem Soc 107:7446
75. Ciobanu O, Kaifer E, Enders M, Himmel HJ (2009) Angew Chem Int Ed 48:5538
76. Braunschweig H, Guethlein F (2011) Angew Chem Int Ed 50:12613
77. Braunschweig H, Claes C, Guethlein F (2012) J Organomet Chem 706:144
78. Braunschweig H, Brenner P, Dewhurst RD, Guethlein F, Jimenez-Halla JOC, Radacki K, Wolf J, Zollner L (2012) Chem Eur J 18:8605
79. Kim S-K, Han W-S, Kim T-J, Kim T-Y, Nam SW, Mitoraj M, Piekoś Ł, Michalak A, Hwang S-J, Kang SO (2010) J Am Chem Soc 132:9954
80. Alcaraz G, Chaplin AB, Stevens CJ, Clot E, Vendier L, Weller AS, Sabo-Etienne S (2010) Organometallics 29:5591
81. Tang CY, Thompson AL, Aldridge S (2010) Angew Chem Int Ed 49:921
82. Tang CY, Phillips N, Bates JI, Thompson AL, Gutmann MJ, Aldridge S (2012) Chem Commun 48:8096
83. Vidovic D, Addy DA, Kramer T, McGrady J, Aldridge S (2011) J Am Chem Soc 133:8494
84. MacInnis MC, McDonald R, Ferguson MJ, Tobisch S, Turculet L (2011) J Am Chem Soc 133:13622
85. Cassen A, Gloaguen Y, Vendier L, Duhayon C, Poblador-Bahamonde A, Raynaud C, Clot E, Alcaraz G, Sabo-Etienne S (2014) Angew Chem Int Ed 53:7569
86. Jiang YF, Blacque O, Fox T, Frech CM, Berke H (2009) Organometallics 28:5493
87. Alcaraz G, Grellier M, Sabo-Etienne S (2009) Acc Chem Res 42:1640
88. Clark TJ, Russell CA, Manners I (2006) J Am Chem Soc 128:9582
89. Luo Y, Ohno K (2007) Organometallics 26:3597
90. Forster TD, Tuononen HM, Parvez M, Roesler R (2009) J Am Chem Soc 131:6689
91. Wolstenholme DJ, Traboulsee KT, Decken A, McGrady GS (2010) Organometallics 29:5769
92. Helten H, Dutta B, Vance JR, Sloan ME, Haddow MF, Sproules S, Collison D, Whittell GR, Lloyd-Jones GC, Manners I (2013) Angew Chem Int Ed 52:437
93. Beweries T, Hansen S, Kessler M, Klahn M, Rosenthal U (2011) Dalton Trans 40:7689
94. Beweries T, Thomas J, Klahn M, Schulz A, Heller D, Rosenthal U (2011) ChemCatChem 3:1865
95. Pun D, Lobkovsky E, Chirik PJ (2007) Chem Commun 3297
96. Miyazaki T, Tanabe Y, Yuki M, Miyake Y, Nishibayashi Y (2011) Organometallics 30:2394
97. Rousseau R, Schenter GK, Fulton JL, Linehan JC, Engelhard MH, Autrey T (2009) J Am Chem Soc 131:10516
98. Kawano Y, Uruichi M, Shimoi M, Taki S, Kawaguchi T, Kakizawa T, Ogino H (2009) J Am Chem Soc 131:14946
99. Hebden TJ, Denney MC, Pons V, Piccoli PMB, Koetzle TF, Schultz AJ, Kaminsky W, Goldberg KI, Heinekey DM (2008) J Am Chem Soc 130:10812
100. Dietrich BL, Goldberg KI, Heinekey DM, Autrey T, Linehan JC (2008) Inorg Chem 47:8583
101. Paul A, Musgrave CB (2007) Angew Chem Int Ed 46:8153

102. Keaton RJ, Blacquiere JM, Baker RT (2007) J Am Chem Soc 129:1844
103. Yang X, Hall MB (2008) J Am Chem Soc 130:1798
104. Yang X, Hall MB (2009) J Organomet Chem 694:2831
105. Zimmerman PM, Paul A, Musgrave CB (2009) Inorg Chem 48:5418
106. Zimmerman PM, Paul A, Zhang Z, Musgrave CB (2009) Angew Chem Int Ed 48:2201
107. Ai D, Guo Y, Liu W, Wang Y (2014) J Phys Org Chem 27:597
108. Douglas TM, Chaplin AB, Weller AS (2008) J Am Chem Soc 130:14432
109. Rossin A, Bottari G, Lozano-Vila AM, Paneque M, Peruzzini M, Rossi A, Zanobini F (2013) Dalton Trans 42:3533
110. Robertson APM, Leitao EM, Manners I (2011) J Am Chem Soc 133:19322
111. Butera V, Russo N, Sicilia E (2014) ACS Catal 4:1104
112. Vogt M, de Bruin B, Berke H, Trincado M, Grützmacher H (2011) Chem Sci 2:723
113. Wallis CJ, Dyer H, Vendier L, Alcaraz G, Sabo-Etienne S (2012) Angew Chem Int Ed 51:3646
114. Chen X, Zhao J-C, Shore SG (2013) Acc Chem Res 46:2666
115. Johnson HC, Leitao EM, Whittell GR, Manners I, Lloyd-Jones GC, Weller AS (2014) J Am Chem Soc 134:1520
116. Kubas GJ (2004) Adv Inorg Chem 56:127
117. Lu ZY, Conley BL, Williams TJ (2012) Organometallics 31:6705
118. Conley BL, Guess D, Williams TJ (2011) J Am Chem Soc 133:14212
119. Schreiber DF, O'Connor C, Grave C, Ortin Y, Muller-Bunz H, Phillips AD (2012) ACS Catal 2:2505
120. Phillips AD, Laurenczy G, Scopelliti R, Dyson PJ (2007) Organometallics 26:1120
121. Chapman AM, Haddow MF, Wass DF (2011) J Am Chem Soc 133:8826
122. Rosello-Merinó M, López-Serrano J, Conejero S (2013) J Am Chem Soc 135:10910
123. Stubbs NE, Robertson APM, Leitao EM, Manners I (2013) J Organomet Chem 730:84
124. Xiong ZT, Yong CK, Wu GT, Chen P, Shaw W, Karkamkar A, Autrey T, Jones MO, Johnson SR, Edwards PP, David WIF (2008) Nat Mater 7:138
125. Diyabalanage HVK, Shrestha RP, Semelsberger TA, Scott BL, Bowden ME, Davis BL, Burrell AK (2007) Angew Chem Int Ed 46:8995
126. Spielmann J, Jansen G, Bandmann H, Harder S (2008) Angew Chem Int Ed 47:6290
127. Spielmann J, Harder S (2009) J Am Chem Soc 131:5064
128. Spielmann J, Piesik D, Wittkamp B, Jansen G, Harder S (2009) Chem Commun 3455
129. Spielmann J, Bolte M, Harder S (2009) Chem Commun 6934
130. Spielmann J, Piesik DFJ, Harder S (2010) Chem Eur J 16:8307
131. Bellham P, Hill MS, Kociok-Kohn G, Liptrot DJ (2013) Chem Commun 49:1960
132. Liptrot DJ, Hill MS, Mahon MF, MacDougall DJ (2010) Chem Eur J 16:8508
133. Bellham P, Hill MS, Kociok-Köhn G (2014) Organometallics. doi:10.1021/om500467b
134. Butera V, Russo N, Sicilia E (2014) Chem Eur J 20:5967
135. Hill MS, Kociok-Kohn G, Robinson TP (2010) Chem Commun 46:7587
136. Lu E, Yuan Y, Chen Y, Xia W (2013) ACS Catal 3:521
137. Hill MS, Hodgson M, Liptrot DJ, Mahon MF (2011) Dalton Trans 40:7783
138. Cui P, Spaniol TP, Maron L, Okuda J (2013) Chem Eur J 19:13437
139. Cowley HJ, Holt MS, Melen RL, Rawson JM, Wright DS (2011) Chem Commun 47:2682
140. Hansmann MM, Melen RL, Wright DS (2011) Chem Sci 2:1554
141. Less RJ, Simmonds HR, Dane SBJ, Wright DS (2013) Dalton Trans 42:6337
142. Harder S, Spielmann J (2011) Chem Commun 47:11945
143. Erickson KA, Wright DS, Waterman R (2014) J Organomet Chem 751:541
144. Daly SR, Bellott BJ, Kim DY, Girolami GS (2010) J Am Chem Soc 132:7254
145. Welch GC, Juan RRS, Masuda JD, Stephan DW (2006) Science 314:1124
146. Stephan DW, Erker G (2010) Angew Chem Int Ed 49:46
147. Miller AJM, Bercaw JE (2010) Chem Commun 46:1709
148. Whittell GR, Balmond EI, Robertson APM, Patra SK, Haddow MF, Manners I (2010) Eur J Inorg Chem 3967

149. Appelt C, Slootweg JC, Lammertsma K, Uhl W (2013) Angew Chem Int Ed 52:4256
150. Burg AB, Wagner RI (1953) J Am Chem Soc 75:3872
151. Burg AB (1959) J Inorg Nuc Chem 11:258
152. Dorn H, Singh RA, Massey JA, Lough AJ, Manners I (1999) Angew Chem Int Ed 38:3321
153. Dorn H, Singh RA, Massey JA, Nelson JM, Jaska CA, Lough AJ, Manners I (2000) J Am Chem Soc 122:6669
154. Dorn H, Vejzovic E, Lough AJ, Manners I (2001) Inorg Chem 40:4327
155. Dorn H, Rodezno JM, Brunnhöfer B, Rivard E, Massey JA, Manners I (2003) Macromolecules 36:291
156. Jaska CA, Manners I (2004) J Am Chem Soc 126:1334
157. Snow SA, Shimoi M, Ostler CD, Thompson BK, Kodama G, Parry RW (1984) Inorg Chem 23:511
158. McNamara WF, Duesler EN, Paine RT, Ortiz JV, Koelle P, Noeth H (1986) Organometallics 5:380
159. Frank N, Hanau K, Flosdorf K, Langer R (2013) Dalton Trans 42:11252
160. Merle N, Koicok-Köhn G, Mahon MF, Frost CG, Ruggerio GD, Weller AS, Willis MC (2004) Dalton Trans 3883
161. Kawano Y, Yamaguchi K, Miyake S-y, Kakizawa T, Shimoi M (2007) Chem Eur J 13:6920
162. Macías R, Rath NP, Barton L (1999) Angew Chem Int Ed 38:162
163. Volkov O, Macías R, Rath NP, Barton L (2002) Inorg Chem 41:5837
164. Ingleson M, Patmore NJ, Ruggiero GD, Frost CG, Mahon MF, Willis MC, Weller AS (2001) Organometallics 20:4434
165. Shuttleworth TA, Huertos MA, Pernik I, Young RD, Weller AS (2013) Dalton Trans 42:12917
166. Jaska CA, Dorn H, Lough AJ, Manners I (2003) Chem Eur J 9:271
167. Jaska CA, Lough AJ, Manners I (2005) Dalton Trans 326
168. Paine RT, Noeth H (1995) Chem Rev 95:343
169. Vogel U, Hoemensch P, Schwan K-C, Timoshkin AY, Scheer M (2003) Chem Eur J 9:515
170. Schwan K-C, Timoskin AY, Zabel M, Scheer M (2006) Chem Eur J 12:4900
171. Thoms C, Marquardt C, Timoshkin AY, Bodensteiner M, Scheer M (2013) Angew Chem Int Ed 52:5150
172. Lee K, Clark TJ, Lough AJ, Manners I (2008) Dalton Trans 2732
173. Huertos MA, Weller AS (2012) Chem Commun 48:7185
174. Huertos MA, Weller AS (2013) Chem Sci 4:1881
175. Hooper TN, Huertos MA, Jurca T, Pike SD, Weller AS, Manners I (2014) Inorg Chem 53:3716
176. Clark TJ, Rodezno JM, Clendenning SB, Aouba S, Brodersen PM, Lough AJ, Ruda HE, Manners I (2005) Chem Eur J 11:4526
177. Pandey S, Lonnecke P, Hey-Hawkins E (2014) Eur J Inorg Chem 2456
178. Pandey S, Lönnecke P, Hey-Hawkins E (2014) Inorg Chem 53:8242
179. Denis JM, Forintos H, Szelke H, Toupet L, Pham TN, Madec PJ, Gaumont AC (2003) Chem Commun 54
180. Kalviri HA, Gartner F, Ye G, Korobkov I, Baker RT (2014) Chem Sci 6:618
181. Esteruelas MA, Lopez AM, Mora M, Onate E (2014) ACS Catal 5:187